

**Analysis and control of adhesion behavior
of solid fuel combustion ash at high
temperature**

2020.6

東京農工大学大学院

生物システム応用科学府

生物機能システム科学専攻

高 居冠

Doctoral Thesis

Analysis and control of adhesion behavior of solid fuel combustion ash at high temperature

GAO JUGUAN

Graduate School of Bio-Applications and Systems Engineering

Tokyo University of Agriculture and Technology

Contents

CHAPTER 1

Introduction

1.1 The situation of energy supply and consumption in the world-----	1
1.2 The situation of energy supply and changing trend in Japan-----	5
1.3 Environmental problems caused by energy consumption-----	8
1.4 The situation of disposal of sewage sludge-----	9
1.5 Deposition phenomena of combustion ashes at high temperature-----	13
1.5.1 Generation of fly ash-----	14
1.5.2 Process of ash transportation and deposition-----	15
1.5.3 Accumulation and growth of deposits-----	17
1.5.4 Different types of forces acting on ash particles-----	19
1.5.5 Ash forming elements-----	21
1.5.6 Ash generated from biomass combustion-----	24
1.5.7 Control of deposition phenomena by combustion additives-----	25
1.6 Purpose of this study and structure of this thesis-----	38
1.7 References-----	42

CHAPTER 2

Analysis and adhesion control of sewage sludge combustion ashes at high temperature

2.1 Introduction-----	46
2.2 Experimental and analysis-----	49
2.2.1 Ash samples and characterization-----	49
2.2.2 Tensile strength and thermomechanical properties of ash powder beds----	49
2.2.3 Thermodynamic calculations for ash samples-----	50
2.3 Results and discussions-----	52
2.3.1 Characterization of ash samples-----	52
2.3.2 Tensile strength and thermomechanical properties of ash samples-----	53

2.3.3 Thermodynamic calculations for ash samples-----	54
2.3.4. Adhesion behavior control by additives-----	55
2.4. Conclusions-----	66
2.5 References-----	67

CHAPTER 3

Research on the effect of specific elements on adhesion phenomena in sewage sludge combustion ashes using model ash systems

3.1 Introduction-----	69
3.2 Experimental-----	73
3.2.1 Real ash samples and characterization-----	73
3.2.2 Raw materials of model ash-----	74
3.2.3 The synthetic method of model ash-----	75
3.2.4 Characterization of model ash samples-----	76
3.2.5 Tensile strength measurements-----	77
3.2.6 Thermodynamic calculation of each ash sample-----	77
3.3 Results and discussions-----	80
3.3.1 Particle characterization of model ash particles and comparison with real ash-----	83
3.3.2 Comparison of tensile strength in ash powder bed for real and model ash--	83
3.3.3 Effects of Ca and Mg on tensile strength of ash powder bed-----	83
3.3.4 Estimation of tensile strength increasing mechanism of each model ash sample-----	87
3.3.5 Microscopic observation of model ash particles before and after heat treatment -----	89
3.3.6 Estimation of different compounds in ash deposition control-----	90
3.4 Conclusions -----	102
3.5 References-----	103

CHAPTER 4

Direct measurement of single-particle adhesion behaviors on metal surfaces at high temperatures

4.1 Introduction-----	105
4.2 Experimental -----	108
4.2.1 Preparations of ash samples-----	108
4.2.2 Characterization of ash samples-----	110
4.2.3 Schematic of adhesion force measurement system-----	111
4.3 Results and discussions-----	118
4.3.1 Shrinkage behaviors of different ash samples at elevated temperature-----	118
4.3.2 Adhesion force of model ash samples prepared from pure silica particles under different conditions-----	119
4.3.3 Adhesion force of coal ash particles prepared by a drop tube furnace-----	121
4.4 Conclusions-----	134
4.5 References-----	135

CHAPTER 5

General Conclusion-----	137
--------------------------------	------------

Acknowledgement-----	142
-----------------------------	------------

CHAPTER 1

Introduction

CHAPTER 1

Introduction

1.1 The situation of energy supply and consumption in the world¹

Figure 1-1 and 1-2 show the world total primary energy supply by region and regional shares. With the development of economics, the supply of primary energy get a significant increase from less than 6000Mtoe in 1970 to about 14000Mtoe in 2017. From regional data it can be seen that the countries in Organization for Economic Co-operation and Development (OECD) have the largest energy supply perennially, however their energy supply is stable in the last 50 years. The energy supply mainly increase in the developing countries and regions, since their societies and economics get significant development in recent years, the energy demands are increasing gradually. The most remarkable countries and regions are China and other non-OECD Asia, as a representative of development in recent years, the energy supply in China and other non-OECD countries has increased from several percentage of the total energy supply to the second and third largest regions in the world. In a word, the increment of energy supply in the world is mainly demanded by the developing countries such as China.

Figure 1-3 and 1-4 represent the energy supply by source all over the world. Fossil fuels including oil, coal and natural gas are always the main energy source in the last 50 years. Oil supply the largest amount of energy all the time, it can not only supply energy products such as gasoline and diesel but also provide the raw materials of industrial manufacture. As a cheap and easily obtainable fossil fuels, coal is a very

popular fuels all over the world. The supply of coal is gradually increasing in the past years. With the development of urbanization, the increase of natural gas supply is rapid and obvious. The growth rates of coal and natural gas combustion are higher than oil. Energy with the largest growth rate is nuclear energy and other new energy, which is due to the diversification of energy supply and meet the demand of low carbon plans. However, although the growth rate is remarkable, the share of nuclear and other new energy is still small.

World TPES from 1971 to 2017 by region (Mtoe)

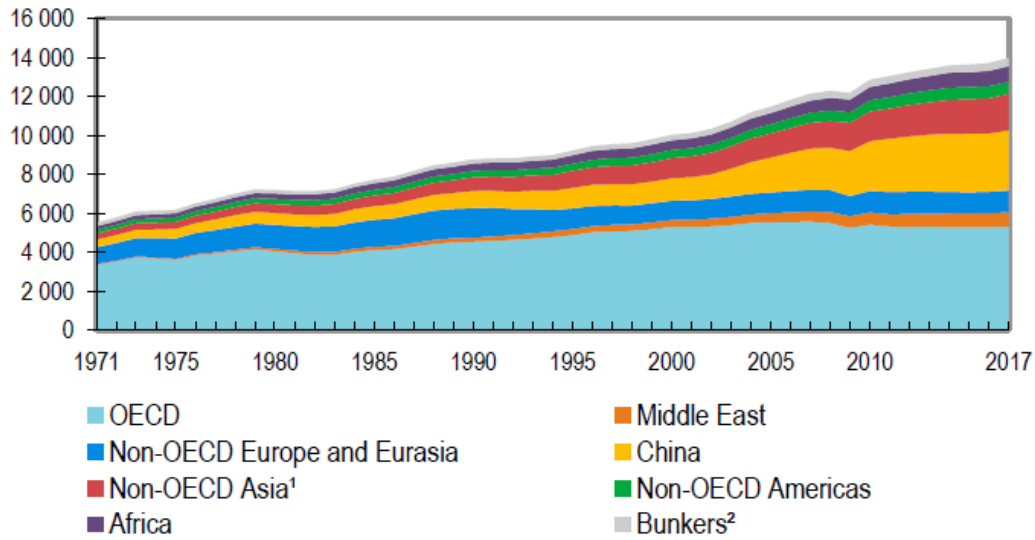
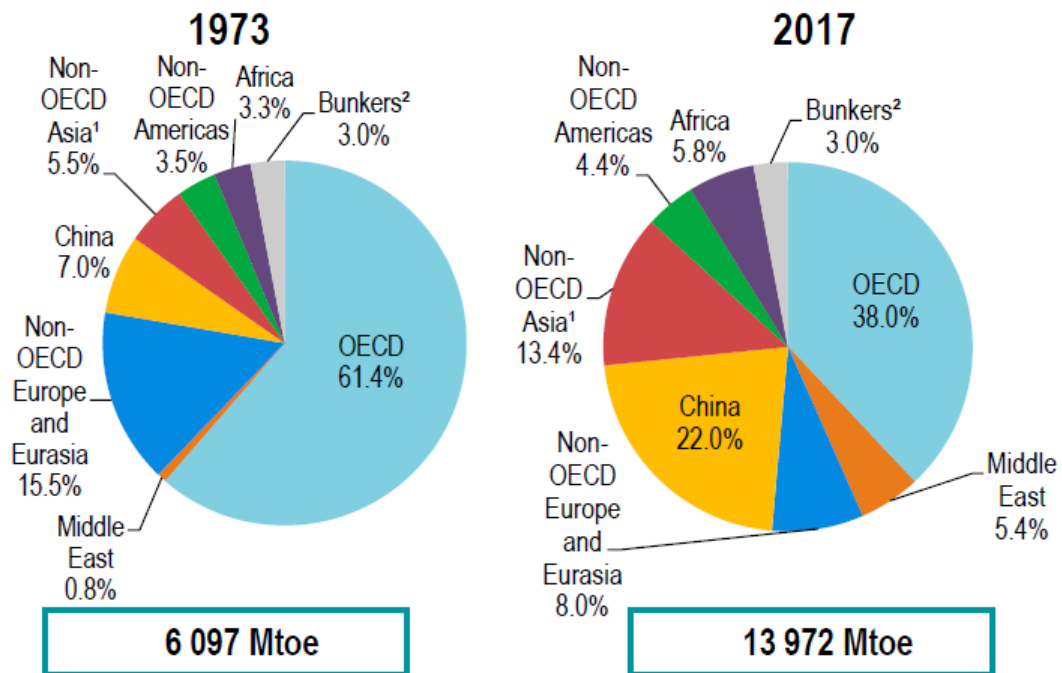


Figure 1-1 World total primary energy supply by region.¹



1. Non-OECD Asia excludes China.

2. Includes international aviation and international marine bunkers.

Figure 1-2 Regional shares of total primary energy supply.¹

World¹ TPES from 1971 to 2017 by source (Mtoe)

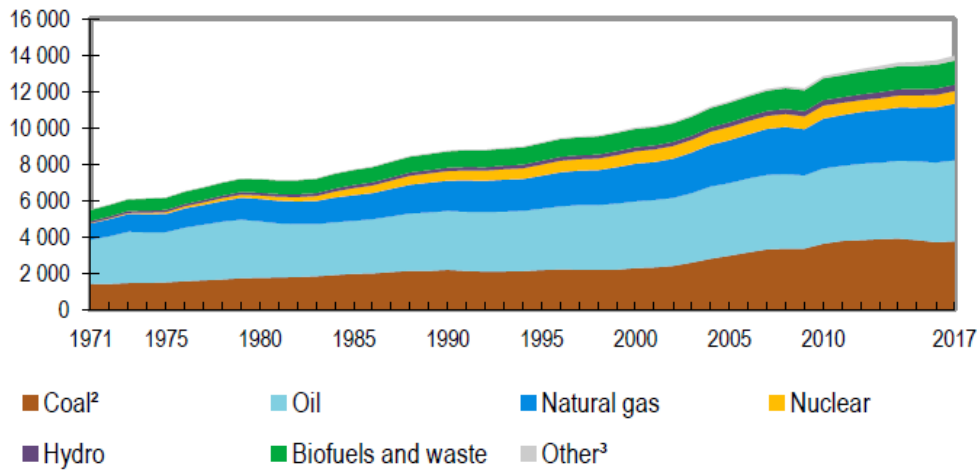
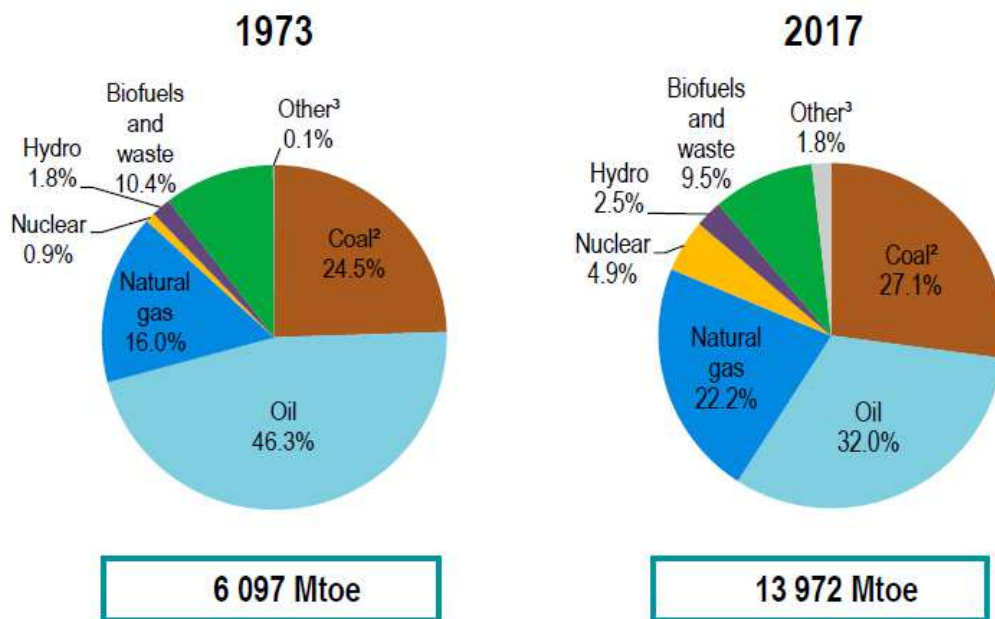


Figure 1-3 World total primary energy supply by source.¹



1. World includes international aviation and international marine bunkers.
 2. In these graphs, peat and oil shale are aggregated with coal.
 3. Includes geothermal, solar, wind, tide/wave/ocean, heat and other sources.
- Source: [IEA, World Energy Balances, 2019](#).

Figure 1-4 source share of total primary energy supply.¹

1.2 The situation of energy supply and changing trend in Japan²⁻³

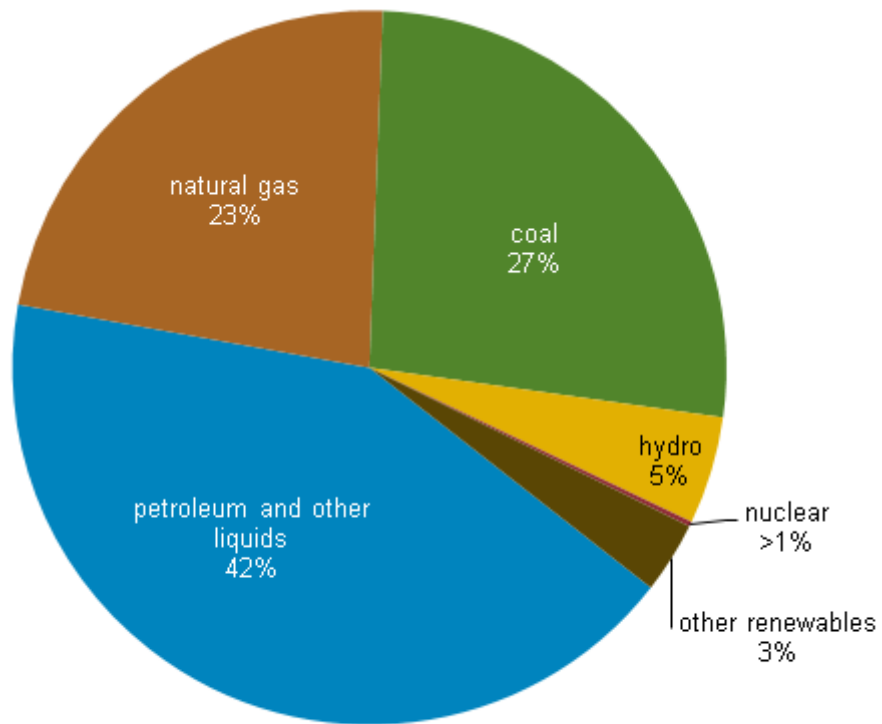
Japan is a country that lacks of energy sources, its self-efficiency ratio of energy was less than 10% in 2017. Most of the required energy sources need to be imported from overseas. Now, Japan is the largest liquefied natural gas importer in the world, meanwhile the rank of coal imports was only behind China and India in the world. More than that, Japan was the third largest consumer of crude oil that behind the United States and China, according to U.S. Energy Information Administration.

In the year of 2010, Japan's domestic energy resources met more than 20% of the country's total primary energy use, which reached to a high level. However, after the nuclear plant accident caused by Great East Japan Earthquake in 2011, the energy self-efficiency ratio of Japan showed a sharp decline due to the shutdown of nuclear power plants. This situation exacerbated the consumption of fossil fuels in the domestic of Japan and forced Japan import more primary energy resources to meet the demands. In 2018, the total imports of coals, natural gas (LNG) and crude oil reached to about 114 million tons, 83 million tons and 1.1 billion barrels respectively. The costs for additional imports of fossil fuels were about \$30 billion every year.

Due to the accident of the Fukushima nuclear power station, the previous share of nuclear energy was replaced by more fossil fuels and renewable energy. In 2017, oil remained the largest source of primary energy in Japan, reached to 39%. This data was about 75.5% in 1973. The increase of other fuels and advanced power efficiency are the main reasons of the decline of oil consumptions. In 1973, the share of coal-sourced fuels was 16.9%, then the data increased to 22.7% in 2010 before the earthquake and

slightly increased to 25.1% in 2017. Data shows the coal is still accounted for a significant share of energy consumption. In the past decades, the consumption of natural gas got significant increase, which was changed from 1.6% in 1973 to 23.4% in 2017. This great demand of natural gas promoted Japan to be the largest LNG importer in the world now. Before the 2011 earthquake, Japan was the third-largest consumer of nuclear power, after the United States and France, and nuclear power reached to 11.2% of the total energy in 2010. After the accident, the attitude of Japan's government to nuclear power was very cautious, by 2018, the share of nuclear power declined to only about 1.4%. Although fossil fuels are still the dominant energy source in Japan, hydroelectric power and other renewable energy sources are in favor gradually and start to grow as an alternative fuel source.

Japan's government currently intends to restart using nuclear energy as a baseload power source with necessary safety measures. The new energy policy plans to balance the country's fuel portfolio. New policies contain enhancing the share of renewable and alternative energy sources, diversifying from oil to reduce dependence in the transportation sector, and developing advanced and efficient generation technologies for fossil fuel use.




 Sources: EIA International Energy Statistics, BP Statistical Review of World Energy 2016

Figure 1-5 Japan's total energy consumption, 2015.²

1.3 Environmental problems caused by energy consumption

Since the industrial revolution the fossil fuels have become the main energy source. The Industrial Revolution modified the whole energy structure of the world society. The consumption of fossil fuels motivate the economic development all over the world and make the lives of human beings more comfortable and convenient. On the other hand, the huge consumption of fossil fuels causes increasingly serious environmental issues at the same time. As the concentration of greenhouse gases increase steadily, the trend of global warming phenomenon is increasingly obvious. Nowadays, the global warming and the related environmental issues, which are cause by the excessive emission of greenhouse gases, have been the focus of the world. Facing the situations of global warming issues, sea level rise, increasing frequency of extreme weathers and other phenomenon which seriously affect the life of humankind and the health of earth ecological system(IPCC, 2007), decreasing the emission of greenhouse gases is one of the efficient choice.

According to the Greenhouse Gas Bulletin of World Meteorological Organization (WMO)⁴, the globally average concentrations of greenhouse gas such as carbon dioxide (CO₂) and methane (CH₄) reached the new high level since the Industrial Revolution. Carbon dioxide is the most important greenhouse gas in the atmosphere and it contributes about 64% of the radiative forcing (WMO, 2011).

In addition to the emission of greenhouse gas, NO_x and SO_x could also emit to the atmosphere during the fuel combustion process. The NO_x and SO_x can dissolve into the rain drops and lead to the acid rains. The drops of acid rains can acidulate soil,

causing serious environmental and biological problems. Meanwhile, the acid rains can also corrode buildings and cause harm to humanity assets.

1.4 The situation of disposal of sewage sludge

With the development of society and economic, the city scale is growing rapidly, the urban population is also increasing rapidly. At the same time, the discharge of waste water and the production of sewage sludge also have increase year by year. Sewage sludge is a kind of outcomes during waste water treatment processes, which is complex heterogeneous bodies composed of bacterial micelles that formed by various microorganisms and absorbed organic and inorganic substances.⁵ Urban sewage sludge usually contains large amount of organic nutrient such as nitrogen and phosphorous which make the sludge as a potential energy source, on the other hand, the harmful substances including heavy metals, pathogenic micro-organisms, bacteria, viruses and toxins need to be processed legally and harmlessly.⁶⁻⁸

There are many methods to dispose sewage sludge, such as sanitary landfilling, ocean dumping, soil utilization, incineration, thermal treatment and resourceful treatment.

Sanitary landfilling refers to the process of direct fill sewage sludge wastes in a landfill site. The sanitary landfill sites require scientific assessment and onsite protection treatment. The main advantage of this disposal method is low cost, however there are still many disadvantages. Firstly landfilling requires large area of land, Secondly the filled sewage sludge may have anaerobic decomposition in the soil and generate some toxic gases. Thirdly the heavy metal and other persistent organic toxics

may permeate into deeper soils and underground water, resulting in secondary pollutions. Nowadays, countries in the world have decrease the proportion of landfilling gradually to reduce damage to environment.

Ocean dumping is a disposal method which was applied in early stage. The direct dumping sewage sludge into the ocean can damage the marine ecological environment and marine biological resources seriously. Most countries have prohibited this disposal method.

Soil utilization means utilize the sewage sludge on the surface or inside of soil to improve soil conditions or increase soil fertility by methods including covering, injection, spray and others. Similar to landfilling, this method also have potential to cause further environment pollution if without scientific and harmless treatment before utilization.

Incineration of sewage sludge is the most widely used disposal method now. Incineration method can achieve targets of volume reduction, harmless, stabilization and resource utilization. After incineration, the volume of sludge could even decrease 90%. Meanwhile, the high temperature can kill the bacteria and pathogen thoroughly and increase the stabilization of heavy metals. The heat generated from incineration can be utilized effectively and the ash residue after combustion can be used as building materials. Now the incineration process of sewage sludge has been wildly used in developed countries.^{5, 9-11}

Thermal treatment refers to using some thermochemical treatment process to separate the organic matters from solid residues in the sludge. Except for incineration,

thermochemical treatment also include wet oxidation, gasification and other techniques,¹⁰ as shown in Figure 1-6.

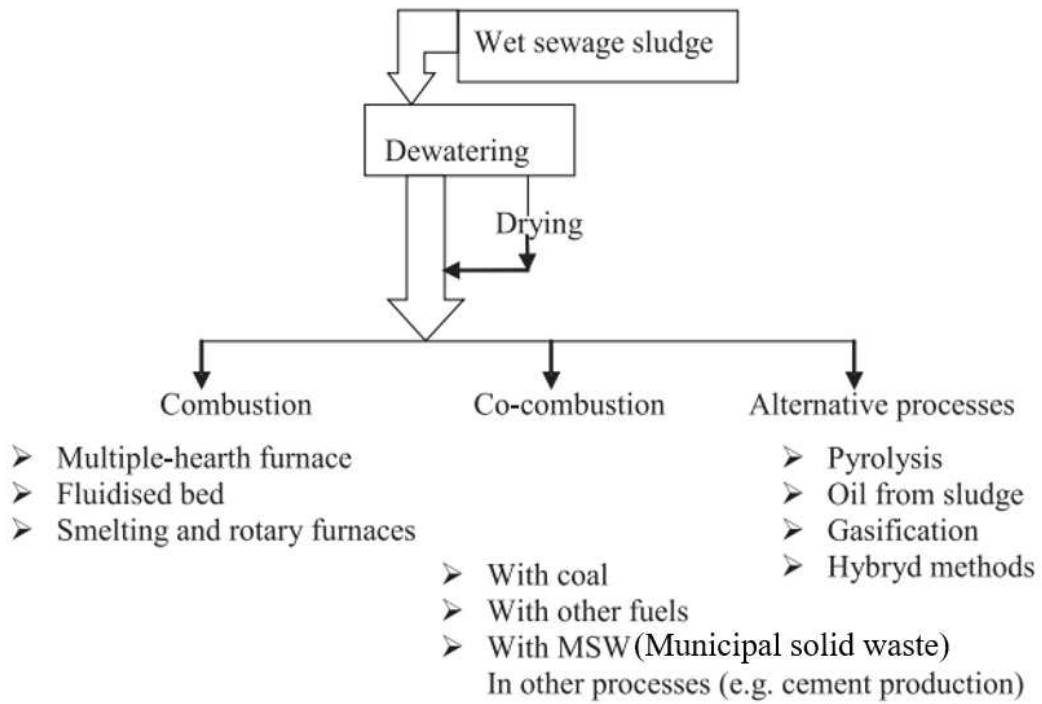


Figure 1-6 Main methods of thermal sewage sludge disposal.¹⁰

1.5 Deposition phenomena of combustion ashes at high temperature

To a coal combustion plant or a sewage sludge treatment plant, steady operation is an eternal subject and objective, however ash deposition phenomena is a traditional and a tough challenge. In systems including solid fuels direct combustion, gasification or power generation, ash particles generate from a combustion furnace could adhere to and grow on the walls of the furnace or heat transfer tubes. These ash deposition phenomena may cause many serious consequences including heat transfer inhibition, gas flow blockage, corruptions on the deposit contact areas and reducing thermal transfer efficiency in heating exchange sections. In some cases, operation temperatures in the plants would be decreased to reduce the possibilities of deposit growth or even the plants would be temporary shutdown when technicians do operations to remove the deposits. For example Figure 1-7 illustrates the deposition and slagging problem of ashes on the screen tubes before and after operation in a Danish boiler.¹² All of these issues and operations could lead to the low efficiency in daily operation and hinder the long-term stable operation of plants, therefore the seriousness of ash deposition phenomena is an important factor which affects the safe and efficient operation of relevant plants. Therefore, it is essential to have a better understanding about the whole process of ash deposition issues from the combustion of fuels, to generation of ash particles, to ash transportation, to ash aggregation and deposition, to the growth of deposit, until the removal of ash deposits. These fundamental researches are conducive to the long-term establishment and development of highly efficient plant systems.

1.5.1 Generation of fly ash

During the combustion of solid fuels including coals and biomass wastes, the non-combustible inorganic contents transform into gas, liquid and solid ash intermediates. Ashes are the incombustible inorganic residues after complete combustion of fuels. These inorganic constituents are called ash-forming compounds. The ash-forming compounds may be composed of included and excluded minerals, salts, or organically bound into the fuel hydrocarbon matrix, simply shown in Figure 1-8.¹³ Generally, the ash content in coals is about 10% and the ash contents in biomass fuels such as woods are only about several percent.¹⁴ In a coal combustion power plant, the combustion ashes stay at the bottom of boiler as incombustible inorganic residues are called bottom ashes, the other ashes will transfer to the convective heat transfer surfaces with the flue gas flow and lead to deposition issues and these ashes are called fly ashes. There are many factors can affect the emission and properties of particulate materials during coals combustions, such as coal characteristics,¹⁵ temperatures^{16 17} and coal sizes.¹⁸ Besides, the existence forms of ashes are also affected by the facilities in the plants, for example, in the vibrating boilers, the ratio of fly ash to bottom ash from bituminous coal combustion is about 60%/40% while the ratio in pc-fired boilers is about 95%/5%.¹⁹

Classical theories suggest that the size distribution model of fly ashes show bimodal distribution due to the ash vaporization and fragmentation as shown in Figure 1-9.²⁰ With the deeper understanding of ash generation during combustion, three modes are used to explain the ash formation from pulverized-coal combustion. The ash particles generated during coal combustions can be divided into three groups according

the size. The smallest ultrafine mode ($<0.1\ \mu\text{m}$) is the result of ash vaporization, nucleation and growth mechanisms. Some inorganic components volatilized during the combustion process and the volatile components may form submicron particles by uniform nucleation or non-uniform condensation on the heat transfer surface of existed fly ash particles. The largest coarse particles ($1\sim 10\ \mu\text{m}$) mainly come from the agglomeration of ash within the burning char particles. They are mainly depend on the properties of coals and combustion conditions. The central fine fragmentation mode ($0.1\ \mu\text{m}\sim 1\ \mu\text{m}$) does not depend on the chemical composition but comprises the major portion of primary fine particle mass emissions from pulverized-coal combustion.²⁰⁻²³ Buhre et al¹⁷ presented the mechanisms of ash formation during pulverized coal combustion, as shown in Figure 1-10. Since the biomass contains a large amount of volatile inorganic components, the generation of fly ash particles due to condensation is more apparent than coal ashes.²⁴

1.5.2 Process of ash transportation and deposition

Deposition phenomenon represents fly ash particles generated from combustion move to the convective heat transfer area and adhere on the surface of heat exchanger causing fouling or slagging issues. Now the acknowledged mechanisms of deposition contain five main routes: inertial impaction, thermophoresis, chemical reaction, condensation and eddy deposition²⁵ (Figure 1-11).

Inertial impaction represent the coarse particles move and hit to the surface of deposition areas by inertia effect. When gas flows carrying coarse particles of $10\ \mu\text{m}$ or

more with large inertial force transport near the heat transfer tubes, the coarse particles depart from gas flows and collide with the tubes, the surface of adhesive layer get rough consequently. This effect is evident for particles over 20 μm . Inertial impaction can be affected by many factors such as the shape of object, size distribution of particles, density of particles, angle of collision and characteristics of gas flow.²⁶⁻²⁸

Thermophoresis deposition means the ash particles move and collide with the tube surface motivated by thermophoretic force, this mechanism mainly act on the particles under 10 μm . Thermophoresis phenomena are caused by temperature gradient, particles suspended in fluids with an obvious temperature gradient have interactions with fluid molecules. Since fluid molecules have higher kinetic energy on the side of high temperature than the low temperature which make the fluid molecules move to the low temperature side from high temperature, the ash particle dragged by fluid collide on the surface of tube and cause deposition consequently.²⁹⁻³⁰

Chemical reaction represents the sulfation of basic compounds, oxidation of unburned coals and the corrosion phenomena of acidic materials in the deposits.

Condensation means the gas-phase inorganic components in the flue gas condense on the surface of heat exchange tubes with relatively lower temperature. The condensation usually occurs all around the tubes.³¹⁻³²

Eddy deposition contain two aspects. One is fine particles collide on the surface by eddy effect in the lee-ward eddy regions. Another is eddy occurs in the intervals of large particles then fine particles among large particles are driven to deposit under the action of eddy flow.

In all the five ash deposition mechanisms, the first four terms have the dominate effects. Among of them, inertial impaction dominate the intensity of deposition layers. Figure 1-12 shows the various stages of ash depositions.³³

The affect regions of different deposition mechanism are also different. Inertial impaction mainly occur on the windward sides while thermophoresis related deposits are finer grained and more evenly distributed around the tube surface than deposits formed by inertial impaction. Condensation deposits have no granularity and are more uniformly deposited on the tubes.³⁴ Figure 1-13 illustrate the deposition tendency of different mechanisms.

The whole fate of mineral materials in coal during combustion are depicted in Figure 1-14 by Bryers including extraneous and inherent ash, different types of deposits and modes of transport to the surface.³³

1.5.3 Accumulation and growth of deposits

Collection efficiency determines the accumulation and growth process of ash deposition. Collection efficiency contains two parts: impaction efficiency and capture efficiency. The rate of inertial impaction is the product of total mass flux of particles in flow and impaction efficiency represents the fraction of particles within the projected target cross section that strike on the target. Capture efficiency represents the fraction of particles that remain on the target after they impact.³⁵ The impaction efficiency can be derived and predicted by the conditions of flow fields and expressed as a function of particles, gas and tube properties by numerous investigations. The inertial impaction

can be characterized as a function of the particle Stokes Number, which is defined as

$$I_m(Stk) = q_m \eta_m \quad (1-1)$$

$$Stk = \frac{\rho_p d_p^2 U_p}{9 \mu_g d_c} \quad (1-2)$$

where I_m is the rate of inertial impaction, Stk is the Stokes number, η_m is the impaction efficiency, and q_m is the local particle flux. In Eq. 1-2, ρ_p , d_p and U_p represent particle density, diameter and mean velocity, respectively; μ_g and d_c represent gas viscosity and tube diameter, respectively.³⁶

Compared to impaction efficiency, capture efficiency is more difficult to be determined because it concerns the melt condition of adhered ash particles. Figure 1-15 shows a widely accepted model to describe the capture efficiency by Walsh et al.³⁷ At the beginning stage of deposition process, only those particles which arrive at the surface in a sticky condition contribute to deposition. Since the adhesion layer is thin at the initial stage and the temperature of tube surface is low, the adhered sticky particles are solidified to form a dry primary deposition layer. When the primary deposition layer act as thermal insulation material on the surface of tubes, the temperature of ash layer get increased gradually. With the increase of temperature the adhesiveness of ash layer increased, slagging and sintering phenomena are easy to occur. In addition, particles containing alkali metals generate compounds with low melting points in the ash layer can also increase the stickiness of deposits. Next large sized particles which did not deposit in the initial stage start to adhere and the ash layer grows. Meanwhile, accompanied by the ash impaction, vibration and gravity, some parts of ash layer get peeled off.

1.5.4 Different types of forces acting on ash particles

The adhesion forces between ash particles and deposit surfaces and forces among particles can impact the deposition phenomena severely at high temperature and the term adhesive force generally relates to the minimum force needed to separate particles adhering to one another. A useful classification of the adhesive forces is based on the presence or absence of a material bridge in the contact region.³⁸ Figure 1-16 shows the common adhesion mechanisms between particles. Adhesive forces with material bridges (contact forces) mainly contain capillary force and solid bond force, meanwhile adhesive forces without material bridges (non-contact forces) mainly contain electrostatic forces (conductor/non-conductor) and van der Waals force. All these forces were simply ranked by Berbner et al., in order of increasing adhesion: electrostatic forces (non-conductor) < electrostatic forces (conductor) < van der Waals force < capillary force < solid bridge force.³⁸

Van der Waals force and capillary force are more common researched and considered forces in particle adhesion researches. Van der Waals force was proposed by van der Waals in 1873 and developed by Hamaker³⁹ in 1937, it described the distance-dependent interactions between molecules and can be expressed as:

$$F_{vdw} = \frac{H_A d}{24h^2} \quad (1-3)$$

where F_{vdw} is the van der Waals force between particles, H_A is the Hamaker constant, d is the diameter of single particle and h is the distance between particles.

Capillary force is applied in the particle interactions when liquid bridges exist

between particle and wall or among particles. A model developed by Rabinovich⁴⁰ et al., and corrected by Lambert et al was widely used.

In a particle-wall situation, the expression is given by:

$$F_{p/w} = -\frac{4\pi\gamma R \cos \theta}{1 + \frac{H}{d_{p/w}}} - 2\pi\gamma R \sin \alpha \sin(\theta + \alpha) \quad (1-4)$$

$$d_{p/w} = -H + \sqrt{H^2 + V/(\pi R)} \quad (1-5)$$

where R , V , γ , θ , α and H are particle radius, liquid bridge volume, liquid surface tension, contact angle, “embracing angle” and distance between wall and particle, respectively.

In a particle-particle situation, the expression is given by:

$$F_{p/p} = -\frac{2\pi R\gamma \cos \theta}{1 + \left[\frac{H}{2d_{p/p}(H,V)} \right]} - 2\pi\gamma R \sin \alpha \sin(\theta + \alpha) \quad (1-6)$$

$$d_{p/p} = \left(\frac{H}{2}\right) \times \left[-1 + \sqrt{1 + \frac{2V}{\pi R H^2}}\right] \quad (1-7)$$

Figure 1-17 illustrates the particle/wall interaction and particle/particle interaction with liquid bridges.

Solid bridge force describes the constitutive behavior of a finite-sized piece of cementations materials deposited between two particles.⁴¹ Solid bridge types can occur in several models including diffusion of molecules from particle to particle, crystallization of some ingredients, chemical reactions, hardening of binders and solidification of melted components.⁴² The bonds can transmit forces between particles acting at the contact point. Figure 1-18 shows the formation mechanism of solid bond and structure between two particles, meanwhile a simplified equation⁴³ to determine the strength of solid bridges is given by:

$$F = \pi x^2 \sigma_{neck} \quad (1-8)$$

where F is the solid bridge force, x is the radius of bridge neck, σ_{neck} is the stiffness of the neck.

1.5.5 Ash forming elements

The main ash forming elements in coal and biomass combustion fuels are potassium, sodium, calcium, magnesium, aluminum, phosphorus, iron, sulfur and chlorine. Different elements have different effects on the deposition properties at different temperature. Generally, researchers categorize the ash forming elements based on the acid-base property, given by Table 1-1. To predict ash behavior and deposition tendencies at high temperature, some empirical indices and formulas were proposed based on chemical composition,⁴⁴⁻⁴⁶ given by:

$$R_B = (\text{Fe}_2\text{O}_3 + \text{CaO} + \text{MgO} + \text{Na}_2\text{O} + \text{K}_2\text{O}) \quad (1-9)$$

$$R_{B/A} = (\text{Fe}_2\text{O}_3 + \text{CaO} + \text{MgO} + \text{Na}_2\text{O} + \text{K}_2\text{O}) / (\text{SiO}_2 + \text{Al}_2\text{O}_3 + \text{TiO}_2) \quad (1-10)$$

$$S_R = 100\text{SiO}_2 / (\text{SiO}_2 + \text{eq}(\text{Fe}_2\text{O}_3) + \text{CaO} + \text{MgO}) \quad (1-11)$$

$$R_S = R_{B/A} S^d \quad (1-12)$$

$$F_u = R_{B/A} (\text{Na}_2\text{O} + \text{K}_2\text{O}) \quad (1-13)$$

where R_B represents basic constituents, $R_{B/A}$ represents (base to acid) character, S_R represents viscosity index, R_S represents slagging index, S^d represents the fraction of S in dry fuel, F_u represents fouling index.

Except for using chemical compounds related indices or formulas to predict ash deposition tendency, the typical and potential chemical reactions among these elements

during ash formation processes are also key research topics.

(1) Alkali metals

Alkali metals refer to potassium and sodium. They exist as organic materials in the fuels. During the combustion process, alkali metals transform into oxides, chlorides, sulfates and so on. These substances can react to silicon and generate eutectic compounds with low melting points, ash deposition phenomena get worse consequently.

(2) Alkaline-earth metals

Alkaline-earth metals refer to calcium and magnesium in fuels. Compared to alkali metals, the deposition issues caused by calcium and magnesium are weakened.⁴⁷ Calcium and magnesium can react to silicon and generate eutectic phases just like alkali metals in some cases, the ash deposition gets promoted consequently. However in some other cases, the melting points of ashes show a tendency of decreasing first and then increasing with the increase of alkaline-earth metal contents.⁴⁸⁻⁴⁹

(3) Silicon

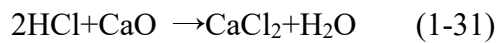
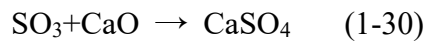
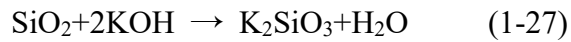
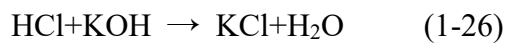
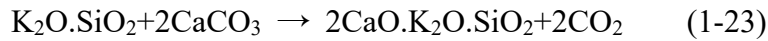
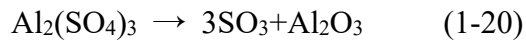
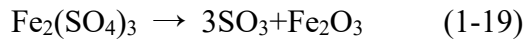
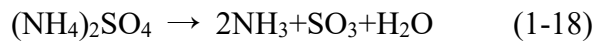
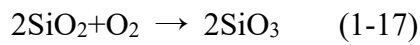
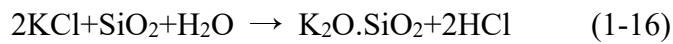
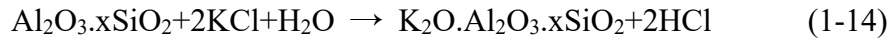
Silicon is the main inorganic element in ashes. The silicate forms would not relate to ash deposition since the high melting temperatures. However, when alkali metals exist in ashes, silicon is easy to react to alkali metals and generate eutectic materials with low melting points, which could result in serious depositions.⁵⁰⁻⁵¹

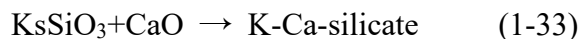
(4) Aluminum

Aluminum is also one of the main elements in ashes. In the situation of high aluminum contents in ashes, aluminum prefers to react to silicon and generate aluminosilicate with high melting temperatures, which contributes to decreasing

ash deposition issues.

Some main chemical reactions during ash formation process are summarized and listed below:⁵²⁻⁵³





1.5.6 Ash generated from biomass combustion

Compared with other fossil fuels, such as coal, bio-based fuels including sewage sludge usually contain higher content of alkali metals, phosphate and chloride, eutectic phase with relatively low melting points and corrosive materials are easy to generate in their combustion ashes, therefore biomass ashes usually have stronger potential to relate to deposition issues at high temperature compared with coal ashes. In addition, since the chemical composition of biomass varies a lot, it is difficult to predict the occurrence of deposition problems.^{50-51, 54-56} If ash-related problems caused from biomass combustion can be suppressed, further utilization of biomass fuels would become possible. Table 1-2 shows the general chemical composition of some typical fuel samples.⁵⁷⁻⁵⁸

Different elements in the biomass ash have different effect on the ash particle adhere phenomena. Alkali metals including sodium and potassium are originally abundantly contained in biomass as organic components, during the combustion process the decomposition and volatilization of fine alkali particles react to other elements and generate compounds with low melting points. These alkali fine particles are easy adhere and accumulate on the heat transfer tubes and inner surface of boilers, decreasing heat transfer efficiency and causing blockage. Sulfur can react to calcium and generate CaSO_4 , which acts as a binder between particles and tube surface. Silicon in the ashes are easy to react to alkali metals and generate eutectic materials, the melting

points of eutectic materials are relatively lower and the eutectic phases are easy to form liquid or slag phases, which promote the adhesion and growth of ash layers. Phosphorus can influence the adhesion temperature by changing the distribution of alkali metals in fly ashes. In phosphorus-poor ashes, potassium may exist as KCl and leads to adhesion phenomenon. However in phosphorus-rich ashes, potassium may be captured by phosphorus and form K-Ca/Mg-P compounds with high melting temperature, which can suppress the deposition potential of fly ashes. In addition, in phosphorous-rich ashes, formation of KPO_3 may promote adhesion troubles.^{50, 59-60}

As described before, it has been studied that each element has various effects on ash adhesion. The chemical compositions of combustion ashes can be used to predict the ash deposition potential in some extent by come indexes such as alkali ratio, slag viscosity index, fouling index and so on. However, since the compositions of biomass are complex and diverse, the complexity could lead to adhesion by more complicated mechanisms which still require further research.⁶¹

1.5.7 Control of deposition phenomena by combustion additives

Biomass with high alkali or chlorine contents tends to cause ash deposition problems during combustions. Technologies have be studied to suppress this phenomena including using additives during combustion, co-firing with other fuels and so on. The main target of these methods is increasing the melting points of ash particles in the boiler, thus the deposition problems could be weakened or suppressed.

Using additives in the combustion process is an important research area in

deposition control subject. The additives can change the inorganic components during the combustion process to a more stable form in chemical and physical routes, the melting points of ash particles get increased and the adhesive force among particles can be suppressed consequently. The main additives and mechanisms are listed in Table 1-3.⁵² Now there are mainly 4 categories of additives used: Al-Si based additives, S-based additives, Ca-based additives and P-rich additives. Different additives influence the adhesiveness of ash through different routes. Al-Si based additives mainly suppress the adhesion force of ash particles by capturing K in KCl and generate compounds with higher stability (such as KAlSi_3O_8). The main effect of S-based additives is converting KCl to K_2SO_4 in ashes. Compared with KCl (melting point: 770°C), the melting point of K_2SO_4 is higher (about 840°C), thus the deposition problems can be suppressed. Meanwhile, as a result of sulphation of KCl, the Cl will be released with gas flow, then Cl-related corrosion can be reduced. The Ca-based additive can release Ca into potassium silicate melts and force K release to gas phase, Ca react with Si and form calcium silicates that have higher melting points consequently. In P-rich and K-rich biomass fuels, Ca-based additives can increase the melting temperature of phosphate. For biomass fuels containing high contents of K and Si and a certain amount of Ca, the introduction of P-rich additives can lead to K react with P and further react with Ca. In this way, content of potassium-silicates with low melting points is reduced, K-Ca-P compounds with higher melting temperatures are promoted to generation.⁵²



Screen tubes BEFORE operation



Screen tubes AFTER approx. 14 days of operation

Figure 1-7 Example of deposition problems.¹²

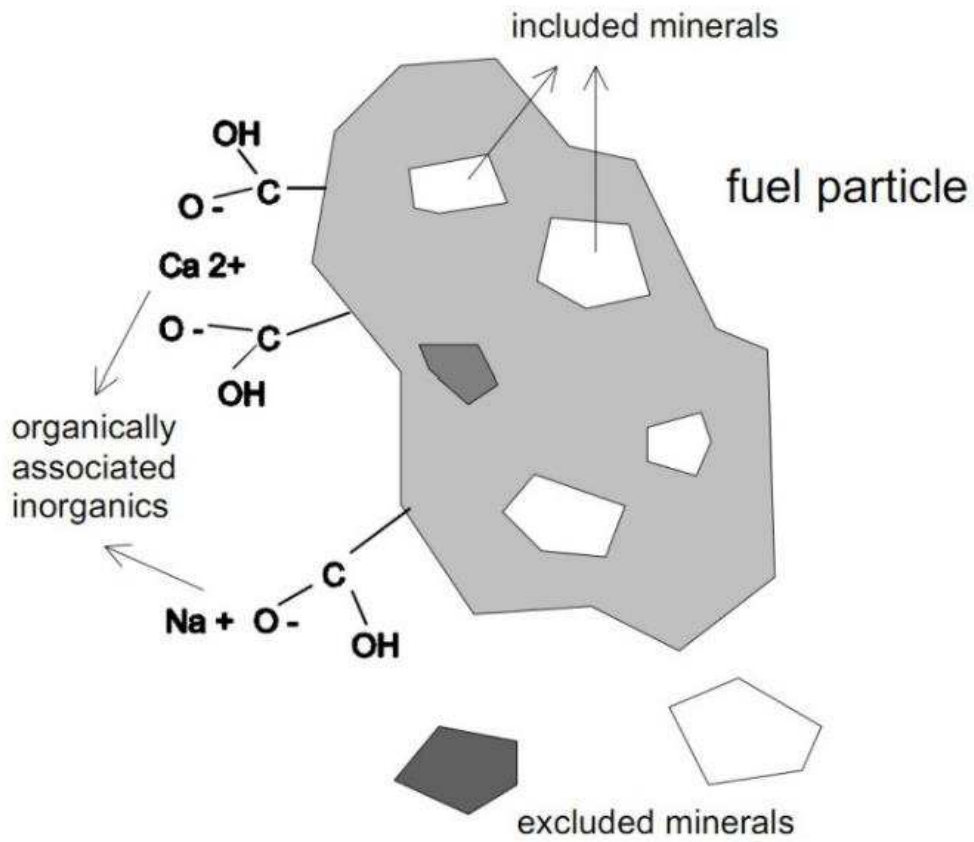


Figure 1.8 A fuel particle containing ash-forming constituents.¹³

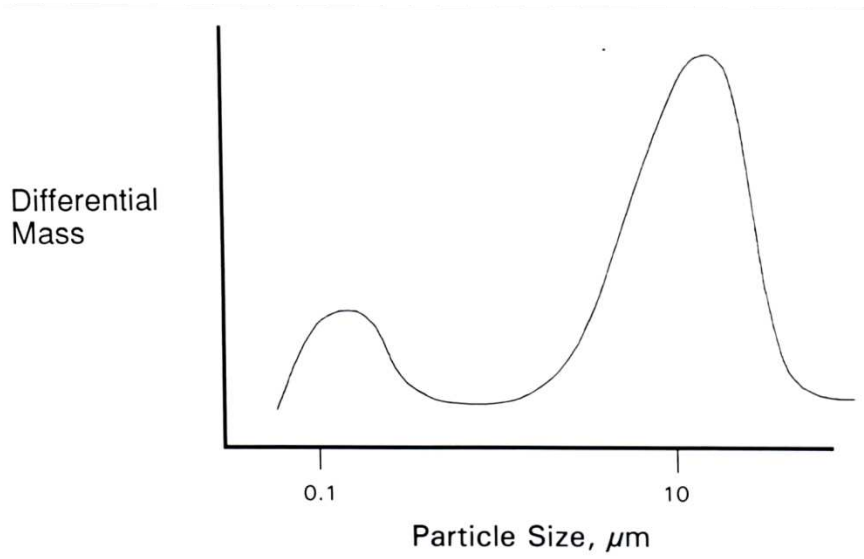


Figure 1-9 Size distribution of combustion fly ashes.²⁰

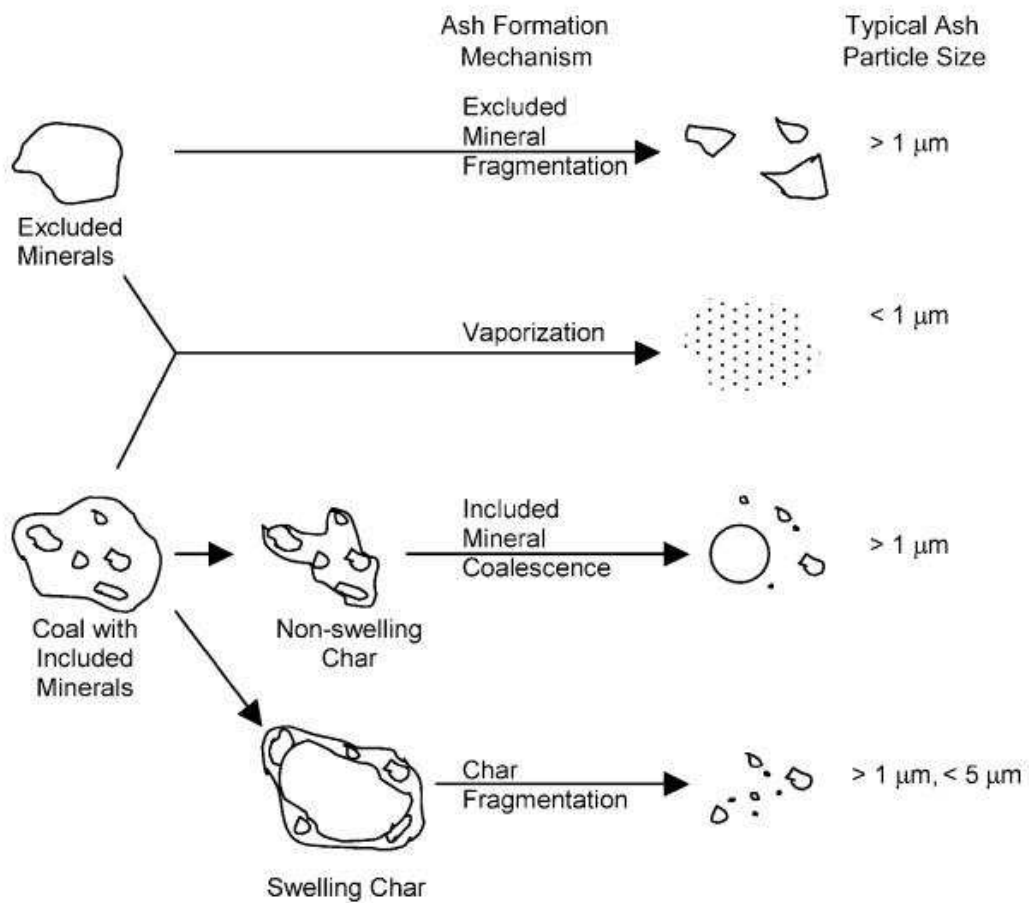


Figure 1-10 Schematic of ash formation mechanisms during pulverized coal

combustion.¹⁷

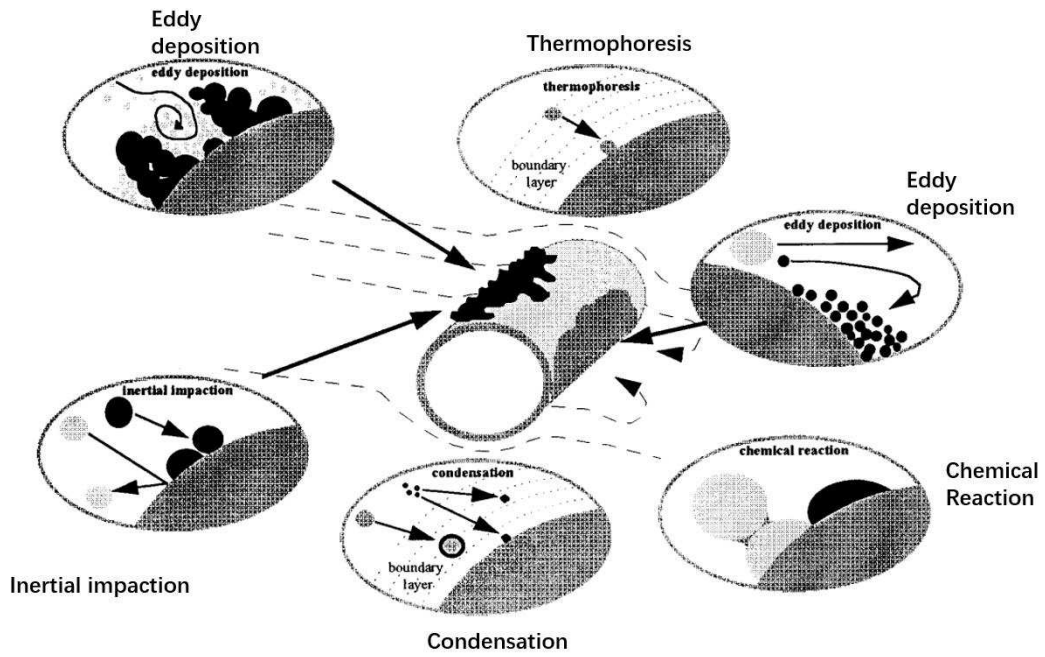


Figure 1-11 Mechanisms controlling the deposition and maturation of ash deposits.²⁵

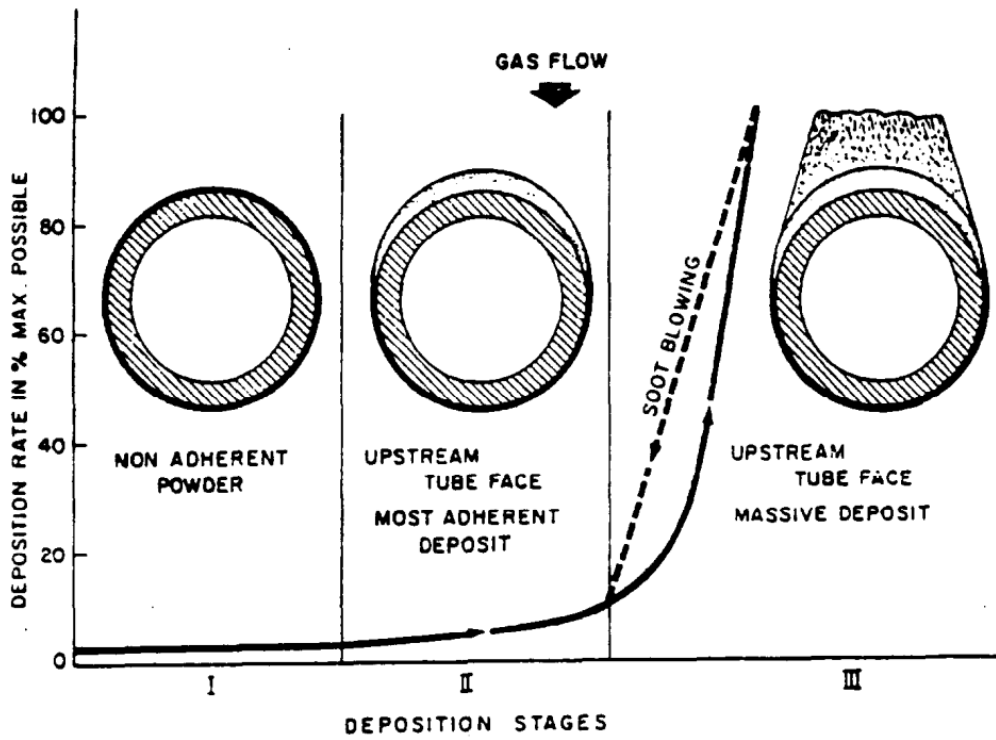
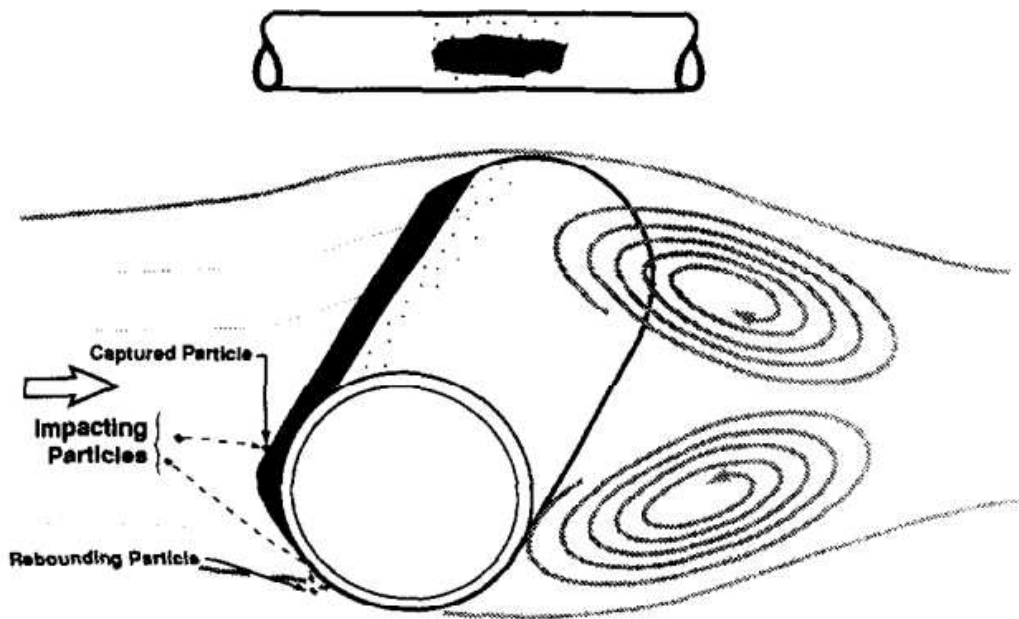


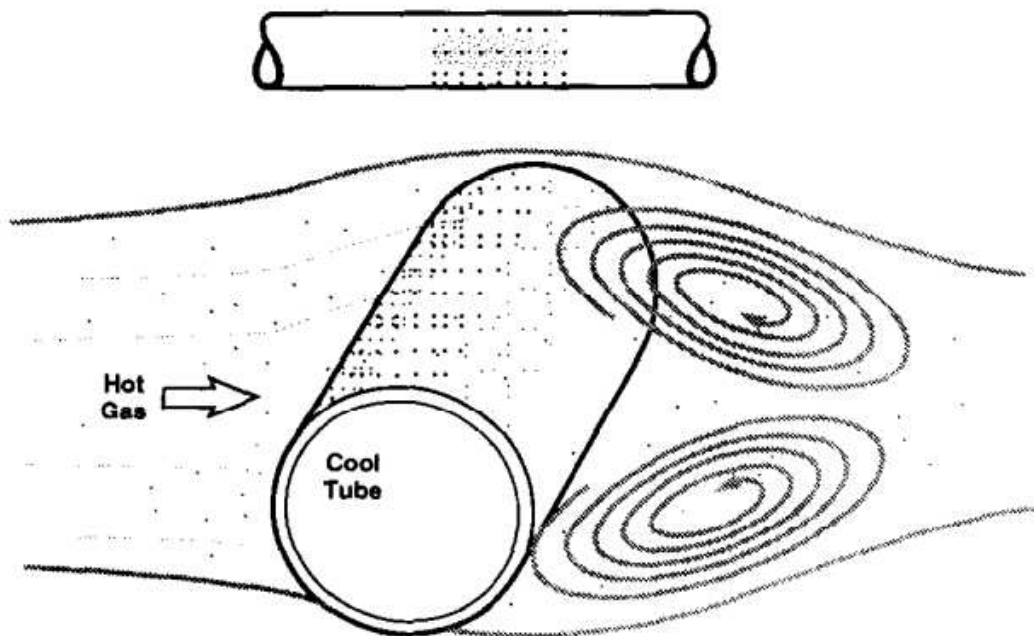
Figure 1-12 Various stages of ash deposition including thermophoresis, condensation and inertial impacts.³³

Particle Impaction

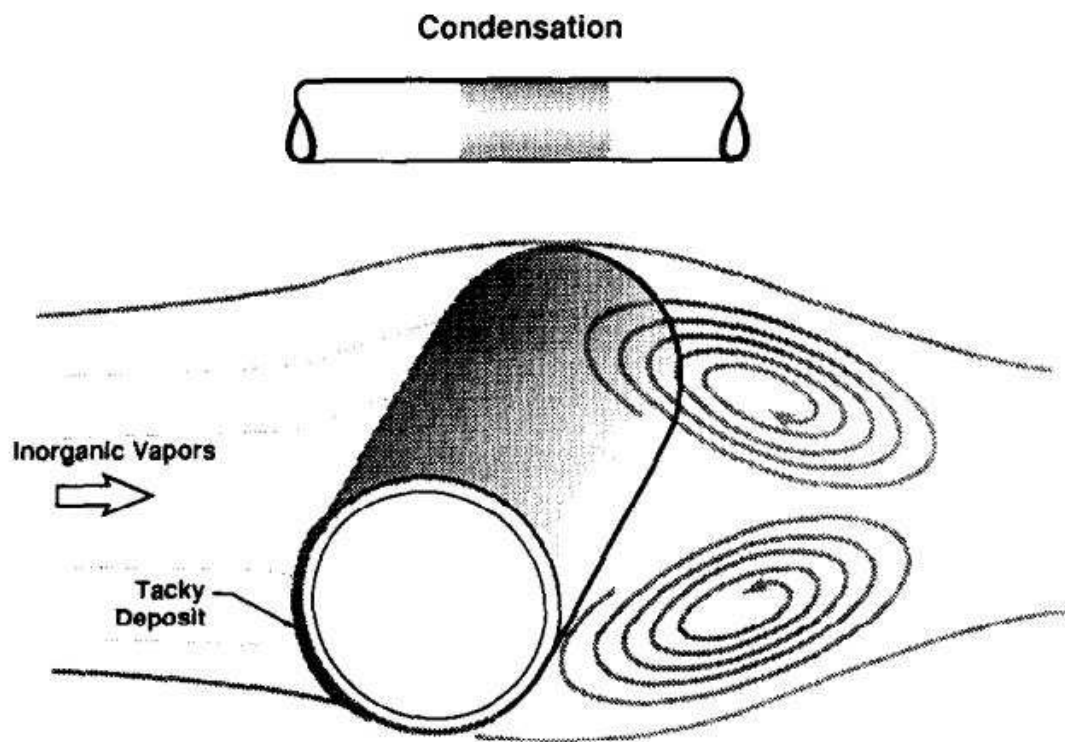


(a) Inertial impaction

Thermophoresis



(b) Thermophoresis



(c) Condensation

Figure 1-13 Schematic illustrations of different mechanism of ash deposition.³⁴

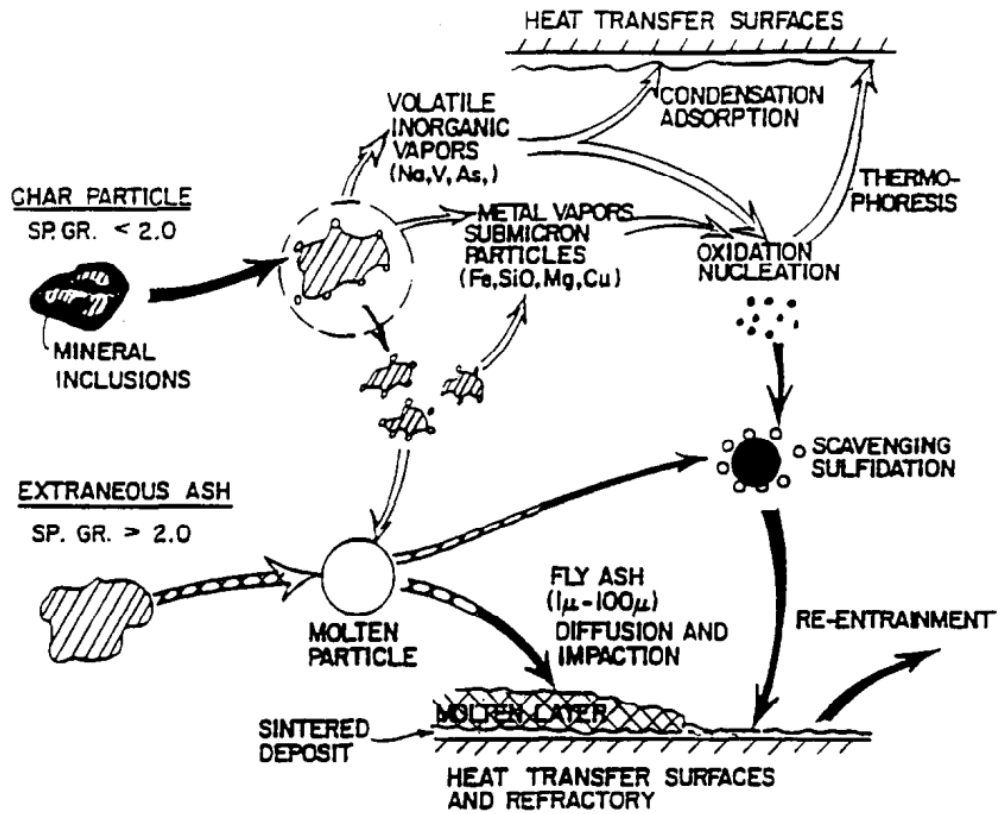


Figure 1-14 Fate of mineral matter in coal during combustion.³³

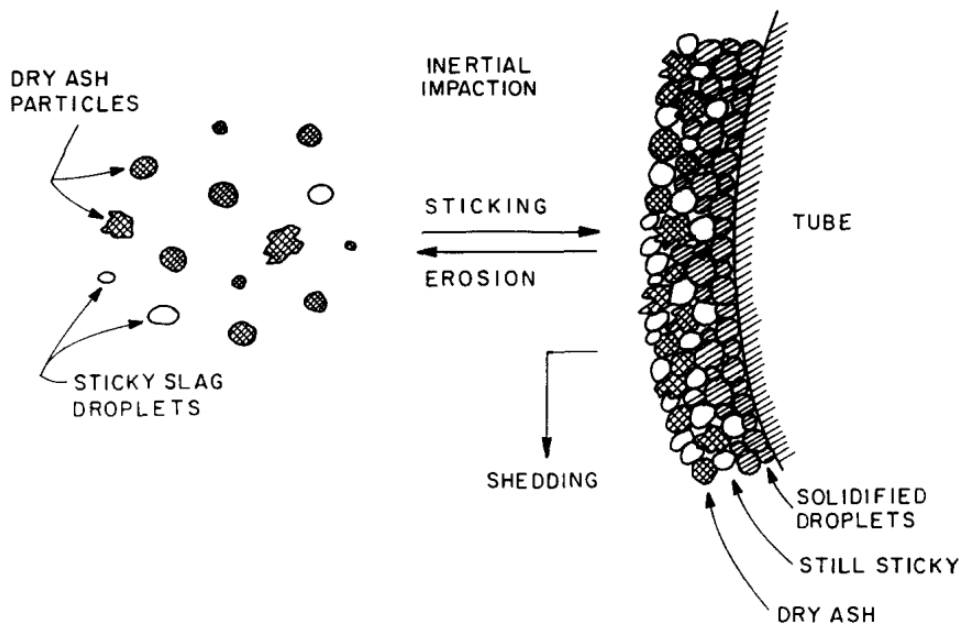
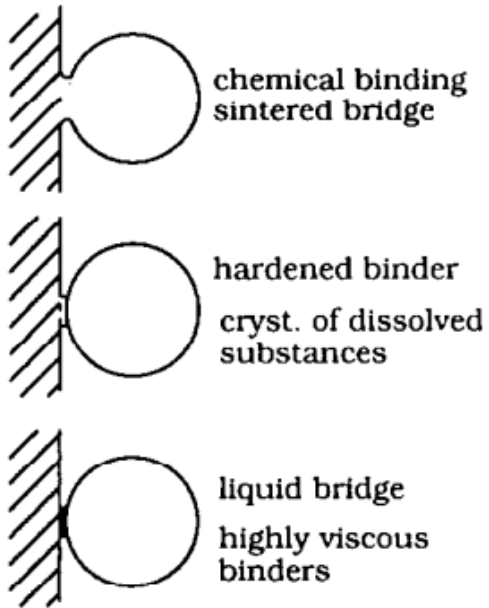


Figure 1-15 Processes contributing to ash deposit growth and removal.³⁷

with material bridges



without material bridges

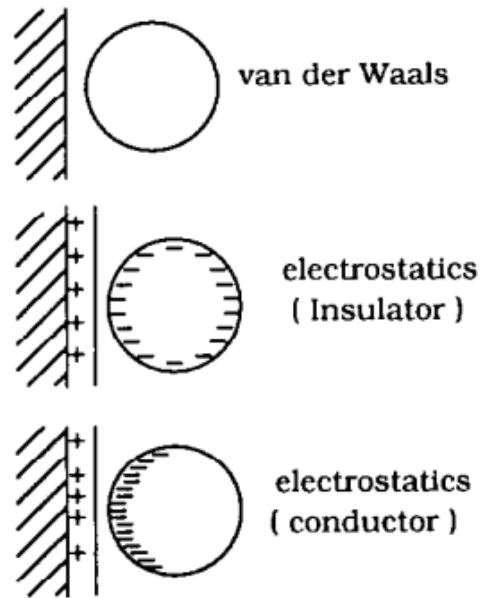
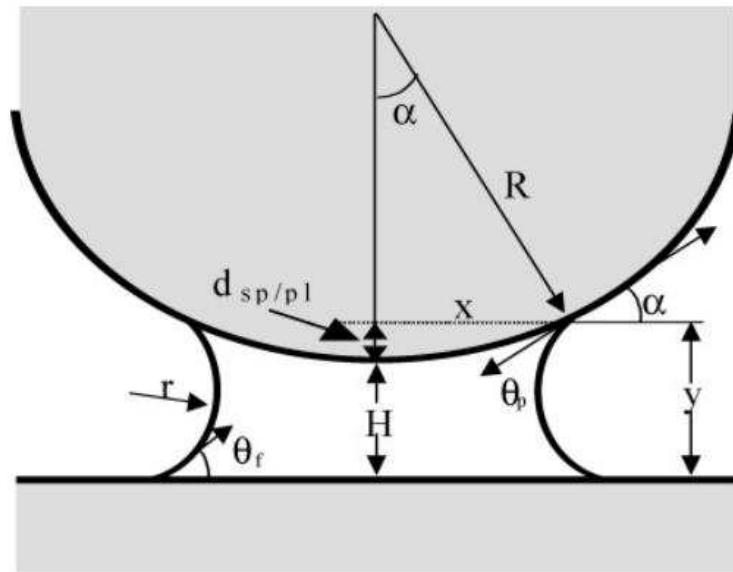
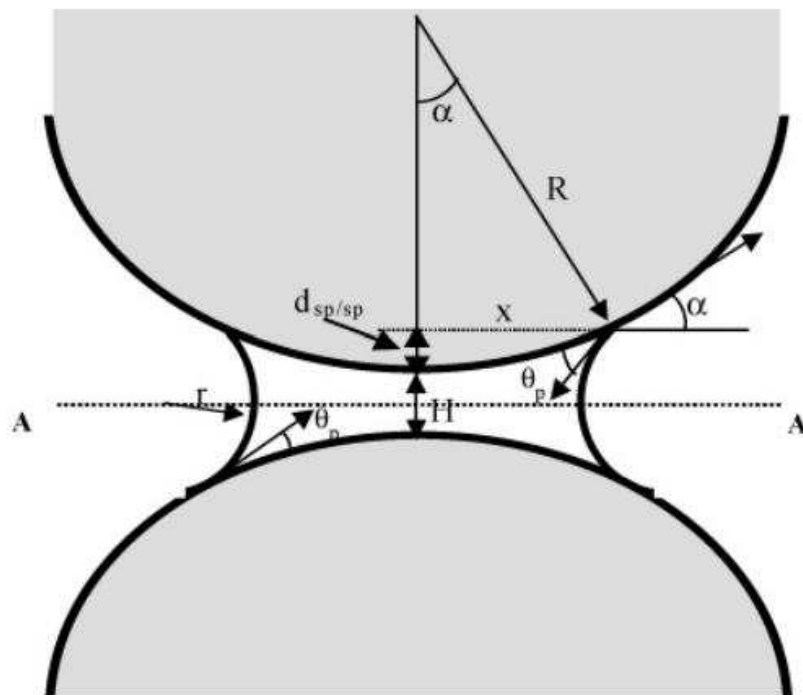


Figure 1-16 Summary of the most common adhesion mechanisms.³⁸



(a) particle-wall



(b) particle-particle

Figure 1-17. Geometry of the particle-wall and particle-particle interaction with a liquid bridge.⁴⁰

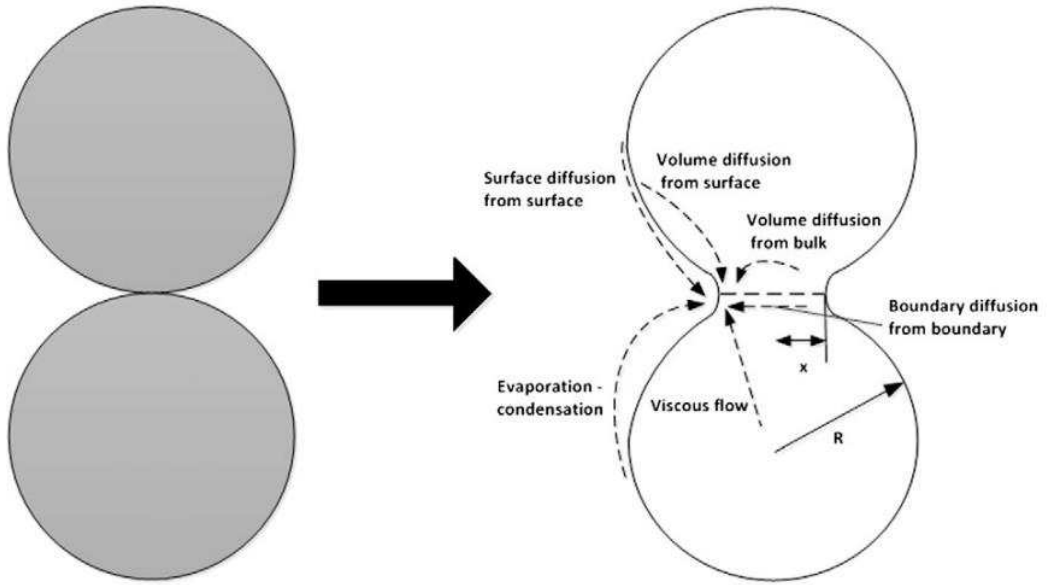


Figure 1-18. Schematic of solid bond.⁴³

Table 1-1. Compounds contain ash relating elements.⁵³

Basic compounds	Acidic compounds
KOH(l,g)(K₂O)	P ₂ O ₅ (g)
NaOH(l,g)(Na₂O)	SO ₂ (g)/SO ₃ (g)
CaO(s)	SiO ₂ (s)
MgO(s)	HCl(g)(Cl ₂)
H₂O(g)	CO ₂ (g)
	H ₂ O(g)

Table 1-2 Chemical compositions (wt%) of some typical fuel samples.⁵⁷⁻⁵⁸

	SiO ₂	Al ₂ O ₃	TiO ₂	Fe ₂ O ₃	CaO	MgO	Na ₂ O	K ₂ O	SO ₃	P ₂ O ₅	Cl
Coal	42.0	20.0	1.2	17.0	5.5	2.1	1.4	5.8	5.8	-	-
Oak	49.0	9.5	-	8.5	17.5	1.1	0.5	9.5	2.6	1.8	0.8
Straw	48.0	3.5	-	0.5	3.7	1.8	14.5	20.0	1.9	3.5	3.6
Sludge	25.1	9.8	-	13.81	23.53	14.17	0.81	0.62	-	8.35	-

Table 1-3 Reviews of additives reported in literatures.⁵²

Suspected effects	Additives	Main components
Chemical adsorption and interaction	kaolin, halloysite, cat litter, enathlite, clay minerals, clay sludge illite detergent zeolites ammonia sulfate, aluminum sulfate, iron sulfate, ammonia phosphate, phosphoric acid DCP limestone, lime, marble sludge sewage sludge, paper sludge, peat ash, coal fly ash dolomite, bauxite, quartz, titanium oxide	$Al_2Si_2O_5(OH)_4$, $Al_4(OH)_8/Si_4O_{10} \cdot 10H_2O$ Mixture of aluminum silicates (i.e. $Al_2Si_4O_{10}$, $Al_2Si_4O_{10}$, silica and alumina one explain $KAl_2Si_2AlO_{10}(OH)_2$ $Na_x [(AlO_2)_x (SiO_2)_y] \cdot zH_2O$ $(NH_4)_2SO_4$, $Al_2(SO_4)_3$, $Fe_2(SO_4)_3$ $(NH_4)_3PO_4$, H_3PO_4 $Ca(H_2PO_4)_2 \cdot H_2O$ $CaCO_3$, CaO $Al_2Si_2O_7$ $CaMg(CO_3)_2$, SiO_2 , Al_2O_3 , TiO_2
Physical adsorption	kaolin, zeolite, halloysite clay minerals clay sludge, sewage sludge, paper sludge lime, limestone, dolomite, calcined dolomite bauxite, gibbsite	$Al_2O_2 \cdot (SiO_2)_2 \cdot (H_2O)_2$, $Al_2Si_2O_5(OH)_4$, aluminum silicates with different Al/Si ratios (i.e. $Al_2Si_4O_{10}$, $Al_2Si_4O_{10}$) Mixture of aluminum silicates (i.e. $Al_2Si_4O_{10}$, $Al_2Si_4O_{10}$), detergent zeolites $CaCO_3$, CaO , $CaMg(CO_3)_2$, $CaO \cdot MgO$ Al_2O_3 , $Al(OH)_3$
Dilution effect and inert elements enrichment	bauxite, lime, limestone, silicon oxide, marble sludge,	Al_2O_3 , $CaCO_3$, CaO SiO_2 , $CaCO_3$
Restraining and powdering effects	lime, limestone	$CaCO_3$, CaO

1.6 Purpose of this study and structure of this thesis

Industrial combustion is closely bound up to human life. Fossil fuels and biomass are the most important source that meet the energy demands of social development and individual usage. Combustion of fuels in incinerator is one of the most important and common method to generate electricity. In addition to that, combustion is also an important method to dispose the domestic wastes generated in daily life. However whether in the combustion of fossil or biomass fuels to generate powers or burning solid wastes as a disposal method in incinerator, the deposition problems are always accompanied. During the combustion process the generated fly ash can adhere to the surfaces of both the incinerator and dust filter and then accumulate over time. Since this grown layer can potentially block the gas flow and damage the filter, thus preventing stable and long-term operation of incineration plants, fly ash adhesion must be monitored carefully and suppressed as much as possible. Especially for some biomass wastes such as sewage sludge, their combustion ashes often contain higher contents of alkali metals, chlorine and phosphorous which lead to the ash melt at relatively lower temperatures, resulting in serious deposition problem. Besides, since the chemical compositions of bio-based fuels and wastes are various, it is difficult to predict the deposition phenomena if without a better understanding of ash adhesion mechanisms. To make sure the normal and efficient operation of plants, it is necessary to fully elucidate the effects of different chemical elements on deposition phenomena and the corresponding mechanisms.

In Chapter 2, the author firstly used different fly ash samples to demonstrate the

cause of different adhesion potentials by the merger of experimental and theoretical approaches. The tensile strength of ash powder beds provided a benchmark for the adhesive properties, which were further studied by thermodynamic calculations. Experimental and theoretical results suggest that the use of alumina nanoparticles is a promising approach to suppress the adhesion of fly ash containing a relatively high concentration of phosphorus components.

In Chapter 3, the research direction is moved from real ashes to model ashes to appeal the effect of specific elements on ash deposition phenomena. Since ash particles included various main and trace elements and chemical compounds, it is impossible to remove certain elements from real combustion ash particles to discuss the effect of target element on the ash adhesion phenomena at high temperature. In order to analyze the effect of certain element on ash adhesion behavior, the preparation method of model ash particles only contained target elements were developed by using pure nano-sized particles and chemical compounds. Firstly, the author focused on main 7 elements, Si, Al, Ca, Mg, Na, K and P in real sewage sludge ash, and synthesized model ashes with almost same chemical compounds of real combustion ash. The synthetic ashes showed similar adhesion property as the real ashes at high temperature condition. The adhesion property of each ash particles was characterized by tensile strength of ash powder bed, which was developed in the previous work of author's group. Secondly, in order to discuss the effect of Ca, Mg and Al on adhesion behavior, 2 kinds of model ash with only included 5 elements, Si, Al, Na, K and P were prepared and characterized adhesion behavior at high temperature. In this model ash, the amount of Ca and Mg was replaced

with Al and the other elements were fixed to the same concentration with 7 element ash. Since the tensile strength of 5 elements model ash was much larger than that of 7 elements model ash, Ca and Mg were important to stabilize phosphorus-rich sewage sludge combustion ashes at high temperature.

In Chapter 4, a new measurement to determine the adhesion force between a fine spherical coal combustion ash particle and a polished flat substrate at high temperature is focused. By controlling the temperature conditions, contact time and compression force on the ash particle prepared from pure silica with alkali metals, author found that only temperature and compression force can influence the adhesion force of between one particle to a flat. Then coal combustion ashes with CaO addition are measured to figure out the effect of different contents of CaO addition on the particle adhesion force.

Chapter 5 mainly summarize the conclusions of this study.

Therefore in Chapter 2, the main research subject about sewage ash deposition phenomena was introduced. Combining experimental results including tensile strength measurements with thermal equilibrium calculation results, it was discussed that partially generation of slag or liquid phases among particles is the main mechanism relating to the high adhesiveness of ashes. Consequently, the main method to suppress the adhesiveness is to reduce the generation of slag phase by increasing melting temperature using physical or chemical routes. In Chapter 2 and 3, the effects of different main elements in ashes on ash adhesion at elevated temperature were discussed. Chapter 2 mainly focused on real ashes while methods of synthesizing model ashes were mainly applied in Chapter 3. In these two chapters, the basic mechanisms

of ash adhesion and deposition phenomena were researched and the roles of seven main elements (Na, K, Al, Si, P, Mg, Ca) were discussed. Then in Chapter 4, the object of research expanded to coal ash samples. New evaluation methods of ash adhesiveness were proposed and the research scale narrowed down from ash bulk to single ash particle. Based on the results in Chapter 2 and 3, simple structured model ash samples with alkali-silicon eutectic compounds were prepared to pre-research the influence factors of adhesion force between single particle to a metal flat. Since Ca is always treated as an additive in coal combustion in industrial scale, based on the researched effect of Ca in sewage sludge ashes in Chapter 3, coal samples with different coal Ca contents were analyzed in Chapter 4 also.

A simplified structure of this thesis are described in Figure 1-19.

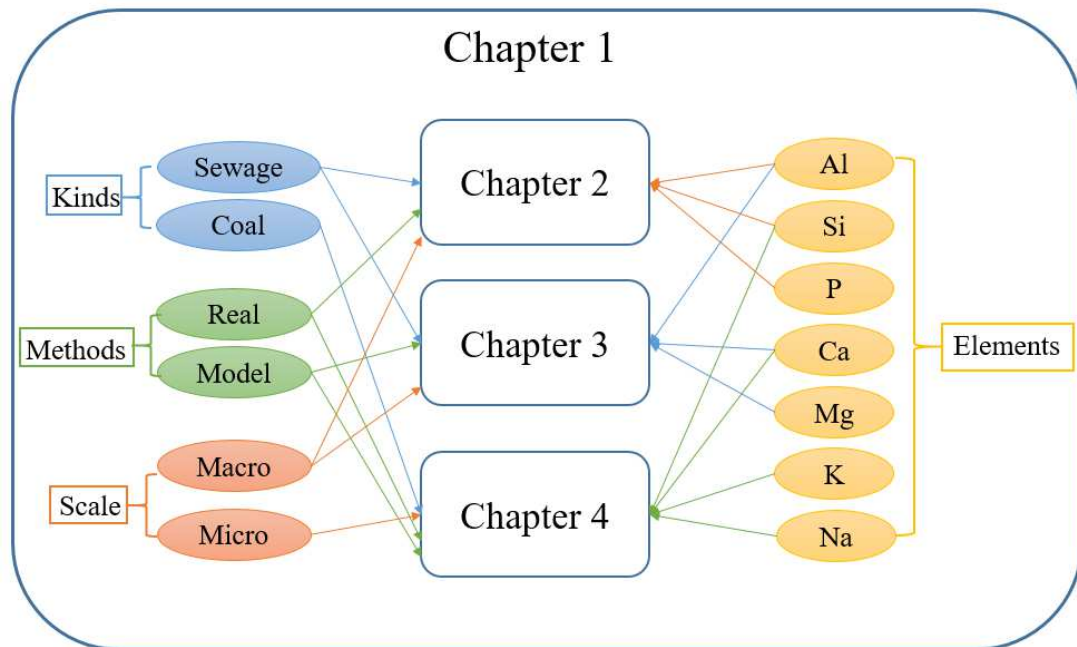


Figure 1-19. A brief structure of this thesis.

1.7 References

1. International Energy Agency, Key world energy statistics 2019.
2. U.S. Energy Information Administration, <https://www.eia.gov/beta/international/analysis.php?iso=JPN>.
3. Ministry of Economy, Trade and Industry, Japan's Energy 2018.
4. WMO Greenhouse Gas Bulletin, The State of Greenhouse Gases in the Atmosphere Based on Global Observations through 2011.
5. Werther, J.; Ogada, T., Sewage sludge combustion. *Progress in Energy and Combustion Science* **1999**, *25* (1), 55-116.
6. Manara, P.; Zabaniotou, A., Towards sewage sludge based biofuels via thermochemical conversion—a review. *Renewable and Sustainable Energy Reviews* **2012**, *16* (5), 2566-2582.
7. Kijo-Kleczkowska, A.; Środa, K.; Kosowska-Golachowska, M.; Musiał, T.; Wolski, K., Mechanisms and kinetics of granulated sewage sludge combustion. *Waste Management* **2015**, *46*, 459-471.
8. Li, W.; Li, W.; Liu, H.; Yu, Z., Influence of sewage sludge on the slurryability of coal–water slurry. *Fuel* **2009**, *88* (11), 2241-2246.
9. Fytili, D.; Zabaniotou, A., Utilization of sewage sludge in EU application of old and new methods—a review. *Renewable and sustainable energy reviews* **2008**, *12* (1), 116-140.
10. Werle, S.; Wilk, R. K., A review of methods for the thermal utilization of sewage sludge: The Polish perspective. *Renewable Energy* **2010**, *35* (9), 1914-1919.
11. Khiari, B.; Marias, F.; Vaxelaire, J.; Zagrouba, F., Incineration of a small particle of wet sewage sludge: A numerical comparison between two states of the surrounding atmosphere. *Journal of Hazard Materials* **2007**, *147* (3), 871-882.
12. Tobiasen, L.; Skytte, R.; Pedersen, L. S.; Pedersen, S. T.; Lindberg, M. A., Deposit characteristic after injection of additives to a Danish straw-fired suspension boiler. *Fuel Processing Technology* **2007**, *88* (11-12), 1108-1117.
13. Lind, T., *Ash formation in circulating fluidised bed combustion of coal and solid biomass*. Technical Research Centre of Finland: 1999.
14. Borman, G. L.; Ragland, K. W., *Combustion engineering*, 1998. McGraw Hill, New York.
15. Quann, R.; Neville, M.; Sarofim, A., A laboratory study of the effect of coal selection on the amount and composition of combustion generated submicron particles. *Combustion Science and Technology* **1990**, *74* (1-6), 245-265.
16. Quann, R.; Sarofim, A. In *Vaporization of refractory oxides during pulverized coal combustion*, Symposium (international) on combustion, Elsevier: 1982; pp 1429-1440.
17. Buhre, B.; Hinkley, J.; Gupta, R.; Nelson, P.; Wall, T., Fine ash formation during combustion of pulverised coal—coal property impacts. *Fuel* **2006**, *85* (2), 185-193.
18. Ninomiya, Y.; Zhang, L.; Sato, A.; Dong, Z., Influence of coal particle size on particulate matter emission and its chemical species produced during coal combustion. *Fuel Processing Technology* **2004**, *85* (8-10), 1065-1088.
19. Dam-Johansen, K.; Glarborg, P.; Frandsen, F.; Østberg, M.; Jensen, A. In *Combustion Chemistry-Activities in the CHEC Research Programme: Separate print from Power Plant Chemical Technology International Conference*, Power Plant Chemical Technology, International Conference, 1996.
20. Smoot, L. D., *Fundamentals of coal combustion for clean and efficient use*. *Coal Science and*

Technology **1993**, 20, 15.

21. McElroy, M.; Carr, R.; Ensor, D.; Markowski, G., Size distribution of fine particles from coal combustion. *Science* **1982**, 215 (4528), 13-19.
22. Linak, W. P.; Miller, C. A.; Seames, W. S.; Wendt, J. O.; Ishinomori, T.; Endo, Y.; Miyamae, S., On trimodal particle size distributions in fly ash from pulverized-coal combustion. *Proceedings of the Combustion Institute* **2002**, 29 (1), 441-447.
23. Jia, Y.; Lighty, J. S., Ash particulate formation from pulverized coal under oxy-fuel combustion conditions. *Environmental Science and Technology* **2012**, 46 (9), 5214-5221.
24. Christensen, K. A.; Stenholm, M.; Livbjerg, H., The formation of submicron aerosol particles, HCl and SO₂ in straw-fired boilers. *Journal of Aerosol Science* **1998**, 29 (4), 421-444.
25. Laursen, K.; Frandsen, F.; Larsen, O. H., Ash deposition trials at three power stations in Denmark. *Energy&Fuels* **1998**, 12 (2), 429-442.
26. Beer, J. M. In *From coal mineral matter properties to fly ash deposition tendencies: A modeling route*, Proceedings of the Engineering Foundation Conference on inorganic transformations and ash deposition during combustion, Palm Coast, 1991; pp 71-94.
27. Rosner, D. E., Total mass deposition rates from "polydispersed" aerosols. *AIChE journal* **1989**, 35 (1), 164-167.
28. Israel, R.; Rosner, D. E., Use of a generalized Stokes number to determine the aerodynamic capture efficiency of non-Stokesian particles from a compressible gas flow. *Aerosol Science and Technology* **1982**, 2 (1), 45-51.
29. Castillo, J. L.; Mackowski, D. W.; Rosner, D. E., Photophoretic modification of the transport of absorbing particles across combustion gas boundary layers. *Progress in Energy and Combustion Science* **1990**, 16 (4), 253-260.
30. Byers, R. L.; Calvert, S., Particle deposition from turbulent streams by means of thermal force. *Industrial & Engineering Chemistry Fundamentals* **1969**, 8 (4), 646-655.
31. Helble, J.; Neville, M.; Sarofim, A. In *Aggregate formation from vaporized ash during pulverized coal combustion*, Symposium (International) on Combustion, Elsevier: 1988; pp 411-417.
32. Castillo, J.; Rosner, D., A nonequilibrium theory of surface deposition from particle-laden, dilute condensable vapor-containing laminar boundary layers. *International Journal of Multiphase Flow* **1988**, 14 (1), 99-120.
33. Bryers, R. W., Fireside slagging, fouling, and high-temperature corrosion of heat-transfer surface due to impurities in steam-raising fuels. *Progress in Energy Combustion Science* **1996**, 22 (1), 29-120.
34. Baxter, L. L.; DeSollar, R. W., A mechanistic description of ash deposition during pulverized coal combustion: predictions compared with observations. *Fuel* **1993**, 72 (10), 1411-1418.
35. Baxter, L. L.; Hencken, K. R.; Harding, N. S. *The dynamic variation of particle capture efficiency during ash deposition in coal-fired combustors*; Sandia National Labs., Livermore, CA (USA); Consolidation Coal Co., Library ...: 1990.
36. Baxter, L. L. *Ash Deposit Formation and Deposit Properties. A Comprehensive Summary of Research Conducted at Sandia's Combustion Research Facility*; Sandia National Labs., Albuquerque, NM (US); Sandia National Labs ...: 2000.
37. Walsh, P. M.; Sayre, A. N.; Loehden, D. O.; Monroe, L. S.; Beér, J. M.; Sarofim, A. F., Deposition of bituminous coal ash on an isolated heat exchanger tube: effects of coal properties on deposit growth. *Progress in Energy and Combustion Science* **1990**, 16 (4), 327-345.
38. Berbner, S.; Löffler, F., Influence of high temperatures on particle adhesion. *Powder Technology*

1994, 78 (3), 273-280.

39. Hamaker, H. C., The London—van der Waals attraction between spherical particles. *Physica* **1937**, 4 (10), 1058-1072.
40. Rabinovich, Y. I.; Esayanur, M. S.; Moudgil, B. M., Capillary forces between two spheres with a fixed volume liquid bridge: theory and experiment. *Langmuir* **2005**, 21 (24), 10992-10997.
41. Shao, Y.; Aoki, N.; Tong, Z.; Zhong, W.; Yu, A.; Kamiya, H., Numerical and experimental study of tensile stresses of biomass combustion ash with temperature variation. *Advanced Powder Technology* **2016**, 27 (1), 215-222.
42. Kaliyan, N.; Morey, R. V., Natural binders and solid bridge type binding mechanisms in briquettes and pellets made from corn stover and switchgrass. *Bioresource Technology* **2010**, 101 (3), 1082-1090.
43. You, C.; Luan, C.; Wang, X., An evaluation of solid bridge force using penetration to measure rheological properties. *Powder technology* **2013**, 239, 175-182.
44. Magdziarz, A.; Wilk, M.; Gajek, M.; Nowak-Woźny, D.; Kopia, A.; Kalembe-Rec, I.; Koziński, J. A., Properties of ash generated during sewage sludge combustion: A multifaceted analysis. *Energy* **2016**, 113, 85-94.
45. Pronobis, M., Evaluation of the influence of biomass co-combustion on boiler furnace slagging by means of fusibility correlations. *Biomass and Bioenergy* **2005**, 28 (4), 375-383.
46. Yang, X.; Ingham, D.; Ma, L.; Srinivasan, N.; Pourkashanian, M., Ash deposition propensity of coals/blends combustion in boilers: a modeling analysis based on multi-slagging routes. *Proceedings of the Combustion Institute* **2017**, 36 (3), 3341-3350.
47. Niu, Y.; Tan, H., Ash-related issues during biomass combustion: Alkali-induced slagging, silicate melt-induced slagging (ash fusion), agglomeration, corrosion, ash utilization, and related countermeasures. *Progress in Energy and Combustion Science* **2016**, 52, 1-61.
48. Song, W. J.; Tang, L. H.; Zhu, X. D.; Wu, Y. Q.; Zhu, Z. B.; Koyama, S., Effect of coal ash composition on ash fusion temperatures. *Energy&Fuels* **2009**, 24 (1), 182-189.
49. Liu, B.; He, Q.; Jiang, Z.; Xu, R.; Hu, B., Relationship between coal ash composition and ash fusion temperatures. *Fuel* **2013**, 105, 293-300.
50. Miles, T. R.; Miles Jr, T. R.; Baxter, L. L.; Bryers, R. W.; Jenkins, B. M.; Oden, L. L., Boiler deposits from firing biomass fuels. *Biomass and Bioenergy* **1996**, 10 (2-3), 125-138.
51. Kamiya, H.; Kimura, A.; Tsukada, M.; Naito, M., Analysis of the high-temperature cohesion behavior of ash particles using pure silica powders coated with alkali metals. *Energy&Fuels* **2002**, 16 (2), 457-461.
52. Wang, L.; Hustad, J. E.; Skreiberg, Ø.; Skjevraak, G.; Grønli, M., A critical review on additives to reduce ash related operation problems in biomass combustion applications. *Energy Procedia* **2012**, 20, 20-29.
53. Bostrom, D.; Skoglund, N.; Grimm, A.; Boman, C.; Ohman, M.; Brostrom, M.; Backman, R., Ash transformation chemistry during combustion of biomass. *Energy&Fuels* **2011**, 26 (1), 85-93.
54. Shao, Y.; Wang, J.; Preto, F.; Zhu, J.; Xu, C., Ash deposition in biomass combustion or co-firing for power/heat generation. *Energies* **2012**, 5 (12), 5171-5189.
55. Hupa, M., Ash-related issues in fluidized-bed combustion of biomasses: recent research highlights. *Energy&Fuels* **2011**, 26 (1), 4-14.
56. Baxter, L. L.; Miles, T. R.; Miles Jr, T. R.; Jenkins, B. M.; Milne, T.; Dayton, D.; Bryers, R. W.; Oden, L. L., The behavior of inorganic material in biomass-fired power boilers: field and laboratory experiences. *Fuel Process Technology* **1998**, 54 (1-3), 47-78.

57. Demirbaş, A., Sustainable cofiring of biomass with coal. *Energy Conversion and Management* **2003**, *44* (9), 1465-1479.
58. Magdziarz, A.; Wilk, M., Thermal characteristics of the combustion process of biomass and sewage sludge. *Journal of Thermal Anal Calorimetry* **2013**, *114* (2), 519-529.
59. Grimm, A.; Skoglund, N.; Bostrom, D.; Boman, C.; Öhman, M., Influence of phosphorus on alkali distribution during combustion of logging residues and wheat straw in a bench-scale fluidized bed. *Energy&Fuels* **2012**, *26* (5), 3012-3023.
60. Lindström, E.; Sandström, M.; Boström, D.; Öhman, M., Slagging characteristics during combustion of cereal grains rich in phosphorus. *Energy&Fuels* **2007**, *21* (2), 710-717.
61. Rizvi, T.; Xing, P.; Pourkashanian, M.; Darvell, L.; Jones, J.; Nimmo, W., Prediction of biomass ash fusion behaviour by the use of detailed characterisation methods coupled with thermodynamic analysis. *Fuel* **2015**, *141*, 275-284.

CHAPTER 2

**Analysis and adhesion control of sewage sludge combustion
ashes at high temperature**

CHAPTER2

Analysis and adhesion control of sewage sludge combustion ashes at high temperature

2.1 Introduction

Sewage sludge, which is the waste produced from water treatment, is burned in an incinerator to reduce sludge volume.¹⁻³ Recently, a high-pressure and -temperature flue gas cleaning system containing a ceramic filter⁴⁻⁵ has been used for energy recycling after ash particle separation in a pressurized fluidized bed combustor (PFBC) system for sewage sludge. However, during the gas scrubbing process, achieving efficient dust layer detachment by reverse pulse jet flow on the ceramic filter is difficult.⁶⁻⁷ The pressure was decreased by dust layer accumulation, until the ceramic filter fractured due to dust layer bridge formation between filters.⁸⁻⁹ Thus, in energy recycling systems using heat exchangers and super heaters, ash deposition and growth phenomena on the surface of the heat exchanger reduced energy recycle efficiency and hindered stable operation of combustion plants. In fluidized bed combustion, de-fluidization of bed materials was promoted by formation of agglomerates and clinkers.¹⁰⁻¹³ These issues were promoted by an increase in ash particle stickiness and adhesion at high temperatures.¹⁴⁻¹⁶ Because the combustion ash from bio-based fuels, including sewage sludge, contains greater amounts of alkali metals, phosphorus, and chlorine compared with other fuels, such as coal,^{10, 17} a eutectics phase with relatively low melting point is generated on the surface of ash¹⁸⁻¹⁹ and melts easily at high temperatures. This slag liquid phase generated between ash particles promotes adhesion and the growth of an ash layer.

To characterize the ash adhesion behavior of pulverized and pressurized fluidized bed combustion of bituminous coal at temperatures below 1000°C, a split-cell tensile strength testing system was designed and prepared on an ash powder bed.²⁰ The tensile strength of the powder beds of pulverized coal combustion ash increased significantly at about 800°C. Ash particle deformation from biomass combustion was observed microscopically by field emission scanning electron microscopy (FE-SEM) using a heating chamber at temperatures above 500°C.²¹ Since biomass combustion ash has relatively high alkali metal concentration compared with bituminous coal combustion ash, the temperature at which a significant increase in ash powder bed strength begins was lower than that of coal combustion ash.

Since phosphorus content in sewage sludge combustion ash generally is much greater than that in other biomass and coal combustion ash,^{17,22} the effect of phosphorus content on adhesion behavior of ash particles at high temperatures has been investigated for its influence on the stable operation of sewage sludge combustion plants. However, the mechanism of the effect of phosphate on adhesion behavior based on a quantitative experimental approach and theoretical analysis has not been reported. Several types of additive have been used for control of combustion ash adhesion from bio-based fuels, including sewage sludge, to promote the stable operation of energy-saving systems using ceramic filters.^{10, 13, 23-27} However, since the mechanism of action for the additives have not been determined, the only approach to selecting the more effective additive is by trial and error; therefore, theoretical design concepts to control ash behavior have not been developed.

In the present study, four samples of fly ash particles were collected from sewage sludge combustion commercial plants. Two of the samples were collected during stable operation from two different plants, and the other two samples were collected during

ash adhesion and ash layer growth problem periods from two different plants. The samples underwent particle size and chemical composition analyses, followed by measurement of the tensile strength of each ash powder bed at temperatures from 400 to 800°C using a split-cell type tensile strength tester. To investigate the mechanism of ash adhesion, thermodynamic equilibrium calculations were obtained for liquid and slag phase formation. Based on the calculation results, an additive was selected to prevent the formation of eutectic phases having low melting points. In addition, the effect of the additive on tensile strength of the ash layer at high temperatures was examined.

2.2 Experimental and analysis

2.2.1 Ash samples and characterization

Four fly ash samples from sewage sludge combustion were collected from dust collectors at different fluidized bed incineration plants. Two samples were collected during stable plant operation (S-1 and S-2) and the other two samples were collected during dust ash deposition and growth trouble periods (T-1 and T-2). Each ash sample was collected using a bag filter placed after the cyclone. Particle size distribution and chemical composition of each ash sample were determined using a FE-SEM and EDS system (Jeol Co., JSM-6335F and JED-2200). A laser diffraction and scattering method (Horiba Co., LA-950ND with air flow cell) was used to measure ash aggregate size distribution in air. The crystal structure of each ash sample was characterized by XRD (Rigaku Co., RINT-2100VPC/N).

2.2.2 Tensile strength and thermomechanical properties of ash powder beds

Tensile strength of sample ash powder beds was determined using a split-cell tensile strength test system, shown in Figure 2-1.²⁰ A shallow cylindrical cell for powder filling (5 cm in diameter and 1 cm deep) placed in a furnace can be divided equally into a fixed portion and a movable portion. During measurement, the powder bed was pulled horizontally by a motor. Since the movable half-cell hung horizontally from three thin metal belts, no friction occurred between the fixed and movable cell parts during measurements.

First, the ash powder sample (8.0 g) was added to a cell and consolidated with a cylindrical weight at a pressure of 2.5 kPa for 10 min. After consolidation, the height

of the powder bed was measured. Temperature of the furnace rose at a rate of 10 K/min to a specified temperature in the range of 400 to 800 °C . This temperature was maintained at that temperature for 10 or 60 min before tensile force loading. The data for tensile stress and displacement of the movable cell were collected during measurements.

To identify the thermal and shrinkage properties of ash samples at elevated temperature, thermomechanical analysis (TMA) (Rigaku Corporation, Thermo plus EVO series, TMA8310) was performed. To investigate the mechanism of ash layer strength increase with temperature, the shrinkage behavior of the ash powder bed was investigated by TMA at high temperature using a heating rate of 10 K/min and at a specific holding temperature for 60 minutes.

2.2.3 Thermodynamic equilibrium calculations for ash samples

To investigate the effect of chemical composition of the ash sample on solid, slag, and liquid phase formation and transformation at elevated temperatures, thermodynamic equilibrium calculations were performed using commercial software (Factsage7.3. Equilib Module). Using thermodynamic equilibrium calculation, given by the system conditions including chemical compositions of reactants, pressure, temperature et al., the situation of a researched system which at an equilibrium under specific temperature can be calculated. The equilibrium follows the principle of minimum Gibbs energy. In this work, author assumed that the system contained the researched ashes and sufficient oxygen, the pressure was set 1atm, the calculations were carried out at elevated temperature conditions which can be used to predict the reaction

trends and system condition in real combustions. Database ‘GTOX’ were selected in the software to perform calculations. Once the chemical compositions, pressure, database were selected, the ideal chemical compounds and physical states of products at specific temperatures can be calculated and predicted. In this work, the initial chemical composition of each ash sample for the calculations was obtained using the FE-SEM/EDS system. Based on the calculated products states, liquid and slag phase formation temperature was defined as the temperature at which slag liquid was detected. The calculated slag formation temperatures were compared with the temperature dependence of tensile strength and linear shrinkage of ash powder beds.

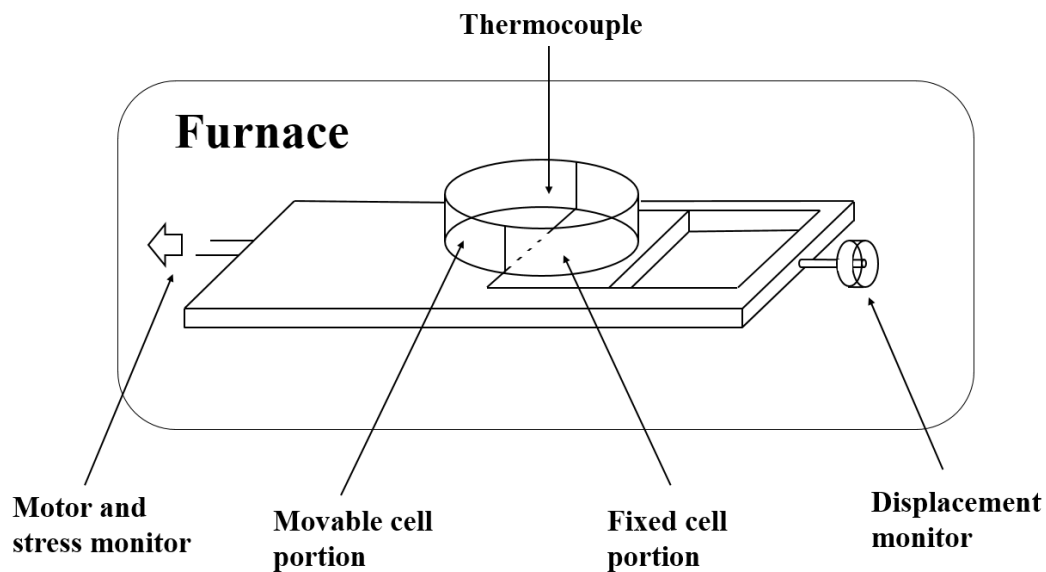


Figure 2-1. Schematic illustration of the split-cell tensile strength test system for ash powder beds at high temperature.²⁰

2.3 Results and discussion

2.3.1 Characterization of ash samples

The SEM images of each ash sample are shown in Figure 2-2. Aggregates were formed from fine primary particles. To determine the primary size distribution of each ash sample, several hundred particles in the SEM images were analyzed using image processing. Number-based cumulative distributions are shown in Figure 2-3(a). The size distributions of the sample was similar for those collected during stable operation ash (S-1 and S-2) and those collected during trouble periods (T-1 and T-2). The mean value for primary particle size diameter ranged from 3.94 to 5.32 μm . Measured mean aggregate diameter of each sample size distribution [Figure 2-3(b)] also was similar among samples and ranged from 8.85 to 14.14 μm , which agreed well with observed aggregate diameters in SEM images.

Elemental analysis of the ash samples was determined by energy dispersive spectrometry (EDS), as shown in Figure 2-4. The major elements in the sewage sludge ash were P, Si, Al, Mg, Ca, Fe, K, and Na. In ashes obtained during stable operation (S-1 and S-2), the Si and Al contents were greater and P and K contents less than those in trouble ashes (T-1 and T-2). Previous reports^{13, 28-29} indicated that P content influenced biomass ash deposition and growth rates on wall and heater surfaces in combustion and heat recovery systems. However, a detail mechanism of phosphorous compound involvement in sewage sludge ash adhesion troubles at high temperatures has not been reported.

Crystal structures of all sample ashes were examined by XRD analysis at room temperature; results are shown in Figure 2-5. The main peak of the quartz phase, SiO_2 , at 26.6° , and peaks of AlPO_4 at 20.3° , 21.5° , and 22.9° were detected in all ash samples. The strong peaks at 29.5° and 31.5° in T-1 and T-2 ashes were determined as calcium

magnesium phosphate (CaMgP_2O_7 , 31.5° , 29.6° and 29.3°). Since AlPO_4 and CaMgP_2O_7 generated by the phosphate in ash have melting temperatures higher than 1300 K (about 1800°C and 1120°C ,³⁰ respectively), these phases are not involved in the increase in ash layer tensile strength. Because the K and Na content was relatively low, the K and Na phases were not able to be detected using XRD.

2.3.2 Tensile strength and thermomechanical properties of ash samples

Examples of the relationship between tensile stress and displacement for S-1 and T-1 ashes at temperatures from 600 to 800°C with a holding time before tensile strength measurement of 10 min are shown in Figure 2-6(a) and 2-6(b). The maximum stress of each curve was the tensile strength of the ash powder bed. The tensile strength of T-1 ash was much greater than that of S-1 ash at temperatures ranging from 600 to 800°C , although the strength was similar for these ash samples at room temperature.

The relationship between tensile strength and temperature using a holding time of 10 min before tensile testing is shown in Figure 2-7. Each mark indicates one measurement, although some measurements were done twice under the same conditions to confirm reproducibility. Data for pure silica powder¹⁹ (FB-6S, Denka Co. Ltd., mean primary particle size: $5.3\ \mu\text{m}$ in diameter, purity: 99.9%) is also shown in Figure 2-7 for comparison. Tensile strength tended to increase for all ash particles from room temperature to 400°C , which was similar to that of pure silica particle. A rapid increase in tensile strength of ash beds was observed from 400 to 500°C in T-1 and T-2 ashes, while the rapid increase in S-1 and S-2 ash occurred from 500 to 600°C . From 600°C to higher temperature, all ash samples have much more stronger tensile strength than pure silica. Meanwhile, tensile strengths of T-1 and T-2 ashes were much greater than

those of S-1 and S-2 ashes in the temperature range of 500 to 800°C. Based on the measurement results, it can be assumed that the adhesiveness of T-1 and T-2 ashes are stronger than S-1 and S-2 ashes, also means T-1 and T-2 ash powder beds can promote more serious ash adhesion and deposition issues on the surface of heat exchangers and walls in waste incineration plants.

To investigate the effect of holding temperature and time on tensile strength of ash powder beds, the linear shrinkage of each ash sample at elevated temperatures and increased holding times was determined using TMA. Results are shown in Figure 2-8. The T-1 and T-2 ashes began to shrink at lower temperatures, approximately 450-550°C, than did S-1 and S-2 ashes (about 650°C), as shown in Figure 2-8. The temperature at which shrinkage began corresponded with the temperature at which tensile strength rapidly increased, as shown in Figure 2-7.

2.3.3 Thermodynamic calculations for ash samples

To examine the relationship between bed strength and increasing temperature more realistically, the database 'GTOX' was used to apply thermodynamic equilibrium calculations. This expanded the applicability of the analysis to the system containing phosphorus. Slag phases were generated by reaction with other elements and chemical compounds at the surface of ash particles. The viscosity and surface tension of molten slag materials were sufficiently high to make strong liquid bridges between particles, which promotes adherence of ash powder beds. Figure 2-9 shows an example of thermodynamic equilibrium calculation results of T-1 ash at elevated temperature, which indicate the change of products and physical states in ideal and equilibrium conditions. The calculated slag phase represents the liquid or molten matters generated

in this system. The calculated slag phase results of all real ashes are shown in Figure 2-10, the formation temperature of slag phase in T-1 ash is expected from 509°C, which can contribute to the increase of tensile strength. In sharp contrast, no slag phase was formed until 703 °C for S-1 ash, also suggesting that S-1 ash is a representative less-adhesive ash in the thermodynamic calculations.

A significant feature of S-1 ash is its low phosphorus content and high silicon and aluminum contents. Thermodynamic calculations were carried out using modified conditions based on T-1 ash as a representative adhesive ash. When 15 wt% phosphorus was subtracted, the slag formation temperature significantly increased up to 703 °C, which was equal to that of S-1 ash (Figure 2-11). These results suggested that high phosphorus content is the key to the adhesive property. Of course, in practice, a subtraction approach cannot be applied to suppress the adhesion of fly ash.

Unfortunately, when silicon was increased by 10-20 wt%, no changes were observed for the slag formation temperatures, suggesting that high silicon content is not directly related to the adhesive property (Figure 2-12). This also means that silicon content is not a promising additive to suppress adhesion of fly ash. When alumina content was increased by 10-20 wt%, however, the slag formation temperatures significantly increased up to 614 °C (Figure 2-13). While this is still lower than that of S-1 (703 °C), aluminum would be a promising additive to suppress adhesion of fly ash.

2.3.4. Adhesion behavior control by additives

To the delight, the tensile strength of T-1 was usefully decreased when alumina nanoparticles were added by dry blending. To evaluate the effect of alumina additives

experimentally, commercial γ -Al₂O₃ powder (Evonik Resource Efficiency GmbH, AEROXIDE Alu130, BET specific surface area: 87 m²/g, purity: >99.8%, weight loss at 425 K for 2 h: < 5%) was used as an additive. The FE-SEM image of γ -Al₂O₃ particles is shown in Figure 2-14; BET particle diameter was 17.4 nm. Ash and γ -Al₂O₃ powders were mixed in a plastic bag and shaken by hand for 10 min under dry conditions. The amount of γ -Al₂O₃ powder added to T-1 ash powder was 1.5 to 6.5 wt%. Tensile strength of ash powder beds with added γ -Al₂O₃ was determined at 700°C.

Figure 2-15 shows the tensile strength measurement results at 700°C of T-1 ash, S-1 ash, and T-1 ash with 1.5 wt%, 3 wt%, and 6.5 wt% added Al₂O₃. Since alumina nanoparticles are not expected to go inside of the ash micro particles, it seems that they adsorb onto the surface. This causes inhomogeneous local high concentrations of alumina toward the ashes and generation of partial slag phase would be suppressed consequently. The tensile strength of 3 wt% Al₂O₃-blended T-1 ash was about 0.8 kPa, which was as low as that of S-1 ash; the reduction compared with original T-ash 1 was about 70%. These results demonstrate that the adhesion force for adhesive ashes with high phosphorus content can be controlled by adding alumina particles before the combustion processes.

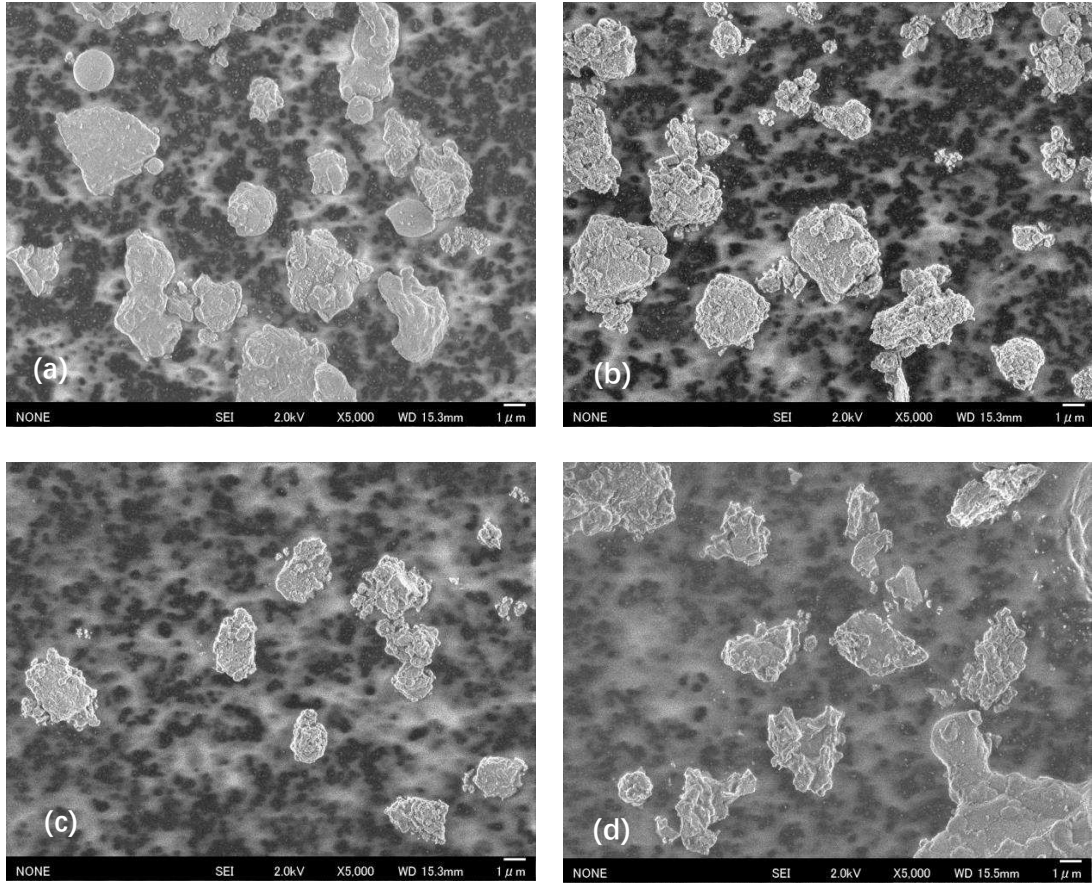
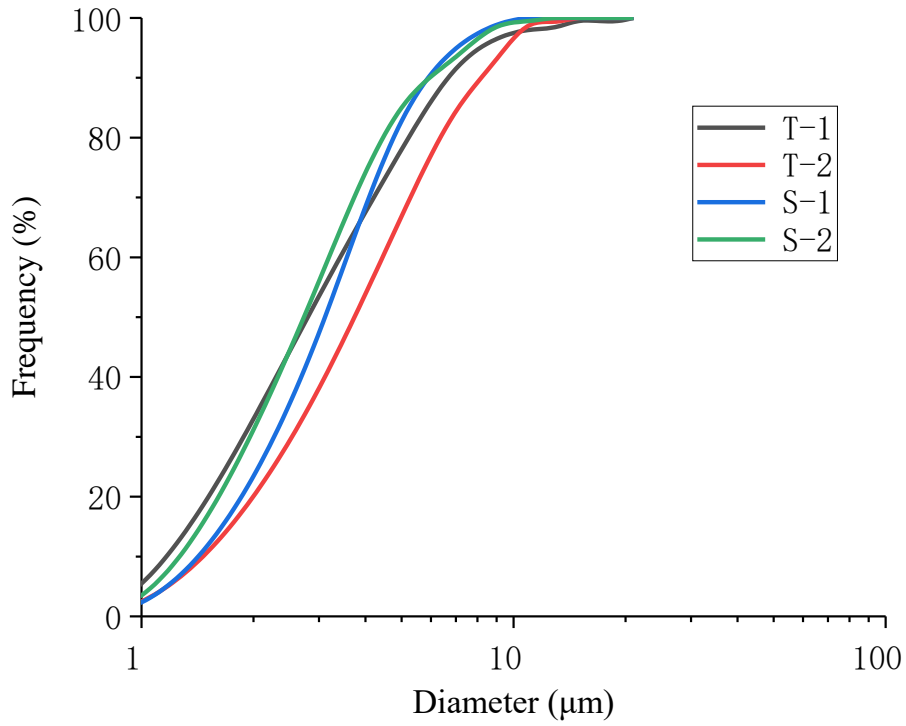
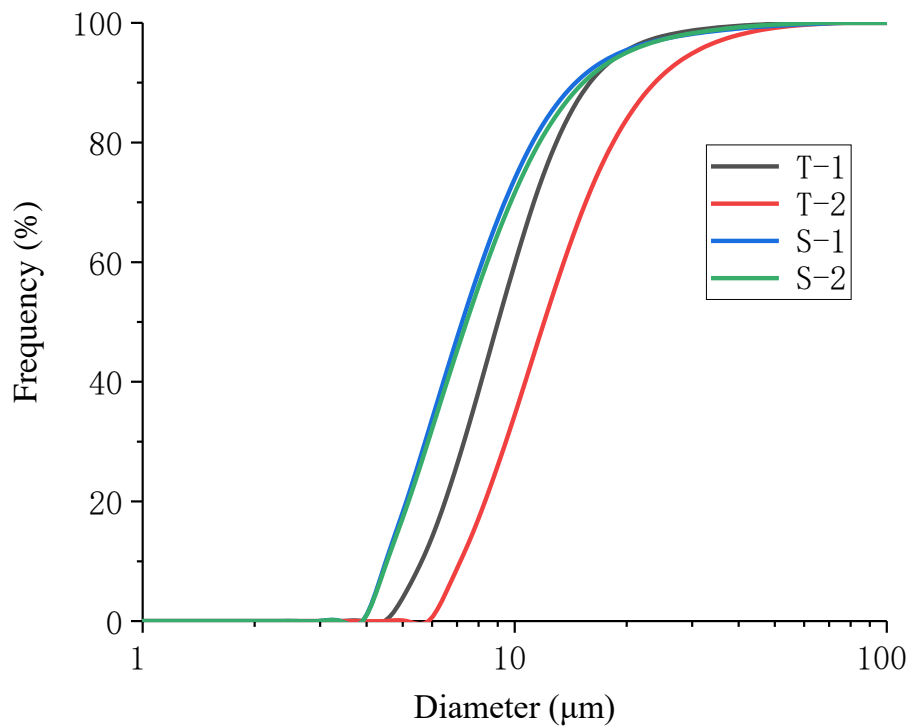


Figure 2-2. SEM images of ash particles: (a) T-1, (b) T-2, (c) S-1, and (d) S-2.



(a) Image processing of FE-SEM pictures



(b) Laser diffraction method

Figure 2-3. Number-based cumulative size distribution of ash samples. (a) Image

processing of SEM observations, (b) Laser diffraction using an air flow cell.

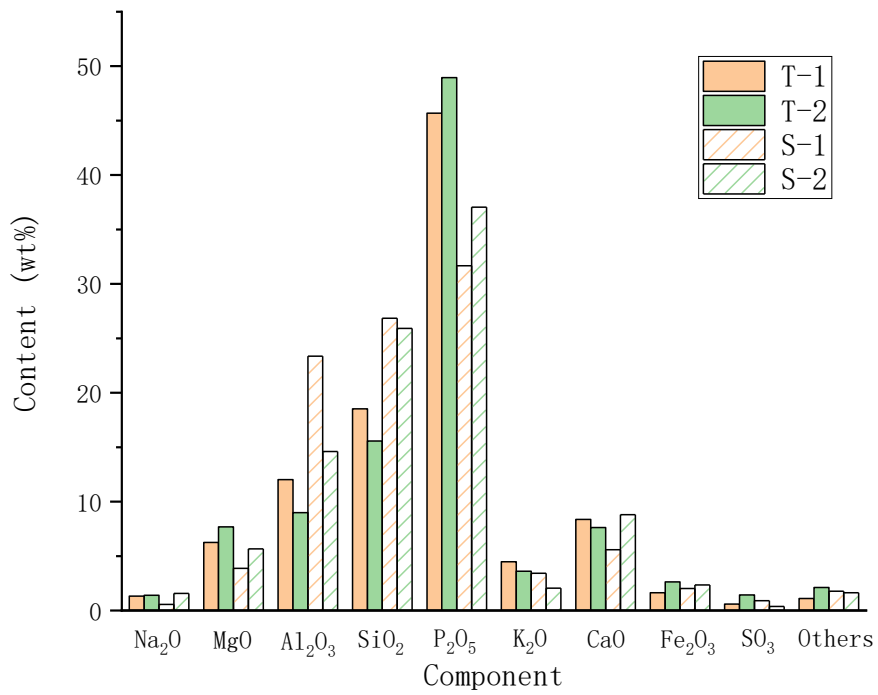


Figure 2-4. Chemical composition of ash samples determined by EDS.

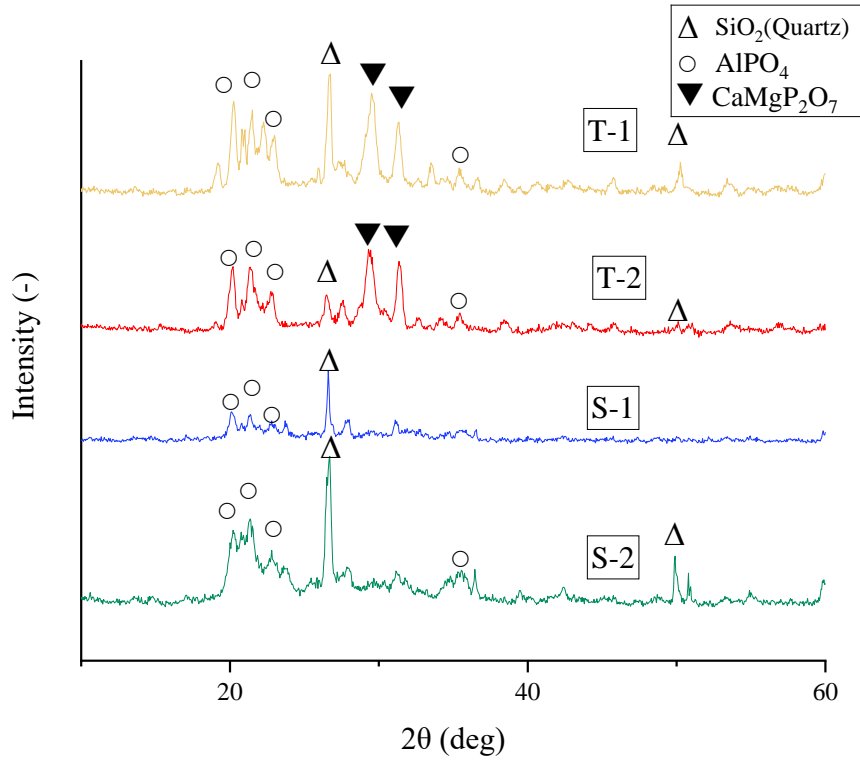
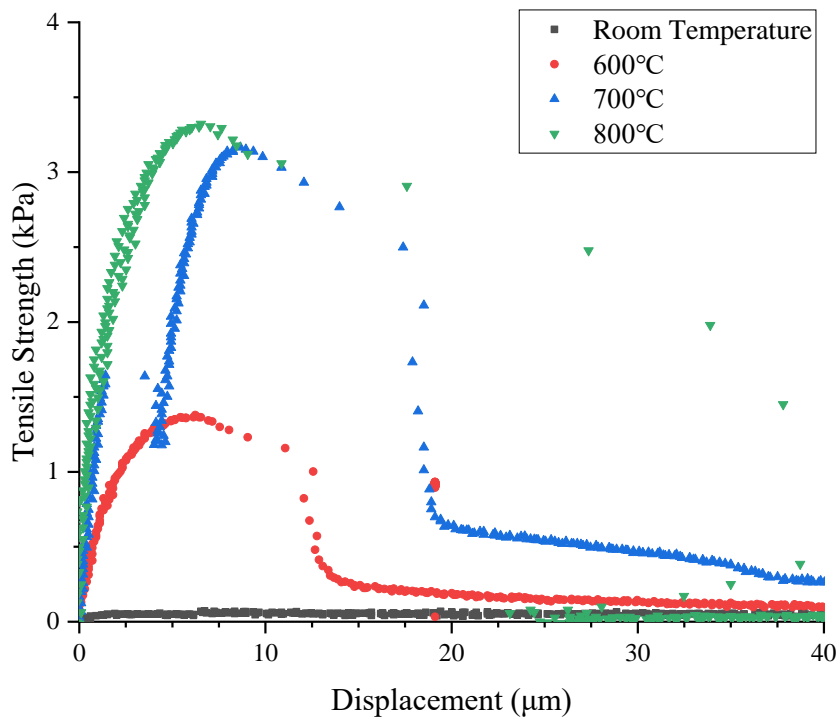
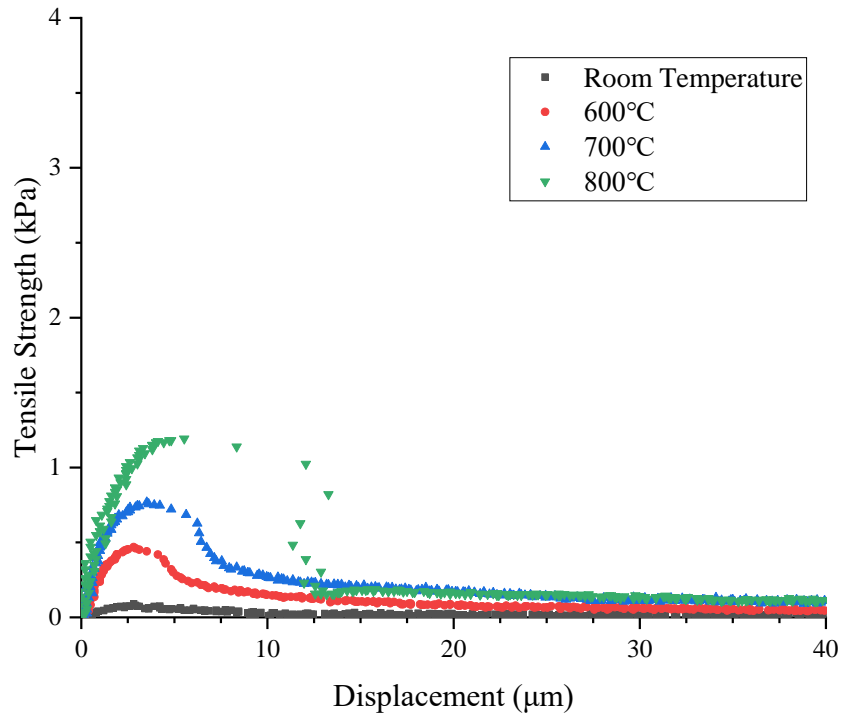


Figure 2-5. XRD patterns for ash samples at room temperature.



(a) Ash deposition for T-1 ash samples



(b) Ash deposition for S-1ash samples
 Figure 2-6. Relationship between stress and displacement

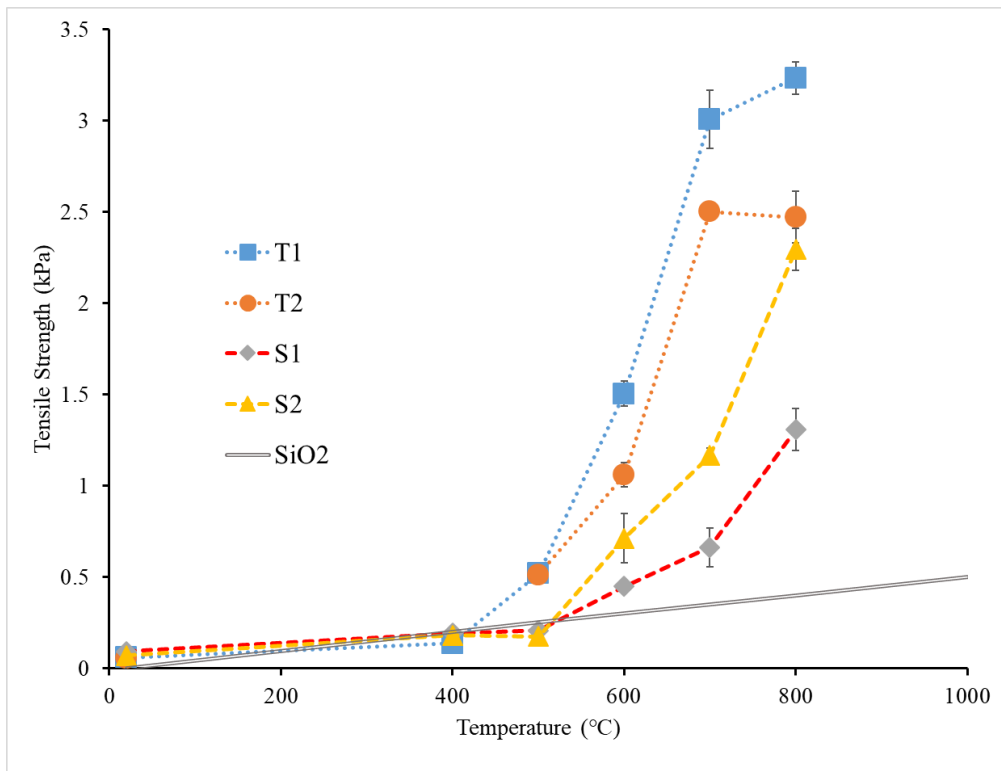


Figure 2-7. Effect of temperature on tensile strength of ash samples and pure silica particles

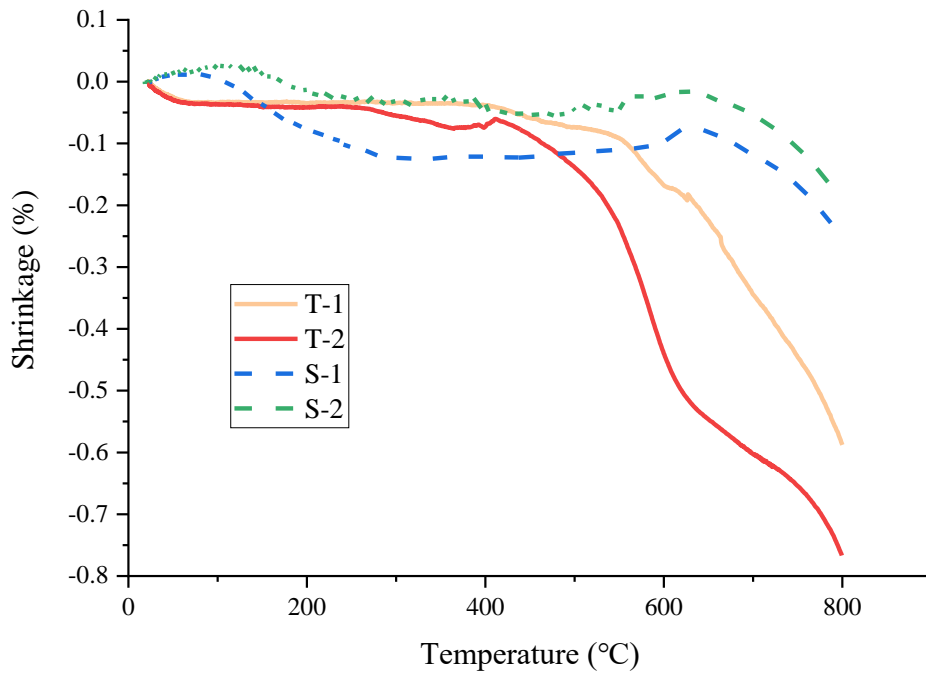


Figure 2-8. Shrinkage behavior of ash samples determined using TMA

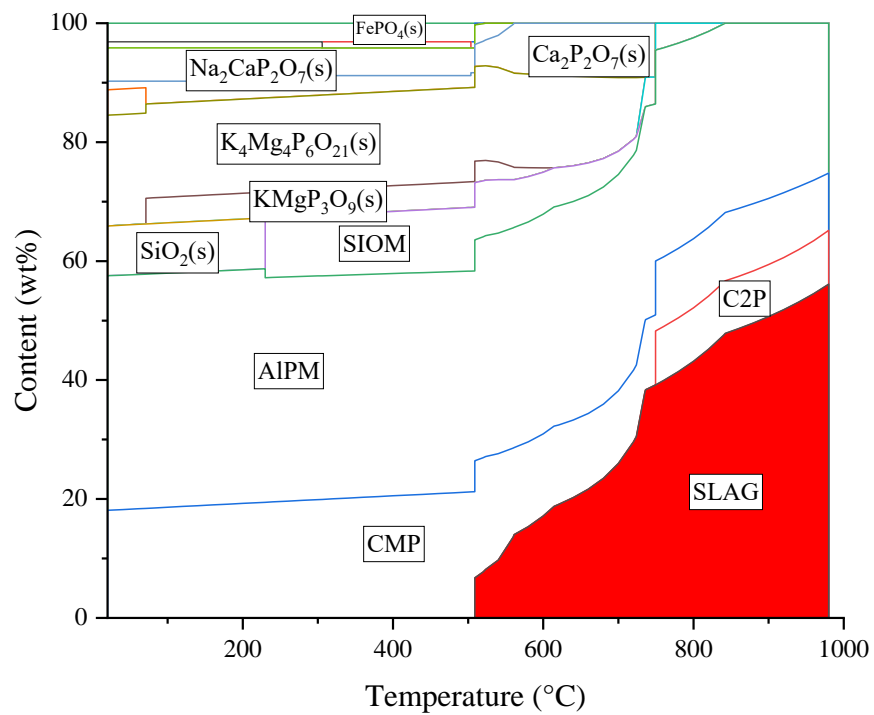


Figure 2-9. Thermodynamic calculation results of T-1 ash at elevated temperature.

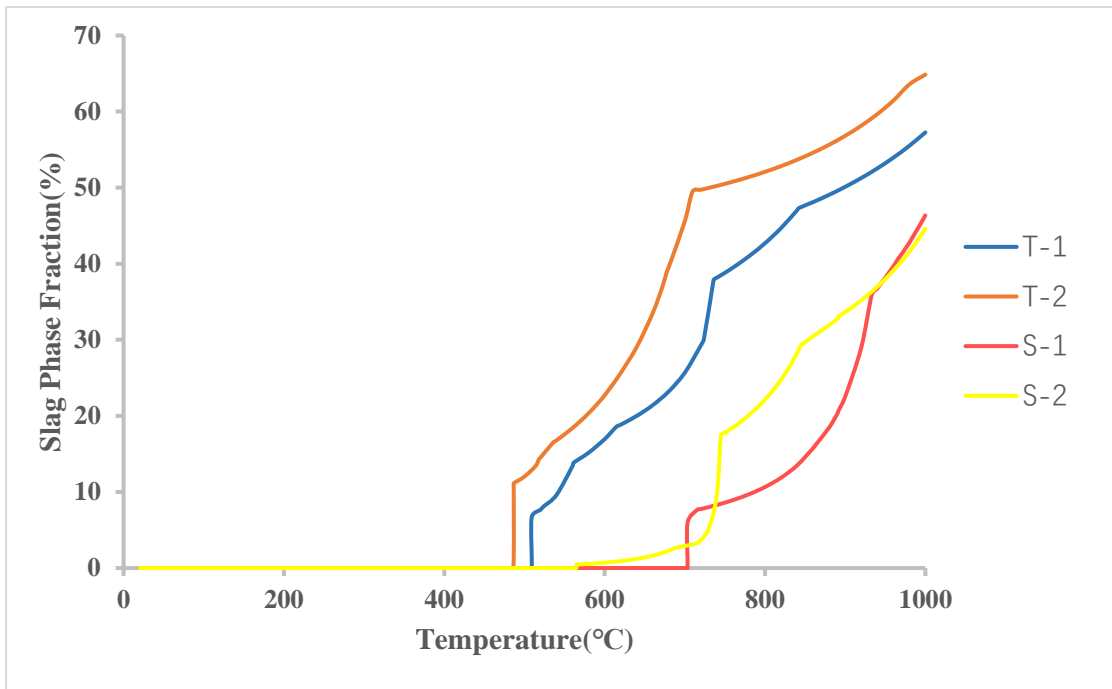


Figure 2-10. Results of thermodynamic equilibrium calculations for all ash samples using GTX database.

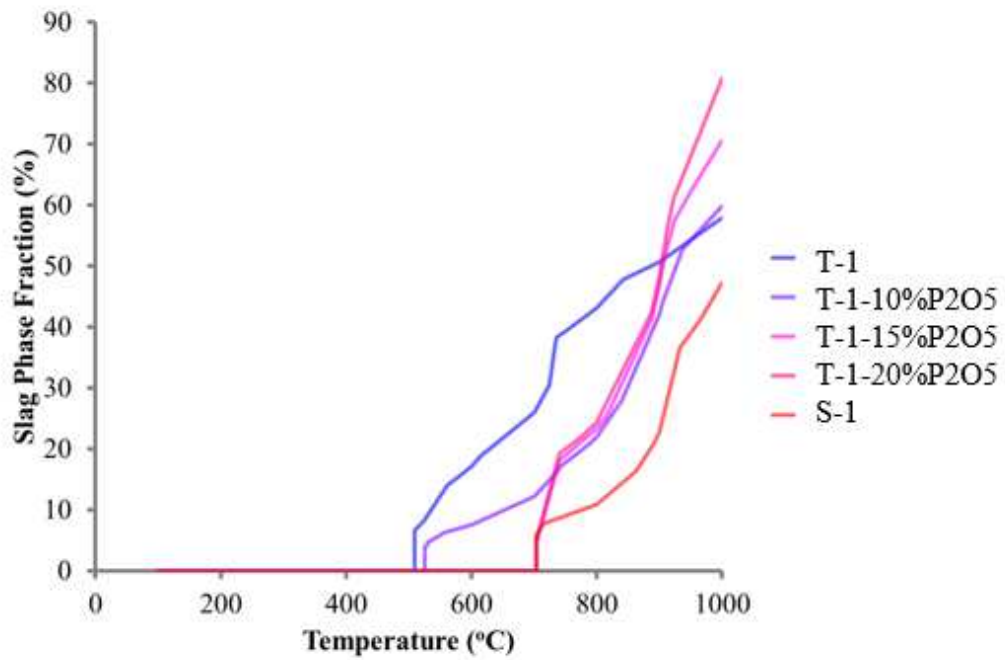


Figure 2-11. Behavior of Slag (Liquid) Phase Formation of T-1 ash with Reduced Phosphorus Content.

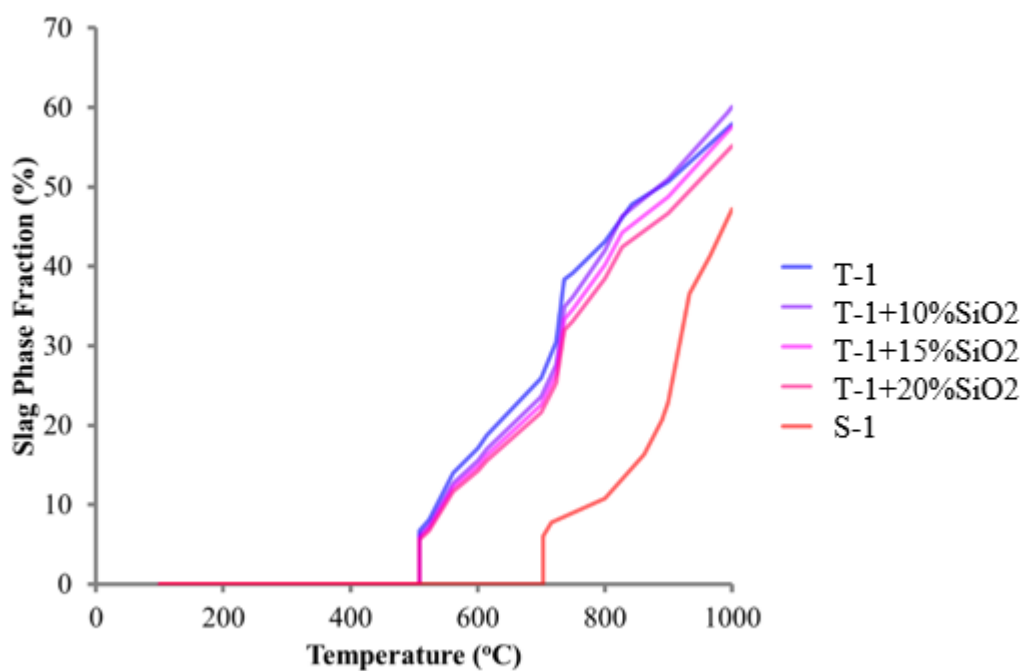


Figure 2-12. Behavior of Slag (Liquid) Phase Formation of T-1 ash with Increased Silicon Content.

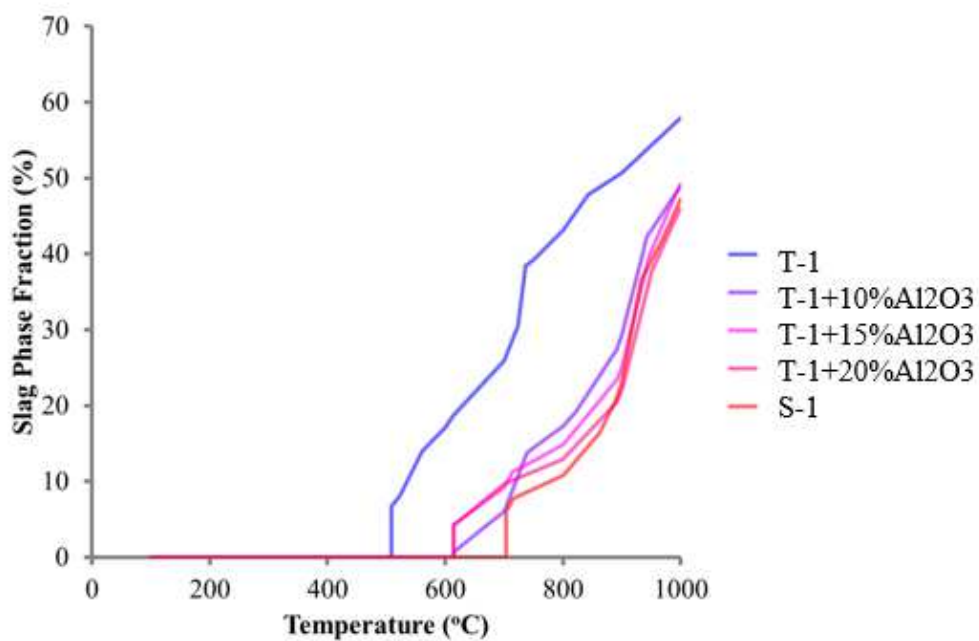


Figure 2-13. Behavior of Slag (Liquid) Phase Formation of T-1 ash with Increased Aluminum Content.

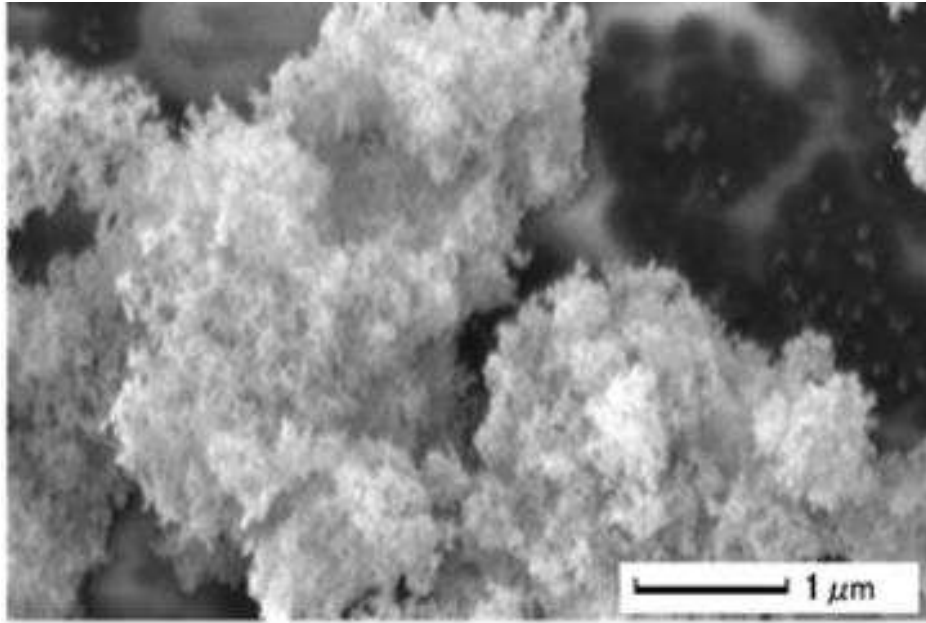


Figure 2-14. FE-SEM image of γ - Al_2O_3 particles.

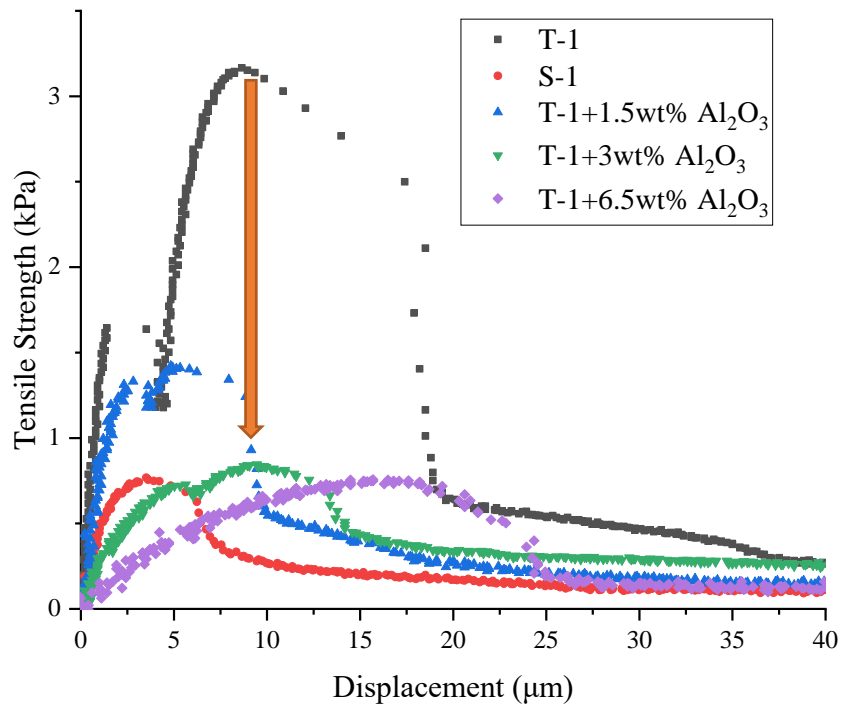


Figure 2-15. Tensile strength measurements of T-1 ash, S-1 ash, and T-1 ash with Al_2O_3 addition (700°C).

2.4. Conclusions

1. The merger of experimental and theoretical approaches has led to the rational finding that alumina nanoparticles are promising additives to suppress the adhesion of fly ash containing a relatively high concentration of phosphorus components.

2. A benchmark for the adhesive properties was provided by the tensile strength of ash powder beds measured by a split-type tester.

3. The behavior of slag phase formation determined by thermodynamic calculations usefully explained the results obtained by the tensile strength measurements.

4. Al_2O_3 was verified that can suppress the adhesive properties of researched ashes.

2.5 References

1. Werther, J.; Ogada, T., Sewage sludge combustion. *Progress in Energy and Combustion Science* **1999**, *25* (1), 55-116.
2. Donatello, S.; Cheeseman, C. R., Recycling and recovery routes for incinerated sewage sludge ash (ISSA): a review. *Waste Management* **2013**, *33* (11), 2328-40.
3. Murakami, T.; Suzuki, Y.; Nagasawa, H.; Yamamoto, T.; Koseki, T.; Hirose, H.; Okamoto, S., Combustion characteristics of sewage sludge in an incineration plant for energy recovery. *Fuel Processing Technology* **2009**, *90* (6), 778-783.
4. Heidenreich, S., Hot gas filtration – A review. *Fuel* **2013**, *104*, 83-94.
5. Lee, K.-S.; Sohn, J.-R.; Park, Y.-O., Filtration performance characteristics of ceramic candle filter based on inlet structure of high-temperature and high-pressure dust collectors. *Journal of Industrial and Engineering Chemistry* **2015**, *21*, 101-110.
6. Walsh, P. M.; Sayre, A. N.; Loehden, D. O.; Monroe, L. S.; Beér, J. M.; Sarofim, A. F., Deposition of bituminous coal ash on an isolated heat exchanger tube: effects of coal properties on deposit growth. *Progress in Energy and Combustion Science* **1990**, *16* (4), 327-345.
7. Kamiya, H.; Deguchi, K.; Gotou, J.; Horio, M., Increasing phenomena of pressure drop during dust removal using a rigid ceramic filter at high temperatures. *Powder Technology* **2001**, *118* (1-2), 160-165.
8. Sharma, S. D.; Dolan, M.; Park, D.; Morpeth, L.; Ilyushechkin, A.; McLennan, K.; Harris, D. J.; Thambimuthu, K. V., A critical review of syngas cleaning technologies — fundamental limitations and practical problems. *Powder Technology* **2008**, *180* (1-2), 115-121.
9. Simon, X.; Chazelet, S.; Thomas, D.; Bémer, D.; Régnier, R., Experimental study of pulse-jet cleaning of bag filters supported by rigid rings. *Powder Technology* **2007**, *172* (2), 67-81.
10. Shao, Y.; Wang, J.; Preto, F.; Zhu, J.; Xu, C., Ash deposition in biomass combustion or co-firing for power/heat generation. *Energies* **2012**, *5* (12), 5171-5189.
11. Namkung, H.; Kim, C.-H.; Kim, D.; Yuan, X.; Kang, T.-J.; Kim, H.-T., Effect of bed agglomeration by mineral component with different coal types. *Journal of the Energy Institute* **2016**, *89* (2), 172-181.
12. Van Caneghem, J.; Brems, A.; Lievens, P.; Block, C.; Billen, P.; Vermeulen, I.; Dewil, R.; Baeyens, J.; Vandecasteele, C., Fluidized bed waste incinerators: Design, operational and environmental issues. *Progress in Energy and Combustion Science* **2012**, *38* (4), 551-582.
13. Wang, L.; Hustad, J. E.; Skreiberg, Ø.; Skjevraak, G.; Grønli, M., A Critical Review on Additives to Reduce Ash Related Operation Problems in Biomass Combustion Applications. *Energy Procedia* **2012**, *20*, 20-29.
14. Werther, J.; Saenger, M.; Hartge, E. U.; Ogada, T.; Siagi, Z., Combustion of agricultural residues. *Prog Energy Combust Sci. Progress in Energy & Combustion Science* **2000**, *26* (1), 1-27.
15. Laursen, K.; Frandsen, F.; Larsen, O. H., Ash deposition trials at three power stations in Denmark. *Energy&Fuels* **1998**, *12* (2), 429-442.
16. Arjunwadkar, A.; Basu, P.; Acharya, B., A review of some operation and maintenance issues of CFBC boilers. *Applied Thermal Engineering* **2016**, *102*, 672-694.
17. Hupa, M., Ash-Related Issues in Fluidized-Bed Combustion of Biomasses: Recent Research Highlights. *Energy&Fuels* **2011**, *26* (1), 4-14.
18. Miles, T. R.; Miles Jr, T. R.; Baxter, L. L.; Bryers, R. W.; Jenkins, B. M.; Oden, L. L., Boiler

- deposits from firing biomass fuels. *Biomass and Bioenergy* **1996**, *10* (2-3), 125-138.
19. Kamiya, H.; Kimura, A.; Tsukada, M.; Naito, M., Analysis of the high-temperature cohesion behavior of ash particles using pure silica powders coated with alkali metals. *Energy&Fuels* **2002**, *16* (2), 457-461.
 20. Kamiya, H.; Kimura, A.; Yokoyama, T.; Naito, M.; Jimbo, G., Development of a split-type tensile-strength tester and analysis of mechanism of increase of adhesion behavior of inorganic fine powder bed at high-temperature conditions. *Powder Technology* **2002**, *127* (3), 239-245.
 21. Tsukada, M.; Yamada, H.; Kamiya, H., Analysis of biomass combustion ash behavior at elevated temperatures. *Advanced Powder Technology* **2003**, *14* (6), 707-718.
 22. Franz, M., Phosphate fertilizer from sewage sludge ash (SSA). *Waste Management* **2008**, *28* (10), 1809-18.
 23. Kupka, T.; Mancini, M.; Irmer, M.; Weber, R., Investigation of ash deposit formation during co-firing of coal with sewage sludge, saw-dust and refuse derived fuel. *Fuel* **2008**, *87* (12), 2824-2837.
 24. Steenari, B.-M.; Lindqvist, O., High-temperature reactions of straw ash and the anti-sintering additives kaolin and dolomite. *Biomass and Bioenergy* **1998**, *14* (1), 67-76.
 25. Llorente, M. J. F.; Arocas, P. D.; Nebot, L. G.; García, J. E. C., The effect of the addition of chemical materials on the sintering of biomass ash. *Fuel* **2008**, *87* (12), 2651-2658.
 26. Thy, P.; Jenkins, B.; Grundvig, S.; Shiraki, R.; Leshner, C., High temperature elemental losses and mineralogical changes in common biomass ashes. *Fuel* **2006**, *85* (5-6), 783-795.
 27. Wu, H.; Glarborg, P.; Frandsen, F. J.; Dam-Johansen, K.; Jensen, P. A., Dust-firing of straw and additives: ash chemistry and deposition behavior. *Energy&Fuels* **2011**, *25* (7), 2862-2873.
 28. Grimm, A.; Skoglund, N.; Boström, D.; Boman, C.; Öhman, M., Influence of phosphorus on alkali distribution during combustion of logging residues and wheat straw in a bench-scale fluidized bed. *Energy&Fuels* **2012**, *26* (5), 3012-3023.
 29. Lindström, E.; Sandström, M.; Boström, D.; Öhman, M., Slagging characteristics during combustion of cereal grains rich in phosphorus. *Energy&Fuels* **2007**, *21* (2), 710-717.
 30. McCauley, R.; Hummel, F.; Hoffman, M., Phase Equilibria and Eu²⁺, Tb³⁺, and Mn²⁺-Activated Luminescent Phases in the CaO-MgO-P₂O₅ System. *Journal of The Electrochemical Society* **1971**, *118* (5), 755-759.

CHAPTER 3

**Research on the effects of specific elements on adhesion
phenomena in sewage sludge combustion ashes using model
ash systems**

CHAPTER 3

Research on the effects of specific elements on adhesion phenomena in sewage sludge combustion ashes using model ash systems

3.1 Introduction

In the main compositions of ashes, alkali metals had been widely researched and confirmed that can lead to deposition issues. In previous chapter, the author researched and discussed the roles of phosphorous, aluminum and silicon in sewage sludge ashes on adhesiveness using real ash samples and proposed the strategy that using alumina powders to suppress the deposition phenomena. However, in addition to these elements, the roles of calcium and magnesium in ashes on adhesiveness are not clear. Therefore, in this chapter, the author tried to discuss the effect of calcium and magnesium in sewage sludge ashes.

Sewage sludge is the residual matter from the treatment of household and industrial waters and it is the largest by-products in volume after waste water treatments.¹⁻² Environmental disposal and utilization of sludge is a very complicated task since the complex composition: on the one hand the organics with high energetic values make the sludge as a potential energy source, on the other hand, the harmful substances including heavy metals, pathogenic micro-organisms, bacteria, viruses and toxins need to be processed legally and harmlessly.^{1, 3-5} Gasification or combustion individually and co-combustion with other fuels are common thermal processes for sludge, which are benefit for energy recovery and volume reduction.⁶⁻¹⁰ Compared to

fossil fuels, such as coal, sewage sludge ashes generally contain higher contents of alkali metals and phosphorus.¹¹⁻¹³ Eutectic phases with low melting points composed from alkali metals are easy to generate, the phases are easy to transform into slag or liquid phase at relatively low temperature and promote adhesion force among powders in the thermal process.¹⁴⁻¹⁶ The existence of P_2O_5 in sewage combustion ash can also result in ash related issues in incinerators such as sintering, slagging, deposition and agglomeration since it seems to decrease the ash melting and slag formation temperature.^{1, 17-19} However, since many main and trace elements were included in sewage sludge ash, the complex phenomena concerned slag and liquid phase formation between particles occurred at elevating temperature. Previous almost all research subjects for ash behavior observation and control usually had been used real combustion ashes with including a lot of main and trace elements. It was difficult to remove some specific elements in real ash to study the effect of each element on adhesion behavior at high temperature. Kamiya. H et al, proposed a method of syntactic model ashes using pure silica powders coated with alkali metals to analyze the cohesion behaviors of ash particles.¹⁶

It has been proved that alkali metals are related to ash deposition issues for generating eutectics phase with relatively low melting points on the surface of ash¹⁵⁻¹⁶. The generated liquid and slag phase among ash particles promoted the adhesion and growth of ash layer. Except for phosphorus and alkali metals, in the previous research (Chapter 2), alumina nanoparticles has been proved as an effective additive to decrease the adhesiveness of sewage fly ashes at high temperature, silica is not direct relate to

the ash adhesion property.²⁰ Besides, calcium and magnesium are also major elements in sewage sludge combustion ashes, they can react with other elements such as phosphorous but few researchers focused on their effects in ash deposition phenomena. To predict the sewage sludge or biomass ash related phenomena, some researcher proposed simple models and formulas based on chemical compositions to research on the ash fusibility.^{1, 21-23} But these models have boundedness since the chemical compositions are extremely various in different sewage sludge. In these researches, CaO and MgO are often treated as basic constitutes in sewage ashes and related to a tendency of decreasing melting temperature. However in some other cases, the results seem different, higher content of calcium can also react with phosphorus and generate refractory minerals, the ash fusion temperatures increase consequently.²⁴ As the main elements in sewage sludge combustion ashes, seldom quantitative experiments focusing on calcium and magnesium in ash deposition phenomena were studied compared to the other elements such as alkali metals, silicon and aluminum. Therefore, it requires more search on the effect of calcium and magnesium in ash deposition issues which benefit the practical industrial disposal of sewage sludge.

Based on this method, synthesis of model ashes is an appropriate way to research on the effect of main elements on sewage sludge ash behaviors at high temperature. Since the existence form and potential reaction routes of Ca and Mg are similar in the target ash samples, author treated the Ca and Mg as a whole instead of processing separately in this work just like the simplification treatment in the research of Bostrom, D et al.²²

In this chapter, based on the above previous work¹⁶, the preparation process of model ash particles from pure fine particles and chemical compounds is developed to study about the roles of each element of this sewage ash deposition phenomena at high temperature condition. Firstly, model ash preparation method from pure inorganic nanoparticles and chemical compounds of 7 main elements (Na, K, Al, Si, P, Ca and Mg) in real sewage sludge ashes were developed to modify the chemical compounds and morphology. The adhesion properties of prepared model ash were compared with a real sewage sludge ash particle at high temperature. After that, to discuss the effect of Ca and Mg on adhesion behavior, 5 elements model ashes replacing calcium and magnesium with aluminum were respectively synthesized and analyzed.

3.2 Experimental

3.2.1 Real ash samples and characterization

The real industrial combustion ashes (referred in Chapter 2) from two different plants with different stickiness and adhesion behaviors were selected as the reference samples. Based on the field deposition performances, these ashes were divided into two groups: one group of ashes from one plant seldom caused deposition issues and the deposits were easy to be removed; the other ashes from another plant were easy to result in deposition issues in daily operations. The main chemical compositions of the real ash samples were examined by energy dispersive spectrometer, EDS system (JEOL Co., JED-2200F) are shown in Figure 2-4. The major elements in the real sewage ashes were Na, K, Al, Si, P, Mg and Ca, the total oxides content of these seven elements is higher than 95%. As a clear difference in chemical composition between T ashes and S ashes, the amounts of Al and Si are higher in S ashes, whereas the amount of P is higher in T ashes.

To reveal the effect of Ca and Mg on ash deposition phenomena at high temperature, synthesizing model ashes is an appropriate method. Model ash is a kind of ash which is synthesized in lab scale. Based on the composition of relevant real ashes or the demand of target composition, raw materials with specific elements are synthesized under mixing, heating, grinding, sieving and other processing approaches, synthetic model ashes having the same or similar chemical compositions as the target ashes are finally obtained. In this work, the synthetic model ashes referred to the Na, K, Al, Si, P, Mg and Ca seven elements.

Two groups of model ashes were synthesized in this work. The first group of ash focused on Na, K, Al, Si, P, Mg and Ca, 7 elements. The target compositions of first group model ashes are based on the average chemical compositions of T-ashes or S-ashes in chapter 2, named M7-1 (represent S-1 and S-2 ashes) and M7-2 ash (represent T1 and T-2 ash). In addition, author designed another group of model ashes to make comparisons between the effect of Ca/Mg and Al. In this group, author synthesized 5-element (Na, K, Si, P and Al) based model ashes. The ratios of Na₂O, K₂O, SiO₂ and P₂O₅ in model ashes followed the average ratios in real ashes yet. However the Al₂O₃ content in this group of ashes was raised to a level which is equivalent to the sum of Al₂O₃, MgO and CaO in real ashes, the Al₂O₃ increasing principle in this group is the molar ratio of Mg and Ca's sum to the increased Al is 1 to 1. Therefore, in this group the ashes contained the Na₂O, K₂O, SiO₂, P₂O₅ and the modified Al₂O₃ content, named after M5-1 and M5-2 ash.

3.2.2 Raw materials of model ash

As the phosphorus contents in the real ash samples are extremely high, micro-sized particles may be easily covered by amorphous phosphorus in the synthetic process, thus the element distribution may be not homogeneous. To achieve a uniform mixing and sufficient reactions among raw material as much as possible, nano-sized raw materials with high specific surface areas should be a better choice. Considering the chemical properties and thermal properties of each element, commercial raw materials including (COONa)₂, (COOK)₂.H₂O, Al₂O₃, SiO₂, NH₄H₂PO₄, MgO and CaCO₃ were selected to be the sources of all elements. Al₂O₃, SiO₂, MgO and CaCO₃ were

used in nano-size powders, the detailed commodity information from manufacturers are listed in Table 3-1.

Particles size distributions of model ashes were measured using a laser-scattering particle size distribution analyzer (Horiba, LA-950ND) in dry condition. In addition, primary particle size were estimated using image processing, the morphological observations of ash powders (Figure 3-1) were carried out by FE-SEM system (JEOL Co., JED-2200F).

3.2.3 The synthetic method of model ash

To synthesize the model ash types, raw materials were first added into ultra-pure water to obtain a primary mix, and the mixed slurry was then filled into a mixer (Thinky, ARE-310) for proper mixing and defoaming (2,000 r/min for 30 s and 2,200 r/min for 30 s). After even mixing, the slurry was placed into a heating furnace under a constant temperature of 120 °C for 24 h to dry out. The dried mixture was then ground in a planetary type pot mill (ITO, LP-1) at 300 rpm for 30 min (WC+Co milling bead, \varnothing 10 mm) and then sieved through a 100 μ m screen, and the precursors of the model ash were then obtained. The heat treatment temperature of the precursors was then determined through a high-temperature X-ray diffraction analysis (Rigaku, RINT2100VPC/N), thermogravimetric analysis, and differential thermal analysis (Rigaku, TG-DTA 8310). Figure 3-2 shows the XRD patterns of the model ash precursors from 300 °C to 800 °C, in which the crystal peaks started to form from 600 °C and became stable from 700 °C. Figure 3-3 shows the TG-DTA curves of the precursors from room temperature to 1,000 °C, in which the weight loss of both samples became

stable at above 650 °C. At approximately 200 °C, the DTA curves showed remarkable endothermic peaks, suggesting that the $\text{NH}_4\text{H}_2\text{PO}_4$ decomposed and generated ammonia gas. With a temperature increase to 650 °C, the decompositions and reactions among the raw materials were completed. When comprehensively considering the results of a high-temperature XRD and TG-DTA, heating at 700 °C for 1 h was chosen as the heat treatment condition during the synthesis of each model ash sample, causing thermal decomposition and synthesis reactions. After heat treatment at 700 °C for 60 min, the samples were ground using a planetary type pot mill (ITO, LP-1) at 350 rpm for 120 min (WC+Co milling bead, \varnothing 10 mm), the heated precursors were sieved through a 100 μm aperture screen, and the target model ash types were then obtained.

3.2.4 Characterization of model ash samples

The chemical compositions of the two groups of model ash types measured using EDS are listed in Table 3-2. The particle size distributions of the model ash types were measured using a laser-scattering particle size distribution analyzer (Horiba, LA-950ND) under dry conditions (Table 3-2). The primary particle size was estimated using image processing, and morphological observations of the ash powders were carried out using the FE-SEM system (JEOL Co., JED-2200F). In addition, to observe the change in morphology of the ash particles after heat treatment, an FE-SEM system equipped with a heating device was applied in this study.

3.2.5 Tensile strength measurements

Tensile strength of real and model ashes powders were measured by a split-cell type tensile strength test system mentioned in chapter 2.²⁵ In this study, because author focused on the adhesion and deposition phenomena on the surface of super heater and heat exchanger, the adhesion behavior need to be characterized ranging from 600 to 1000 °C. Within this temperature range, the remarkable softening, melting and fusion of ash particles were not observed. The slightly increase of adhesion force between ash particles was characterized by using this tensile strength measurement system in this temperature range. Before measurement, 6.5 g of model ash powder was filled in the measurement cell and consolidated at a normal pressure of 2.66 kPa for 10 min. After consolidation, the tensile strength of the powder beds was measured at room temperature (about 20 °C) and at high temperatures (400 °C to 800 °C). The heating rate in the furnace was set to 10 °C /min, and the furnace maintained the specified temperature for 60 min before tensile force loading. To characterize the thermal properties of ash samples, thermomechanical analysis (TMA) was also demonstrated for each ash sample.

3.2.6 Thermodynamic calculation of each ash sample

A thermodynamic calculation is a useful method to help determine the ash deposition by calculating the thermal equilibrium of the ash at different temperatures. Commercial software, FactSage 7.3, was used to conduct the thermodynamic equilibrium calculations in this study. The Equilib module is a Gibbs energy minimization workshop used in FactSage, and calculates the concentrations of the

chemical species when specified elements or compounds react or partially react to reach a state of chemical equilibrium. The database 'GTOX' is suitable for a calculation of an oxide system, particularly under a high concentration of phosphorus, and can estimate the formation temperature of the slag phase in the ash system. The detailed calculated results are listed in Table 3-3. The calculation conditions were set at a temperature ranging from 20 °C to 1000 °C, and the temperature check point interval is 10 °C under a pressure of 1 atm.

Table 3-1. Commodity information of raw materials.

(a) Nanoparticles

Material	Estimated Diameter(nm)*	Specific Surface Area (m ² /g)	Product information
Al ₂ O ₃	12.5	130	Evonik, Aeroxide® Alu130
SiO ₂	9	304	Evonik, AEROSIL® 300
MgO	20	52	Skyspring Nanomaterials, 4810NH
CaCO ₃	15-40	>40	Skyspring Nanomaterials, 1957RH

*Calculated from specific surface area or measured by manufacturers.

(b) Chemical compounds

Chemicals	Purity	Product information
(COONa) ₂	99.5%	Fujifilm Wako, 198-02655
(COOK) ₂ .H ₂ O	99%	Fujifilm Wako, 165-04105
NH ₄ H ₂ PO ₄	99%	Fujifilm Wako, 012-03305

Table 3-2. Particle size distributions and chemical compositions of all model ashes.

ash	mean particle size (µm)		chemical composition (wt%)						
	laser diffraction	FE-SEM	Na ₂ O	K ₂ O	Al ₂ O ₃	SiO ₂	P ₂ O ₅	MgO	CaO
M7-1	8.29	4.64	1.45	2.7	19.61	30.92	35.09	4.09	6.15
M7-2	8.37	5.24	1.85	3.77	10.78	19.5	50	7.19	6.91
M5-1	8.71	5.18	1.47	2.54	29.08	33.3	33.61		
M5-2	8.68	4.49	1.365	4.445	24.44	18.205	51.545		

Table 3-3. Special solutions and end-members information in 'GTOX' database

Phase	End-member
ALPM*	(Al+3)1(P+5)1(O-2)4 (Al+3)1(Si+4)1(O-2)4 (Si+4)1(P+5)1(O-2)4 (Si+4)1(Si+4)1(O-2)4
SIOM*	(Al+3)1(P+5)1(O-2)4 (Al+3)1(Si+4)1(O-2)4 (Si+4)1(P+5)1(O-2)4 (Si+4)1(Si+4)1(O-2)4
C3PL*	Ca+2:P+5:O-2 Mg+2:P+5:O-2
CMP*	Ca+2:Ca+2:P+5:O-2 CaP ₂ MgO ₇
KN2P*	Na ₄ P ₂ O ₇ K ₄ P ₂ O ₇
KP_H*	g-K+1:P+5:O-2 g-Na+1:P+5:O-2

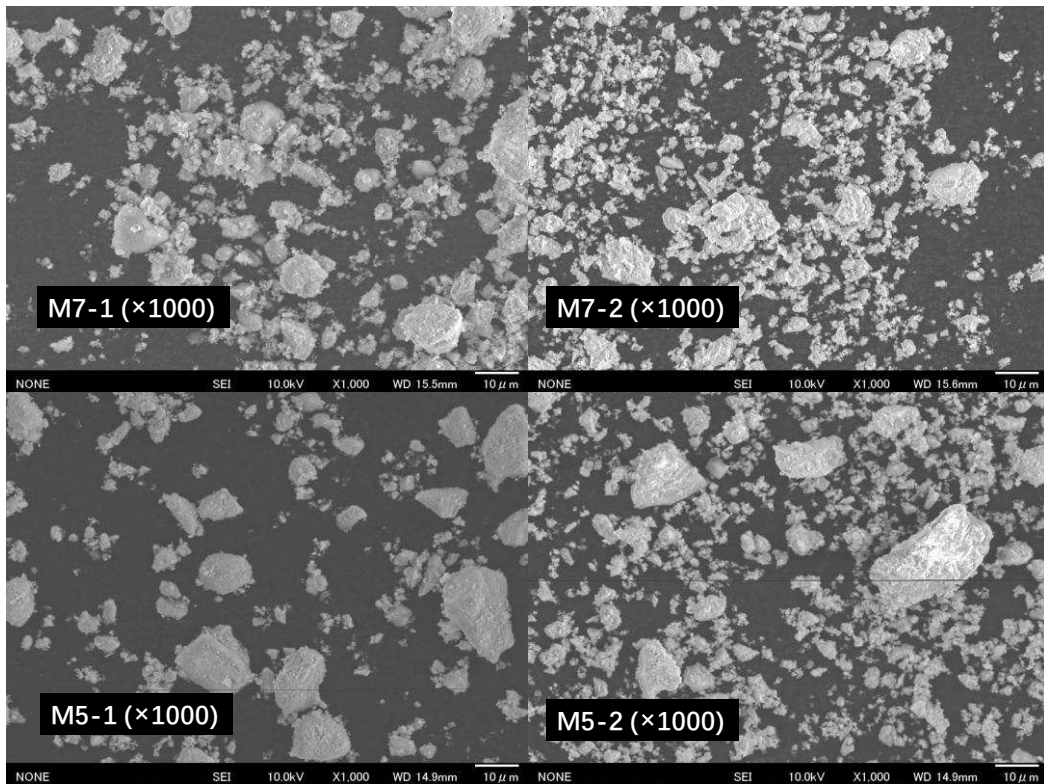


Figure 3-1. Examples of SEM observations of each synthetic ash sample

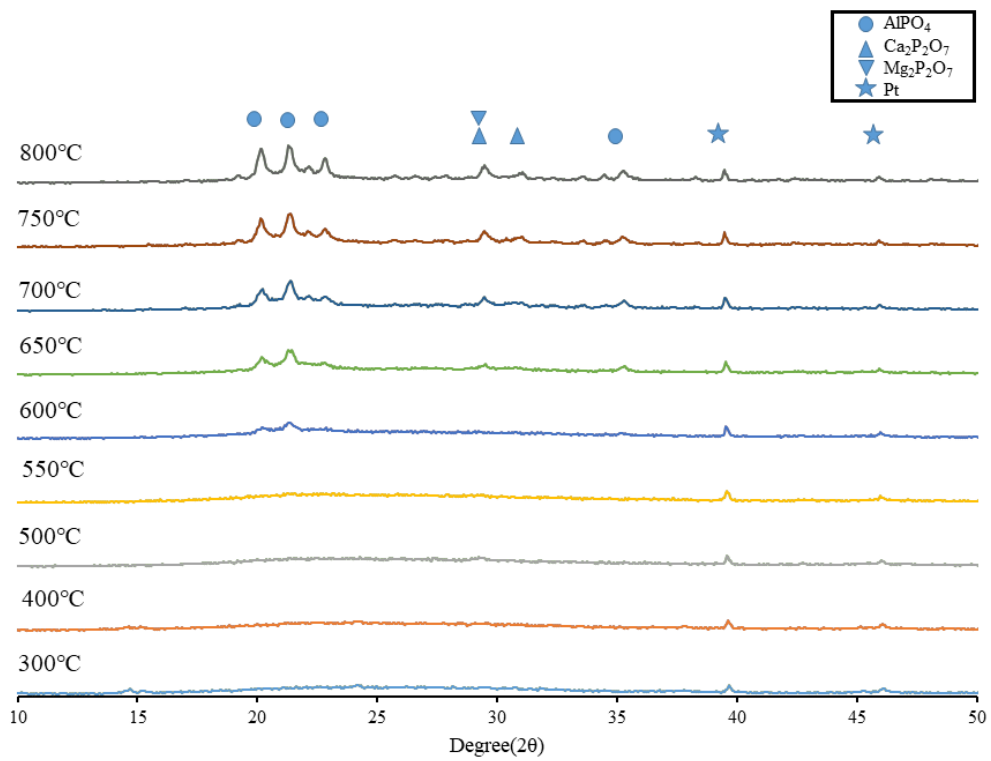


Figure 3-2. Crystal phase detection of M7-1 ash precursors at elevated temperature

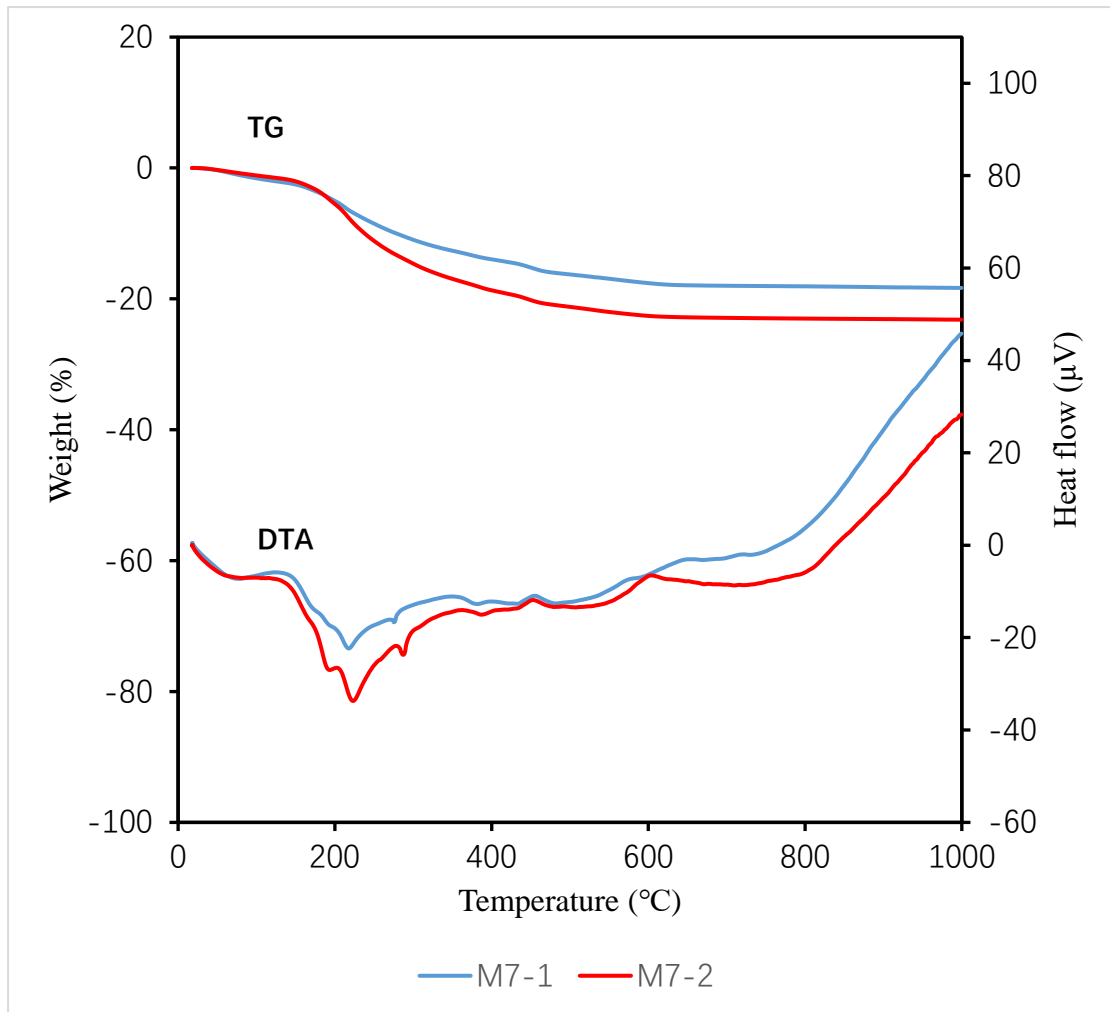


Figure 3-3. TG-DTA curves of M7 ashes precursors at elevated temperature

3.3 Results and discussions

3.3.1 Particle characterization of model ash particles and comparison with real ash

The particle morphology and size distribution of all model ash samples are shown in Figures 3-4 and 3-5. Through control of the grinding and sieving conditions after heat treatment, the morphology and size distribution of the model ash particles were similar with those of the real combustion ash samples.

Based on an EDS analysis of the FE-SEM observation applied to confirm the homogeneity of the elemental distribution in the model ash, Figure 3-6 shows the mapping analysis patterns of M7-1 ash. The distributions of the seven main elements were mostly uniform and no excessive concentrations of a specific element occurred.

The crystal structures of all model samples and their corresponding real ash samples at room temperature as measured using XRD are shown in Figure 3-7. AlPO_4 were strongly detected in all ash samples, CaMgP_2O_7 were observed in the T, M7-1, and M7-2 ashes, and $\text{Ca}_2\text{P}_2\text{O}_7$ peaks were detected in M7-1 and M7-2 ashes. Meanwhile, considering that the Na and K amounts were relatively low in all ash samples, the related crystal phase concerned with alkali metal was not detected through XRD. Because the raw material of SiO_2 was made up of amorphous silica nanoparticles, the peak of the quartz phase in real ash, which was contaminated or generated during the sewage sludge treatment process, was not detected in each model ash type.

TMA results of each ash samples are shown in Figure 3-8. The start shrinking temperatures of S, M7-1 and M7-2 ashes are higher than their corresponding ash samples, T, M7-2 and M5-2, separately. The liner shrinkages of all samples are limited to less than 2% at 800 °C, which suggests that softening characterization of ash samples in this temperature range is not obvious. Tensile strength measurement should be an appropriate method to evaluate the ash adhesion and deposition properties.

3.3.2 Comparison of tensile strength in ash powder bed for real and model ash

To discuss the ash deposition and quantification of ash stickiness at high temperature, the tensile strength of the ash powder bed was characterized using a split-cell type tester. By applying the tensile strength, the stickiness of each ash sample was able to be estimated at each temperature. As phosphorous content is a key element to the adhesive property and aluminum can suppress the adhesiveness of sewage sludge ash (Chapter 2),²⁰ S and M7-1 ashes with higher content of Al₂O₃ and lower content of P₂O₅ showed weaker tensile strengths compared with T and M7-2 ashes at temperatures lower than 800 °C. First, the author confirmed that the tensile strength of the real combustion ash (S and T) at different temperatures can be modified using the seven-element model ash (M7-1 and M7-2) prepared from four pure nanoparticles and three chemical compounds. The tensile strength data of both groups of ashes at different temperatures are shown in Figure 3-9. In the case of M7-1 and S ashes, which chemical composition were almost same, the tensile strength of both ash samples was slightly increased with an increase in temperature from 400 to 700 °C. From 700 °C to 800 °C,

the strengths of both ash samples are significantly increased. The strength of M7-1 was stronger than that of S at 800°C. In the case of M7-2 and T ash, the strengths of both ashes slightly increased from room temperature to 500 °C, and significant increase was observed in the temperature range above 600°C. The strengths of model ashes were always higher than the corresponding real ashes at the same temperatures, at which significant increase of tensile strength was observed, 800°C for M7-1 and S, and from 600 to 800°C for M7-2 and T samples. The reasons why such difference between the strength of model and real ash could be attributed to the synthetic process of model ashes, unlike the generation of real ashes in plants. Model ash particles were prepared from nano-sized raw materials and relatively lower temperature thermal treatment compared with real ashes. In Figure 3-7, quartz phase was observed in S and T ashes, however, was not observed in M7-1 and M7-2 ash. Amorphous SiO₂ phase was remained in model ash, and promoted to generate more slag phase compared with the real ashes. The variation trends of each model ash sample were similar to the corresponding real ash sample.

3.3.3 Effects of Ca and Mg on tensile strength of ash powder bed

Using the model ash preparation process, the tensile strengths of four types of model ash particle bed, M7-1, 2 and M5-1, 2, were prepared and determined at different temperatures, as shown in Figure 3-10. At room temperature, the tensile strength of each sample was almost the same at approximately 0.2 kPa. Until reaching a temperature of 400 °C, the tensile strength of all samples remained at a relatively low

level (< 1.0 kPa). Because slag and liquid phases were not generated among the primary particles, a capillary force caused by the liquid bridges among the particles did not exist, and thus the interactions among the particles were only dominated by the van der Waals force. At 500 °C, the tensile strengths of the M7-1, M7-2, and M5-1 ash types maintained a low tensile strength; however, the data on the M5-2 ash showed an increase to 2.4 kPa. The significant increase in the tensile strength of M7-2 ash was observed at approximately 600 °C (2.42 kPa), which was higher than that of M5-2 ash, but lower than that of M5-1 ash (700 °C, 4.35 kPa). In all ash samples, M7-1 showed almost the weakest tensile strength during the temperature-elevated process as compared with the other ash types, and its strength was significantly promoted at the highest temperature, from 700 °C to 800 °C. Overall, the tensile strength of the model ash types increased with an increase in temperature, but the extent of such increase and the temperatures at which the tensile strength got significant increase are different.

In the vertical comparisons of the M7-1 and M7-2, and M5-1 and M5-2, ash types, the Mg and Ca in the M7 ash were simply replaced using the same molar content of Al. A simple visual method was used to compare the impact of Al and Ca/Mg on the ash stickiness at high temperature. As shown in Figure 3-10, the seven-element based ash types demonstrated a lower tensile strength compared with the corresponding five-element based ash types with excess Al at the same temperature. At this temperature, the low tensile strengths of M7-1 and M5-1 at 400 °C to 600 °C were considered to be dominated by the van der Waals force but not the capillary force promoted by the liquid bridges, and the difference in tensile strength between the two samples was not

remarkable. Because it was estimated that the remarkable increase in tensile strength for each model ash sample at different temperatures was caused by the liquid or slag phase formation between particles, the slag formation temperature of each ash sample was estimated using a thermal equilibrium calculation.

3.3.4 Estimation of tensile strength increasing mechanism of each model ash sample

A thermal equilibrium calculation is a useful method for predicting and explaining the ash behaviors at elevated temperature, and follows the principle of Gibbs free energy minimization. Figure 3-11 shows the prediction of the slag formation and chemical constitution under equilibrium for the model ash types, which represents the potential transformation and reaction trends in the target chemical systems. By using pure raw materials, it is easy to accurately discuss the slag phase formation temperature compared with real combustion ash samples because many trace elements were not included.

In Figure 3-11(a), the slag phase generation started from approximately 778 °C in M7-1. Because a remarkable increase in the tensile strength of M7-1 was observed from 700 °C to 800 °C, it suggests that the slag phase formation between ash particles caused a liquid bridge force among the ash powders. As shown in Figure 3-11(b) for M7-2 ash, the slag phase transformed from other solid phases from 591 °C, which was much lower than that of the M7-1 ash. Because the increase in the tensile strength of M7-2 ash was

also started from 500 °C to 600 °C, the temperature-dependent increase in the tensile strength of M7-2 ash was also able to be explained through this calculation.

By contrast, the calculated slag formation temperature of M5-1 ash was estimated to be 779 °C, as shown in Figure 3-11(c); however, the remarkable increase in the temperature of M5-1 ash was from 600 °C to 700 °, and this model ash sample did not match the calculation results. In the case of M5-2 ash, the slag phase formation temperature is 450 °C, and the tensile strength increased from 400 °C to 500 °C. The temperature at which tensile strength got rapid increase agrees well with the equilibrium calculation results for the slag phase formation temperature in M7-1, M7-2, and M5-2 ash types. Only one mismatch occurred in the case of M5-1 ash at 700 °C, and no slag phase was calculated at this temperature although a rapid increase in tensile strength was observed.

This mismatch might be caused by the inhomogeneity during the ash preparation process from raw nanometer sized particulate materials, and a partial change in the chemical constituent might decrease the formation temperature of the slag phase. As nanoparticles were generally formed aggregates, the inhomogeneity might be generated from remained aggregate structure after general wet mixing process of raw materials. If the author use wet agitation milling process with fine beads, it is possible to disperse aggregate structure, however, the author afraid the effect of contamination from beads and wall on slag phase formation temperature.²⁶ As the previous study by the author's group showed, the generation of a tiny amount of liquid or slag phase can lead to a

strong stickiness of the ash,²⁷ and a remarkable increase in tensile strength might consequently occur at a lower temperature. The verification experiments (morphological change observations) of this assumption are described in the following.

3.3.5 Microscopic observation of model ash particles before and after heat treatment

To verify the formation of molten slag phases in M5-1 ash, SEM images of the model ash at room temperature and after heat treatment at 700 °C under atmospheric pressure were taken using a CC-FE-SEM system equipped with a heating device,²⁸ as shown in Figure 3-12. Using this system, each sample was observed through an FE-SEM under high vacuum condition; however, each sample was also heated under atmospheric pressure in a chamber connected with the FE-SEM. There were no remarkable differences in appearance after heating at 700 °C compared with at room temperature in the M7-1 ash group and no apparent fusion phenomena occurred. By contrast, it can be clearly seen that the morphology of the M7-2 ash changed after heating. At room temperature, there were many tiny-sized particles at spot A and B, but they vanished after treatment at 700 °C and it was considered that the small particles melted and merged into the large particles. The surface of surrounding areas also showed morphological change after heat treatment. At spot C, the shaded gap shrank after heat treatment and some parts of clear boundaries vanished which suggested the partially melt and fusion occurred. The morphology change of M5-2 ash was also

remarkable after heat treatment. Many ash particles fused with each other and the roughness significantly decreased.

It is worth mentioning that the change in morphology after heat treatment can only be observed at a few spots in the M5-1 ash. For example, tiny-sized particles merged with each other and the surface became smooth at spot D at 700 °C, which confirmed the partial melting and deformation of the M5-1 ash. The remarkable increase in the tensile strength of M5-1 ash at 700 °C can be consequently explained by the trace amount of slag phase formation on the ash particles. In brief, these results further confirm the relevance and rationality of the experiments and hypothesis.

3.3.6 Estimation of different compounds in ash deposition control

In brief, the calculated results match and agree well with the experimental results, and therefore the reason why the tensile strength of the ash significantly increases at high temperature can be ascribed to the slag phase formation among the ash particles. Through vertical comparisons between the equilibrium calculation results between the M7-2 and M5-2 ash types, after replacing Ca and Mg with Al, the calculated slag formation temperature decreased and the tensile strength increased at high temperature. In the M7-1 and M5-1 ash groups, although the calculated slag formation temperature is similar, the tensile strength driven by the capillary forces in the M5-1 ash were stronger than those in the M7-1 ash at a high temperature. In general, Ca and Mg are important elements for reducing the tensile strength with Al in phosphorus-rich ash.

Alumina powder was proven to suppress the adhesion potential of sewage sludge ash at high temperature in the previous study (Chapter 2).²⁰ In this chapter, the author found that Ca and Mg achieve a better performance in terms of deposition control of phosphorus-rich sewage sludge ash with Al. Despite this, Al₂O₃ powder is still a recommended additive at the industrial scale. Al₂O₃ powder has a better universality than Ca or Mg products because calcium and magnesium only work under certain phosphorus-rich conditions. In addition, considering its availability and chemical stability, Al₂O₃ should be a better choice of additive.

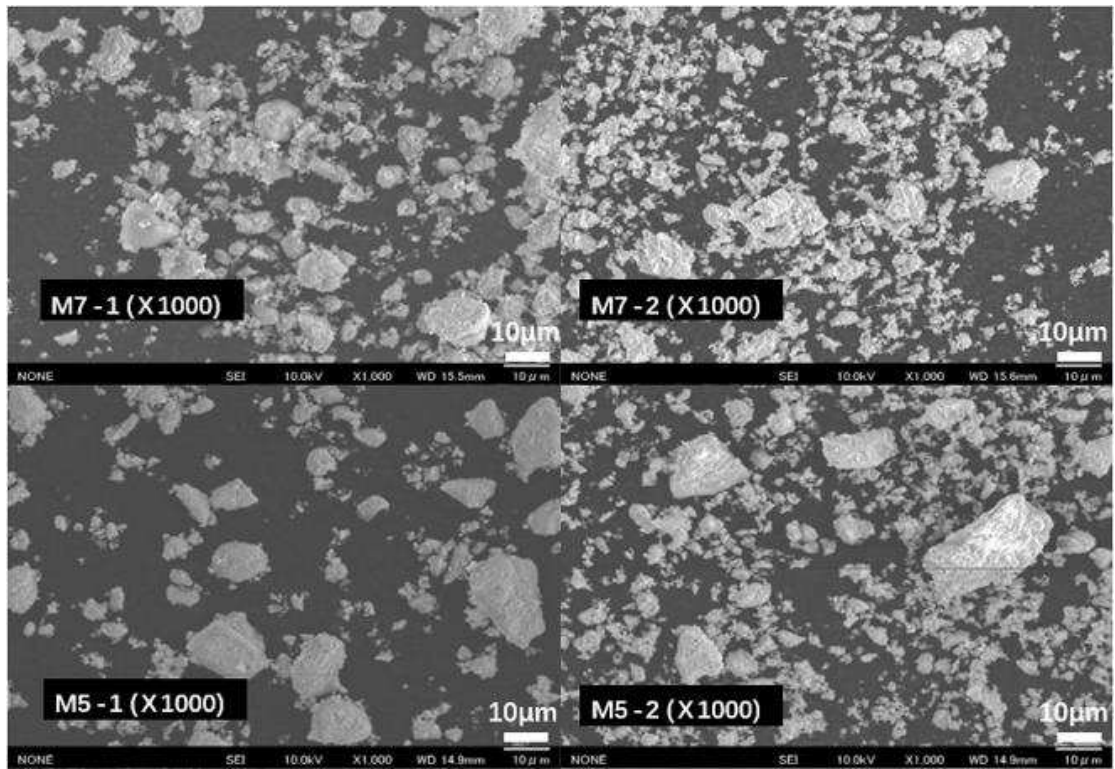
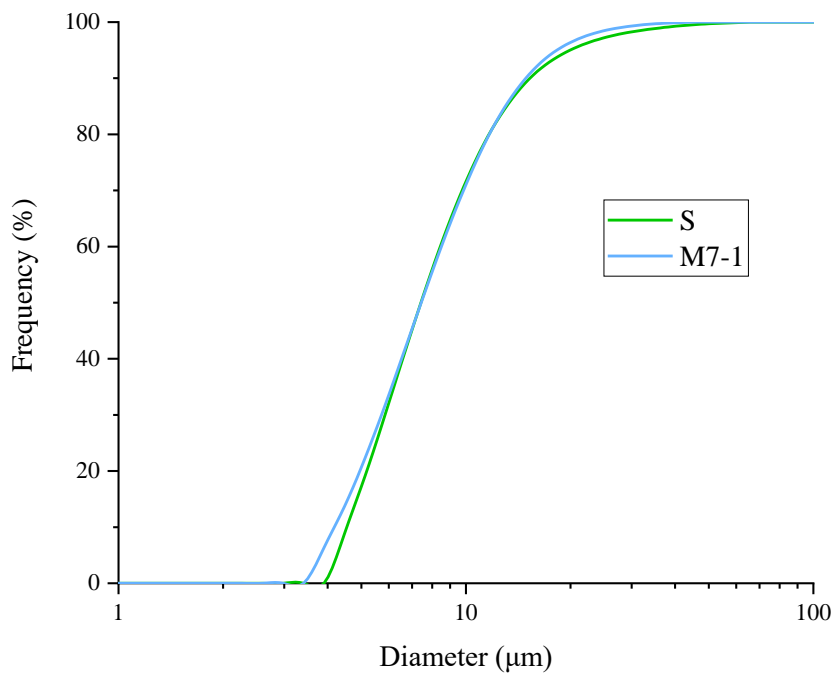
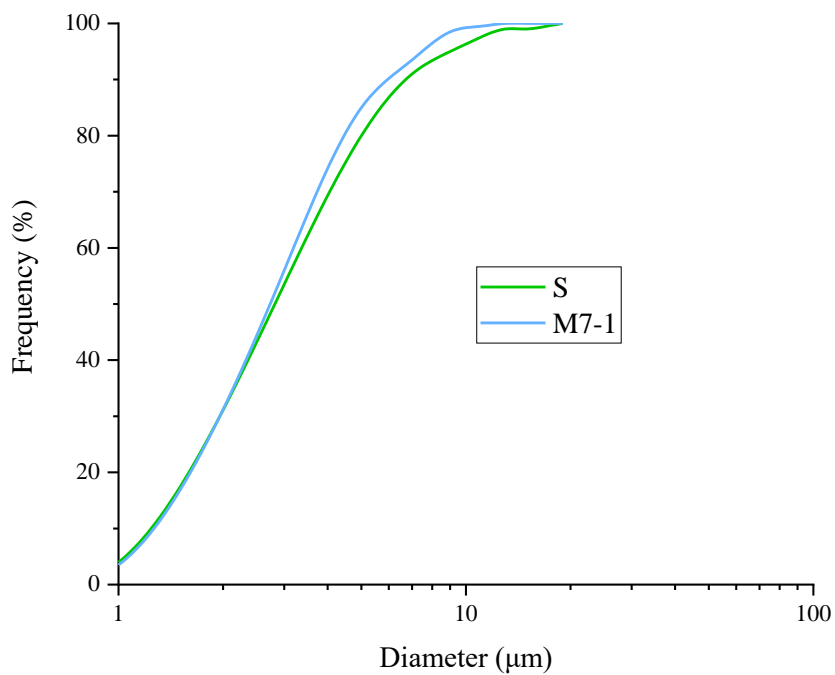


Figure 3-4. Examples of SEM observations of each synthetic ash sample.



(a) Laser diffraction method



(b) Image Processing of FE-SEM observation

Figure 3-5. Number based cumulative size distribution of S-2 and M7-1 samples. (a) Laser diffraction used air flow cell, (b) Image Processing of SEM observation.

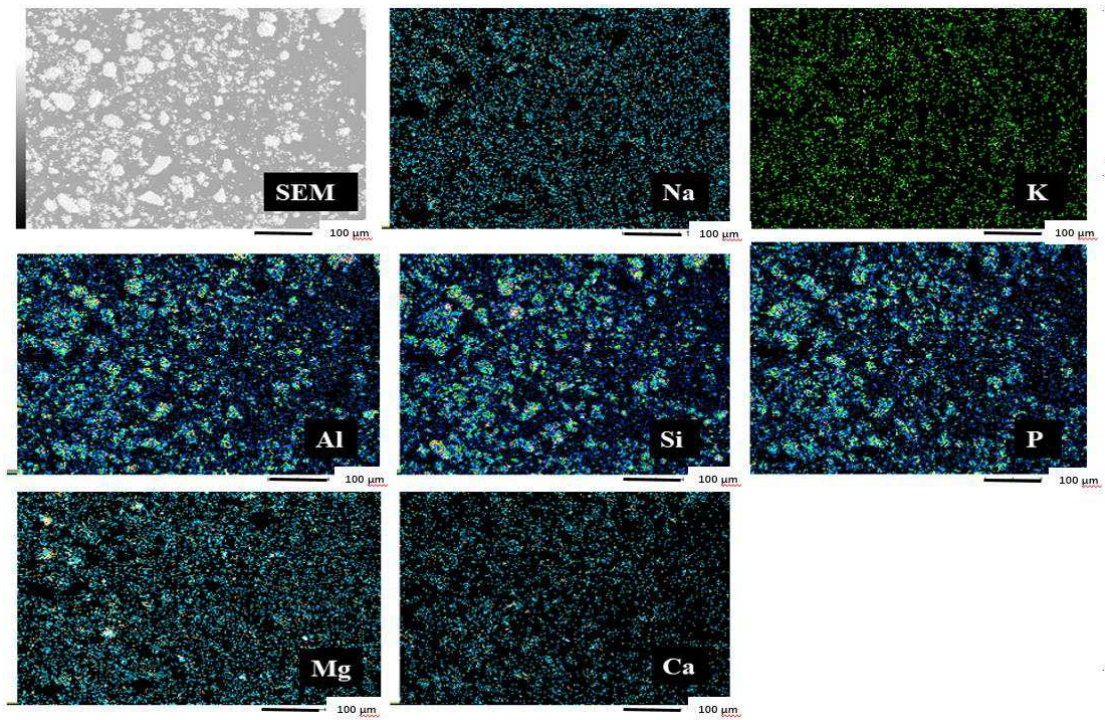
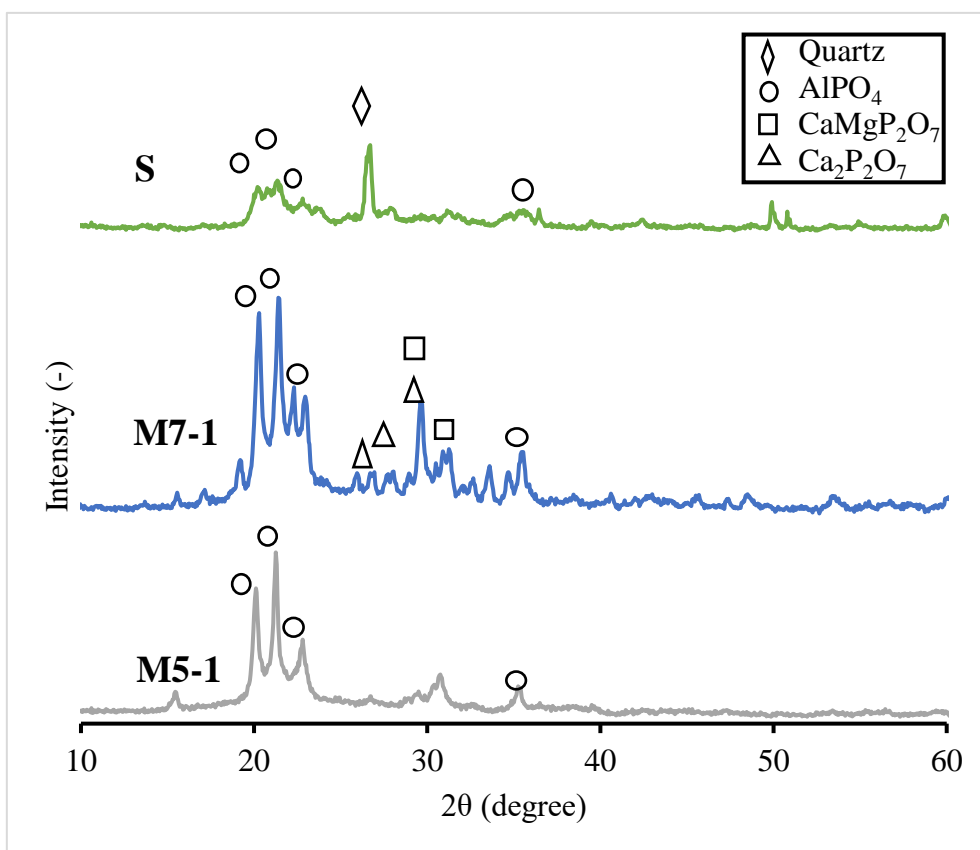
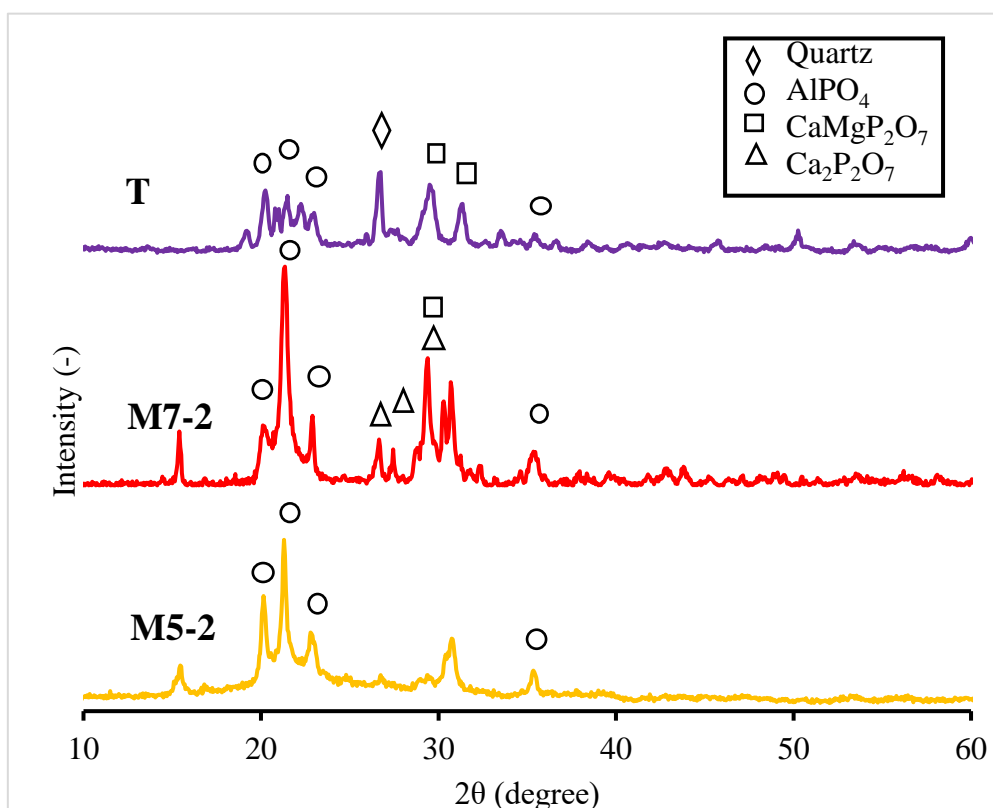


Figure 3-6. Element distribution analysis of 7-element based synthetic ashes using EDS mapping system (M7-1)



(a) S, M7-1 and M5-1 ashes



(b) T, M7-2 and M5-2 ashes

Figure 3-7. XRD patterns of model ashes and real ashes at room temperature.

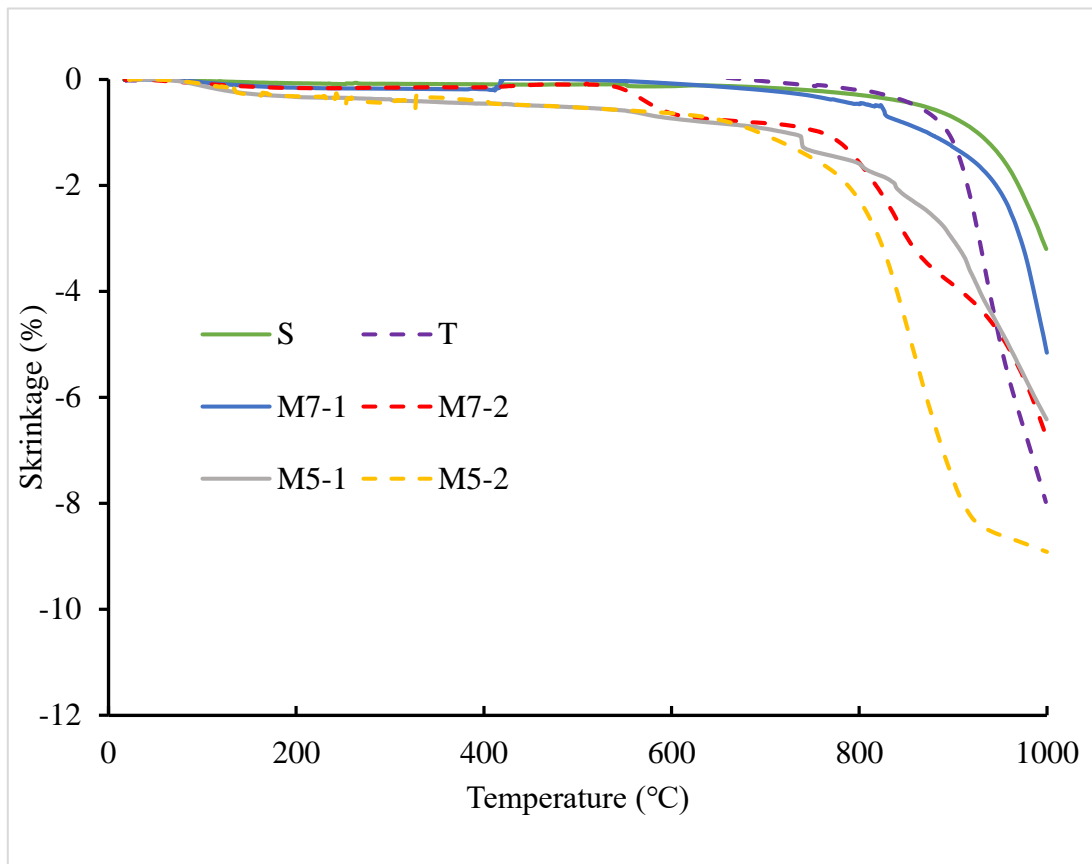


Figure 3-8. Thermomechanical analysis (TMA) curves of all ash samples at elevated temperature.

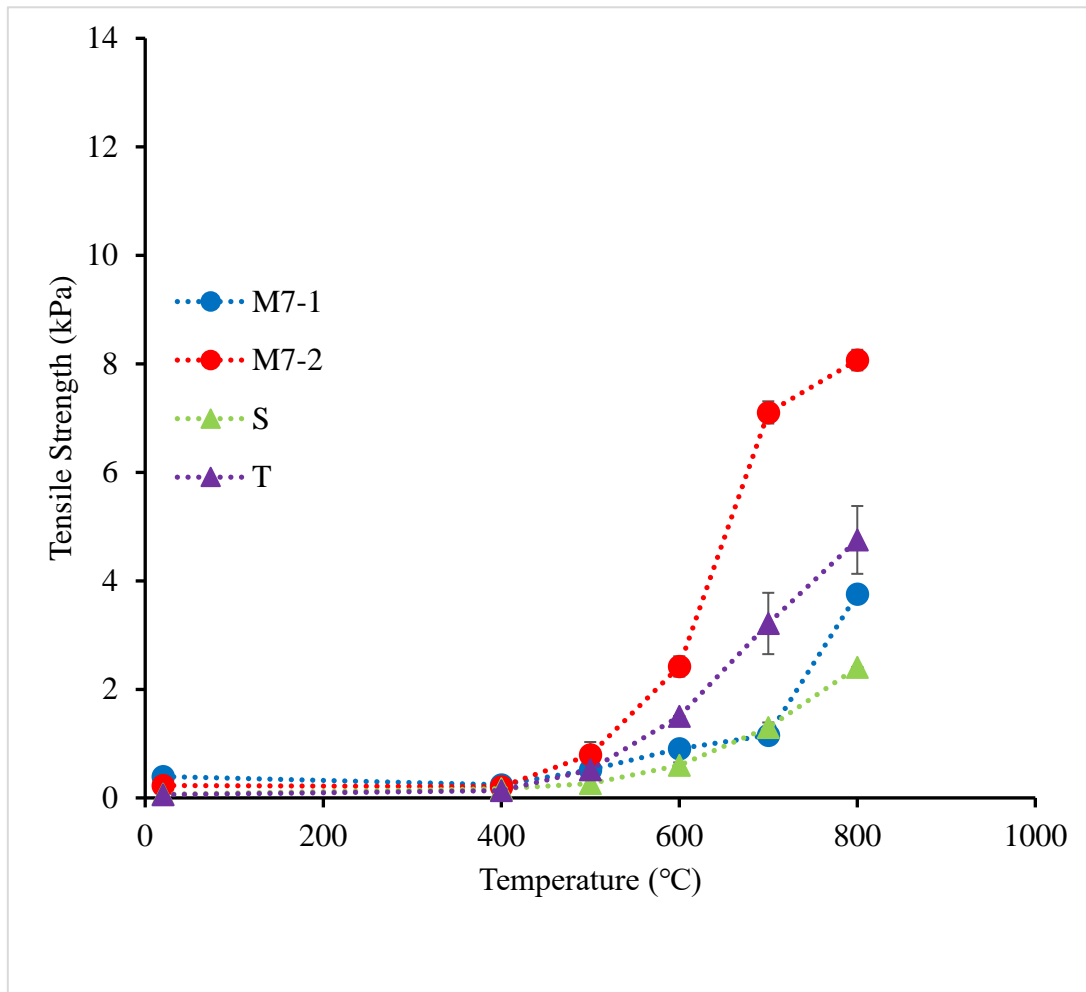


Figure 3-9. Tensile strengths of M7 series ashes and real ashes at various temperatures.

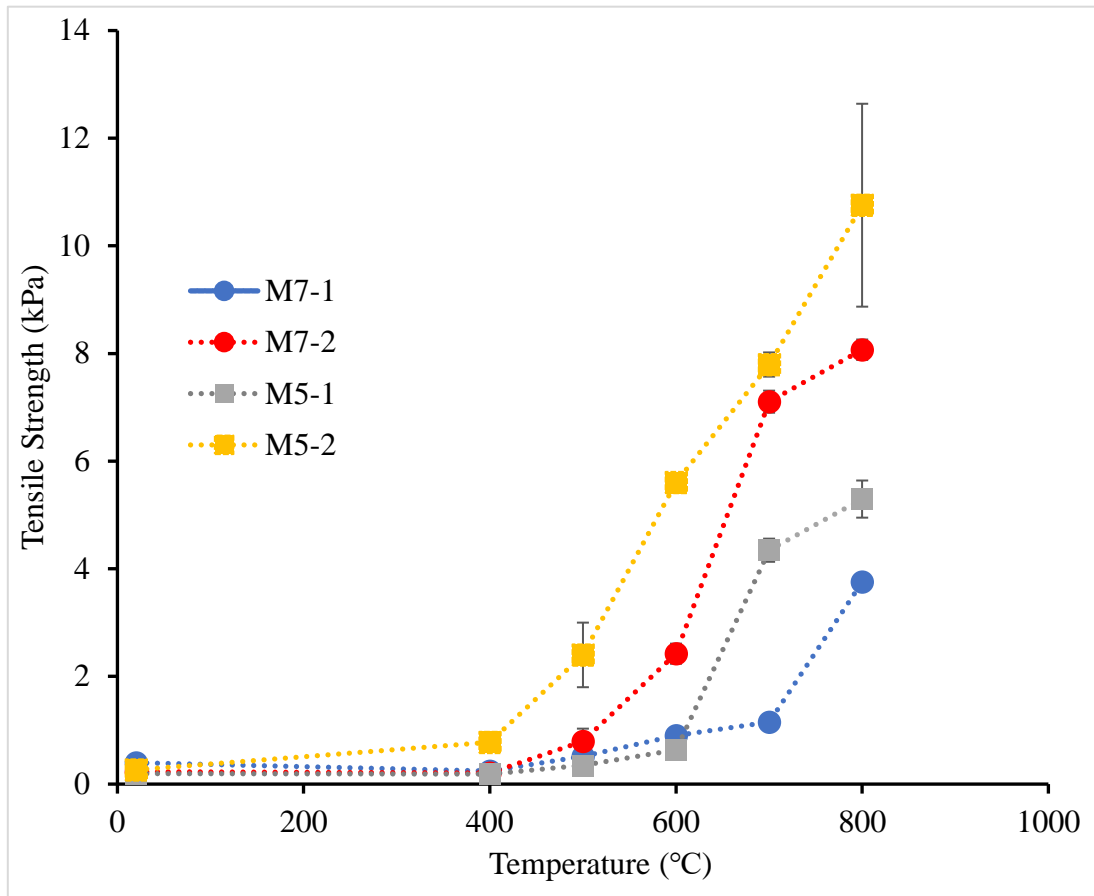
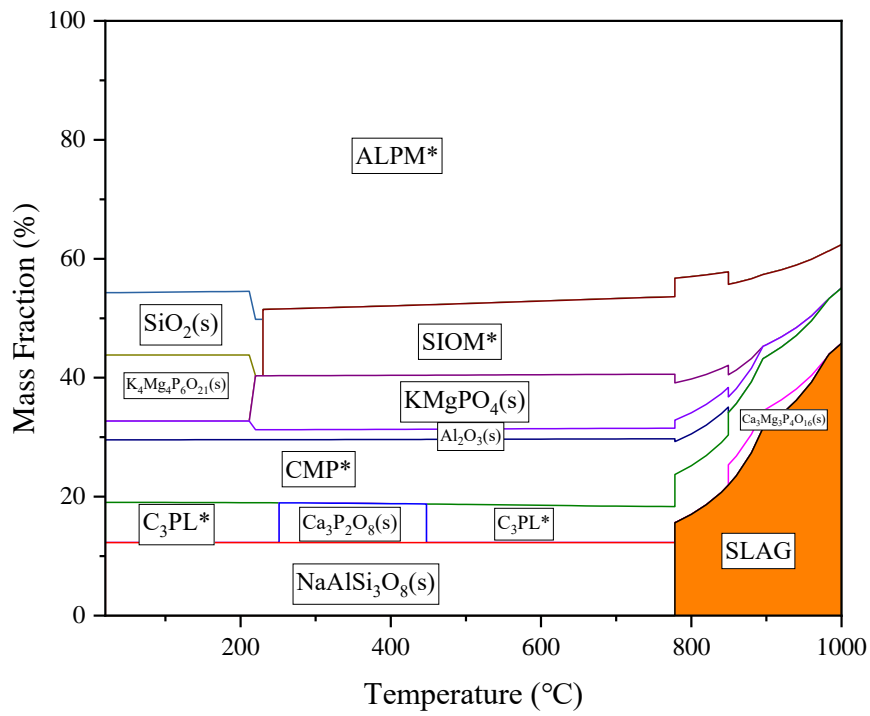
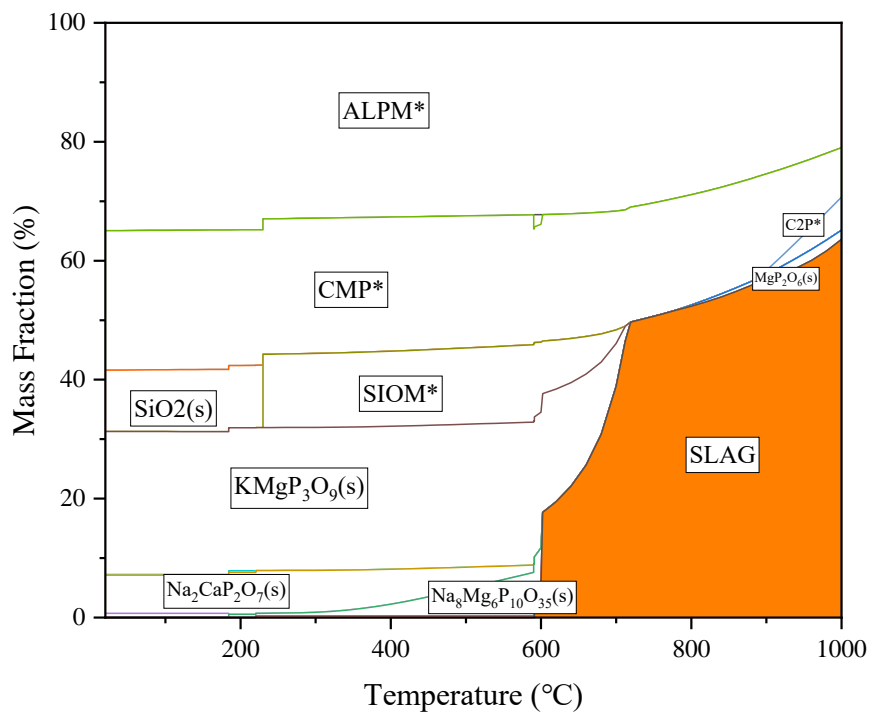


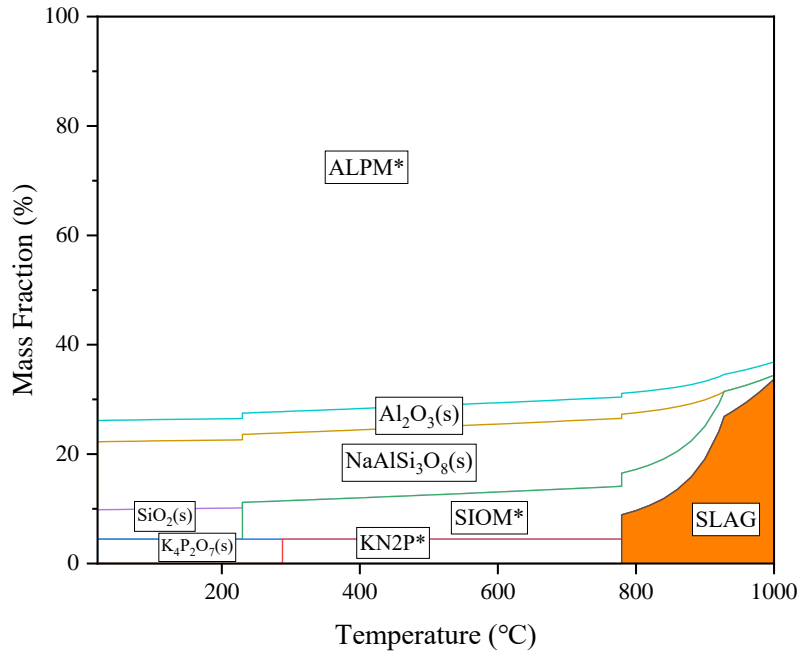
Figure 3-10. Tensile strengths of model ashes at various temperatures.



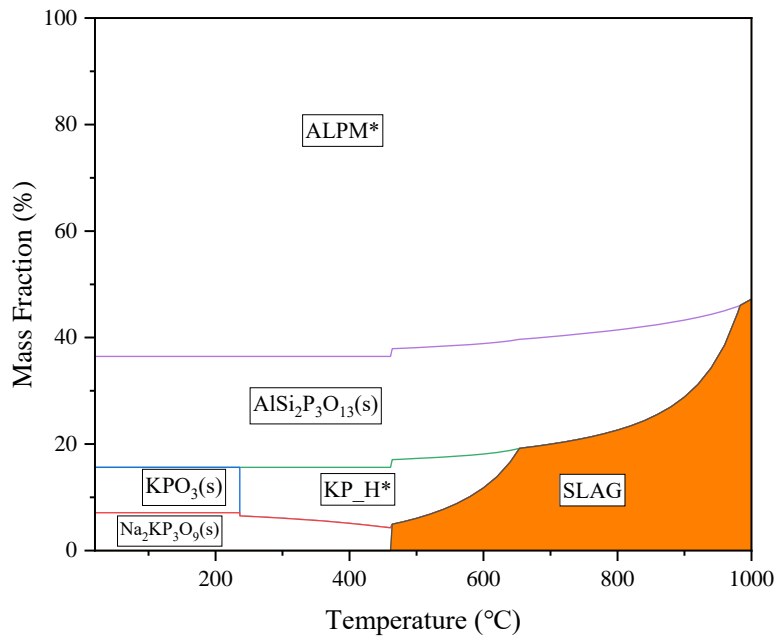
(a) M7-1 ash



(b) M7-2 ash



(c) M5-1 ash



(d) M5-2 ash

Figure 3-11. Results of thermal equilibrium calculations for model ash samples using 'GTOX' database.

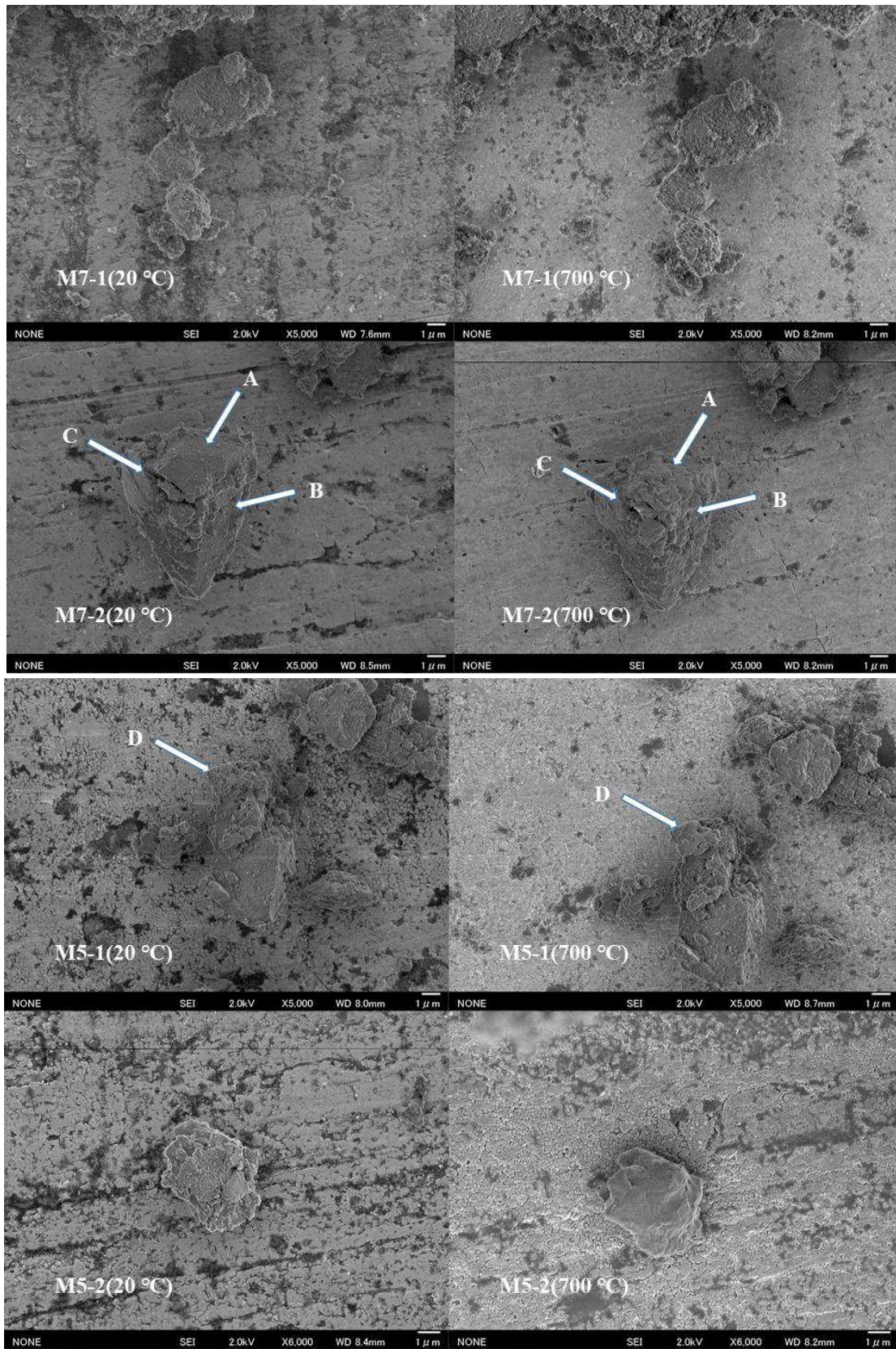


Figure 3-12. Morphology change of synthetic model ashes before and after heat treatment using high temperature FE-SEM system.

3.4 Conclusions

1. A method of synthesizing sewage sludge combustion ashes was proposed and the synthesized model ashes can modify the stickiness of real ashes to some extent.

2. Since the rationality and effectiveness of this synthetic method, it became possible to research on the effect of specific elements on the deposition phenomena of ashes at high temperature by controlling the concentration of specific elements in model ashes.

3. By using the model ash system, it was found that Mg and Ca have a better performance in resistance of slag phase generation compared to Al in the high phosphorus concentration sewage sludge ashes.

3.5 References

1. Magdziarz, A.; Wilk, M.; Gajek, M.; Nowak-Wozny, D.; Kopia, A.; Kalembe-Rec, I.; Kozinski, J. A., Properties of ash generated during sewage sludge combustion: A multifaceted analysis. *Energy* **2016**, *113*, 85-94.
2. Werther, J.; Ogada, T., Sewage sludge combustion. *Progress in Energy and Combustion Science* **1999**, *25* (1), 55-116.
3. Manara, P.; Zabaniotou, A., Towards sewage sludge based biofuels via thermochemical conversion—a review. *Renewable and Sustainable Energy Reviews* **2012**, *16* (5), 2566-2582.
4. Kijo-Kleczkowska, A.; Środa, K.; Kosowska-Golachowska, M.; Musiał, T.; Wolski, K., Mechanisms and kinetics of granulated sewage sludge combustion. *Waste Management* **2015**, *46*, 459-471.
5. Li, W.; Li, W.; Liu, H.; Yu, Z., Influence of sewage sludge on the slurryability of coal–water slurry. *Fuel* **2009**, *88* (11), 2241-2246.
6. Donatello, S.; Cheeseman, C. R., Recycling and recovery routes for incinerated sewage sludge ash (ISSA): A review. *Waste Management* **2013**, *33* (11), 2328-2340.
7. Murakami, T.; Suzuki, Y.; Nagasawa, H.; Yamamoto, T.; Koseki, T.; Hirose, H.; Okamoto, S., Combustion characteristics of sewage sludge in an incineration plant for energy recovery. *Fuel Processing Technology* **2009**, *90* (6), 778-783.
8. Wilk, M.; Magdziarz, A.; Kalembe, I., Characterisation of renewable fuels' torrefaction process with different instrumental techniques. *Energy* **2015**, *87*, 259-269.
9. Folgueras, M. B.; Díaz, R. M.; Xiberta, J.; Prieto, I., Thermogravimetric analysis of the co-combustion of coal and sewage sludge. *Fuel* **2003**, *82* (15-17), 2051-2055.
10. Judex, J. W.; Gaiffi, M.; Burgbacher, H. C., Gasification of dried sewage sludge: status of the demonstration and the pilot plant. *Waste Management* **2012**, *32* (4), 719-723.
11. Hupa, M., Ash-related issues in fluidized-bed combustion of biomasses: recent research highlights. *Energy&Fuels* **2011**, *26* (1), 4-14.
12. Obernberger, I.; Brunner, T.; Bärnthaler, G., Chemical properties of solid biofuels—significance and impact. *Biomass and Bioenergy* **2006**, *30* (11), 973-982.
13. Wang, C.; Feng, S.; Wang, P.; Li, X.; Zou, L., Distribution of phosphorus fractions and bio-available phosphorus forms and their relationships in sewage sludge. *Huan jing ke xue= Huanjing kexue* **2008**, *29* (6), 1593-1597.
14. Bie, R.; Li, S.; Zhao, Y.; Yang, L., Investigation on the control of agglomeration during fluidized-bed incineration of wastewater containing alkali metal salts. *Energy&Fuels* **2009**, *23* (9), 4304-4310.
15. Miles, T. R.; Miles Jr, T. R.; Baxter, L. L.; Bryers, R. W.; Jenkins, B. M.; Oden, L. L., Boiler deposits from firing biomass fuels. *Biomass and Bioenergy* **1996**, *10* (2-3), 125-138.
16. Kamiya, H.; Kimura, A.; Tsukada, M.; Naito, M., Analysis of the high-temperature cohesion behavior of ash particles using pure silica powders coated with alkali metals. *Energy&Fuels* **2002**, *16* (2), 457-461.
17. Beck, J.; Müller, R.; Brandenstein, J.; Matscheko, B.; Matschke, J.; Unterberger, S.; Hein, K. R., The behaviour of phosphorus in flue gases from coal and secondary fuel co-combustion. *Fuel* **2005**, *84* (14-15), 1911-1919.
18. Wang, L.; Skjevrak, G.; Hustad, J. E.; Grønli, M. G., Sintering characteristics of sewage sludge ashes at elevated temperatures. *Fuel Processing Technology* **2012**, *96*, 88-97.

19. Lindström, E.; Sandström, M.; Boström, D.; Öhman, M., Slagging characteristics during combustion of cereal grains rich in phosphorus. *Energy&Fuels* **2007**, *21* (2), 710-717.
20. Gao, J.; Matsushita, M.; Horiguchi, G.; Fujii, R.; Tsukada, M.; Okada, Y.; Kamiya, H., Toward Stable Operation of Sewage Sludge Incineration Plants: The Use of Alumina Nanoparticles to Suppress Adhesion of Fly Ash. *Energy&Fuels* **2019**.
21. Pronobis, M., Evaluation of the influence of biomass co-combustion on boiler furnace slagging by means of fusibility correlations. *Biomass and Bioenergy* **2005**, *28* (4), 375-383.
22. Bostrom, D.; Skoglund, N.; Grimm, A.; Boman, C.; Ohman, M.; Brostrom, M.; Backman, R., Ash transformation chemistry during combustion of biomass. *Energy&Fuels* **2011**, *26* (1), 85-93.
23. Yang, X.; Ingham, D.; Ma, L.; Srinivasan, N.; Pourkashanian, M., Ash deposition propensity of coals/blends combustion in boilers: a modeling analysis based on multi-slagging routes. *Proceedings of the Combustion Institute* **2017**, *36* (3), 3341-3350.
24. Zhang, Q.; Liu, H.; Qian, Y.; Xu, M.; Li, W.; Xu, J., The influence of phosphorus on ash fusion temperature of sludge and coal. *Fuel Processing Technology* **2013**, *110*, 218-226.
25. Kamiya, H.; Kimura, A.; Yokoyama, T.; Naito, M.; Jimbo, G., Development of a split-type tensile-strength tester and analysis of mechanism of increase of adhesion behavior of inorganic fine powder bed at high-temperature conditions. *Powder Technology* **2002**, *127* (3), 239-245.
26. Takebayashi, K.; Sasabe, S.; Iijima, M.; Kamiya, H., Surface modification and dispersion of gas phase synthesized oxide composite nanoparticles in organic solvent by agitation milling process with small beads. *Journal of the Society of Powder Technology, Japan* **2010**, *47* (5), 310-316.
27. Horiguchi, G.; Fujii, R.; Yamauchi, Y.; Okabe, H.; Tsukada, M.; Okada, Y.; Kamiya, H., Toward Stable Operation of Coal Combustion Plants: The Use of Alumina Nanoparticles To Prevent Adhesion of Fly Ash. *Energy&Fuels* **2018**, *32* (12), 13015-13020.
28. Tsukada, M.; Yamada, H.; Kamiya, H., Analysis of biomass combustion ash behavior at elevated temperatures. *Advanced Powder Technology* **2003**, *14* (6), 707-717.

CHAPTER 4

**Direct measurement of single-particle adhesion behaviors on
metal surfaces at high temperatures**

CHAPTER 4

Direct measurement of single-particle adhesion behaviors on metal surfaces at high temperatures

4.1 Introduction

In Chapter 2 and Chapter 3, the author researched on the deposition phenomena of sewage sludge ashes using real ash and model ash samples. The main method to evaluate the adhesiveness of sewage ashes was using the tensile strength tests on ash bulks. Meanwhile, the author discussed the roles of specific main elements in ashes on the adhesion properties such as Al, P, Ca and Mg, based on the experimental results, additives which can suppress the deposition phenomena were proposed. In ash combustion deposition issues, coal ash is another main object, based on the experimental methods and some results in Chapter 2 and 3, the author tried to research on the adhesion behavior of single-particle on a metal surface using a new adhesion evaluation method, which may contribute to the fundamental researches of ashes behaviors.

Adhesion and deposition phenomena of ash particles at high temperatures on the walls of super heaters and heat exchangers prevent the long and stable operation of power generation systems by coal, waste, and biomass combustion and gasification systems. In order to analyze and discuss the increasingly prevalent mechanism of ash particle adhesion at high temperatures and develop a technology for ash adhesion

prevention, characterization methods for ash adhesion behavior at high temperatures are necessary. Conventional analysis methods are available to characterize the ash samples which contain tensile strength tests of ash powder beds,¹⁻³ dilatometry tests on ash powder pellet fracture⁴⁻⁵ and laboratory scale filtration tests to evaluate ash adhesion to filters.⁶⁻⁹ These tests have been performed using ash samples from a variety of fuels. Each method was able to characterize the adhesion force between particles or ceramic filter surfaces.

The acknowledged mechanisms of deposition involve many routes: ash particles move to and collide with the surface of the deposition area due to inertia effects, thermophoretic forces, and other mechanisms.¹⁰⁻¹² During the accumulation and growth of the deposited ash layers, the impaction and capture efficiency of fly ash particles on the surface of a superheater are affected by many factors such as particle density, velocity, and melt conditions of adhered particles.¹³⁻¹⁴ To investigate the ash adhesion behavior on the surface of superheaters and heat exchangers, fundamental studies about interactions and behaviors between individual particles and the surface of a target plate in high-temperature conditions are necessary to provide a more comprehensive understanding of the mechanism of particle adhesion.

In the previous work of author's group, a system which can directly measure the adhesion force of particles with a diameter of 1 mm and greater under high-temperature conditions was designed and developed.¹⁵ However, the measurable size of single particles of the system was much larger than the ash particles generated in a real

combustion condition, which are on the order of 10 μm in magnitude. In contrast, atomic force microscope (AFM) techniques with colloidal probes¹⁶⁻¹⁷ can be used to measure forces on particles with diameters in range of 1 to 50 μm ; however, the operation temperature range is usually limited up to 250 $^{\circ}\text{C}$ in ambient conditions.¹⁸ Therefore, a force measurement system which can consider both, the small particle size and high-temperature conditions, is required to determine the adhesion force of a single ash particle. Previously, a high-resolution measurement system capable of determining the adhesion force between a single particle around 10 μm in diameter and a flat plate at elevated temperatures up to 1000 $^{\circ}\text{C}$ was developed.¹⁹

Compared to sewage sludge ashes, the operation temperatures of coal combustion in real plants are usually higher, reaching to 1000 $^{\circ}\text{C}$ and higher. The morphology of coal combustion ash particles usually shows spherical shapes with smooth boundaries rather than irregular shape. Therefore coal combustion ash particles are more suitable for the direct measurement of adhesion force on single particle compared with sewage sludge ash samples. In this study, using the measurement system described, two kinds of model and modified ash particles were prepared and tested to investigate the effect of various experimental conditions, such as temperature, compressive force, chemical composition, and compression speed, on the adhesion forces between single ash particles and smooth stainless steel plate surfaces at different temperatures. Based on these results, the author discuss the first ash adhesion mechanism of a single particle on a metal plate.

4.2 Experimental

4.2.1 Preparations of ash samples

To determine the influence of factors for the adhesion force of one particle on a metal plate, spherical particles are required. First, the author attempted the synthesis of simplified model ash particles to represent the basic modes of fly ash adhesion. Silica and alkali metals generate eutectic materials with low melting points, which could result in serious depositions.^{2, 20} This phenomenon is one of the main mechanisms related to ash adhesion and deposition issues. Based on this mechanism, model ash particles composed of silica powders and alkali metals were prepared as experimental materials.

Model ash particles were prepared using high-purity fused silica particles with alkali metal addition. Silica particles (FB-74) were manufactured by Denka Company. $(\text{COONa})_2$ and $(\text{COOK})_2 \cdot \text{H}_2\text{O}$ were used as the source of sodium and potassium, and the mass fractions of sodium and potassium in the model ash samples were both set to 0.5 wt%. $(\text{COONa})_2$ and $(\text{COOK})_2 \cdot \text{H}_2\text{O}$ were dissolved in distilled water to prepare a solution, following which high-purity fused silica powders were added into the solution and mixed for 1 min using a planetary centrifugal mixer (Thinky, MX-201) to form a homogeneous slurry. After even mixing, the slurry was transferred to a mortar and placed in a drying machine (Nitto Kagaku, NHK-170). The slurry was stirred with a spatula every 10 min to maintain a homogeneous state in the drying process until it was completely dried out. Subsequently, the precursor was crushed and grinded with a spatula and a pestle, then heated at 630 °C for 1 h in an electric furnace to decompose

and remove organic components of the oxalates, yielding the model ash. The morphology of the model ash particles is shown in Figure 4-1.

Coal ash particles were prepared by the combustion of pulverized coals in a drop tube furnace (DTF). The schematic of the drop tube furnace is shown in Figure 4-2. The original coals, with approximately 13 wt% of ash content (Table 4-1), were processed into powders whose mean diameter was under 150 μm before combustion, and then were fed into the top of DTF. The highest temperature at combustion zone of DTF was about 1400 $^{\circ}\text{C}$ and the average residence time of fuel in the reaction zone was about 4.36s, all inorganic ash contents in coal was once melted and then cooled. Detailed information of combustion conditions are listed in Table 4-2. After combustion treatment in the furnace tube, the generated ash particles were collected with a thimble filter by air suction.

CaO is often considered as a kind of desulfurizer in coal combustion.²¹ However calcium, an alkaline-earth metal, similar to alkali metals, can react with silicon and generate eutectic phases, thereby promoting ash deposition.²² The product after desulfurization, calcium sulfate, also influences the slagging and deposition on convection heating surfaces.²³ However, in some other cases, the melting points of ashes show a tendency to decrease initially and then increase with increasing alkaline-earth metal content.²⁴⁻²⁵ In order to analyze the effect of calcium compound addition into ash particles on the adhesion behavior, 5 or 10 wt% CaO particles (Chichibu Sekkai Co. Ltd., mean particle diameter: 2.5 μm) were added into pulverized coal and mixed

by a planetary centrifugal mixer for 3 min. Ash particles containing Ca were prepared by a drop tube furnace with the same combustion conditions as ash particles without CaO addition. Scanning electron microscope (SEM) images of the prepared ash particles with different Ca contents are shown in Figure 4-3.

4.2.2 Characterization of ash samples

Thermomechanical analysis (TMA) was utilized to measure the shrinkage behavior of each ash particle bulk in elevated temperature conditions. Using shrinkage curves, the deformation behavior at the contact points between particles was discussed at different temperatures.

Morphology observations and size distributions of the ash particles were obtained using the FE-SEM system (JEOL Co., JED-2200F) and image processing. Size distributions were also measured using a laser-scattering particle size distribution analyzer (Horiba, LA-950ND) under wet conditions as shown in Figure 4-4. Chemical compositions of tested sample particles were examined using an energy dispersive spectrometer (EDS) system (JEOL Co., JED-6335F), results of example particles are shown in Figure 4-5, which agree with the pre-designed chemical compositions of ash samples in general. Meanwhile, to identify the effect of high temperature condition on the chemical compositions of ash samples, EDS results of coal ash sample after 950 °C for 30 min were also listed in Table 4-1. Results showed that the heat treatment under 950 °C would hardly change the chemical compositions of coal ash samples.

4.2.3 Schematic of adhesion force measurement system

Figure 4-6(a) shows the schematic of the adhesion force measurement system between single spherical particles and a steel surface. This system primarily contains five parts including a Nano-stage (Nippon Laser & Electronic) with a linear motor that controls the displacement of the stage in the nanoscale, a quartz rod equipped on the Nano-stage for mounting the measured particle, a quartz glass blade spring with a polished SUS310S flat plate, a displacement transducer (Mitz, Nanometric Sensor 613A), and an infrared heating system (Thermo Riko, GA 198).

Prior to measurements, a spherical particle was mounted on the top of the quartz glass rod with $\gamma\text{-Al}_2\text{O}_3$ nanoparticles as a binder, by a micromanipulator (Shimadzu, MMS-77) with a video microscope, which was used to prepare a colloidal probe for atomic force microscopy.¹⁹ Details on the preparation process of the single-particle-mounted quartz glass rod are shown in Figure 4-6(b). Firstly, a dense suspension binder of the $\gamma\text{-Al}_2\text{O}_3$ nanoparticle with a polymer dispersant was used to cover the surface of the top of the glass rod, where a model or modified single ash particle was then picked up. The alumina nanoparticle binder was dried in an oven and treated in a furnace at 800 °C to sinter the alumina particles in the binder and fix the single particle at the top of the quartz rod as shown in Figure 4-7.

The quartz glass rod with a single particle was mounted on the measurement system as shown in Figure 4-6(a). The single particle on the top of the rod was positioned very close to the SUS plate initially. After elevating to the target temperature using an

infrared ray heater, the particle moved to the plate at a set speed driven by the Nano-stage until it reached a target compression force, determined by the deflection of the blade spring. Then, the particle moved backwards to detach from the plate at the same velocity. The adhesion force between the particle and plate was also determined by the maximum deflection of the blade spring during detachment. Figure 4-8 presents an example of signal variation detected by the displacement transducer in one measurement process including compression and detachment. The resolutions for the displacement and force measurements between a particle and the plate are 0.1 μm and 60 nN, respectively.

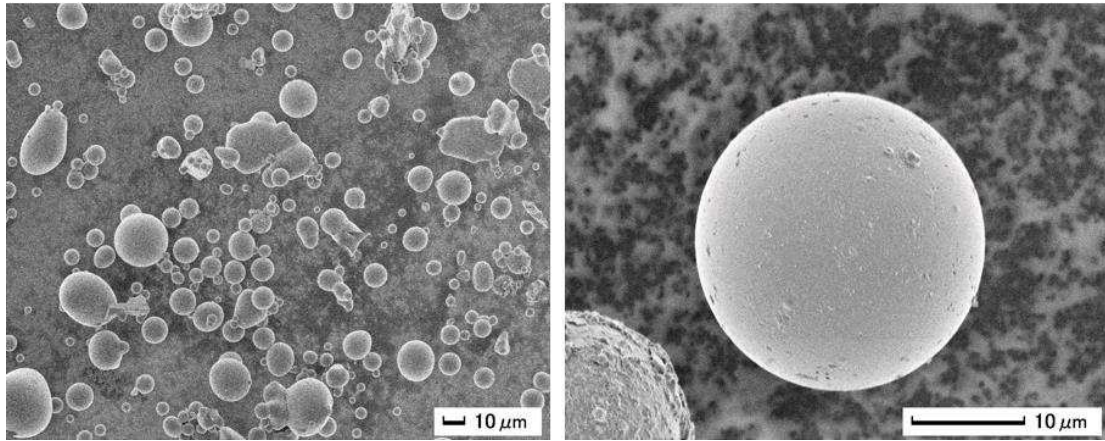


Figure 4-1. Morphology observation of model ash sample prepared from pure silica particles and alkali compounds.

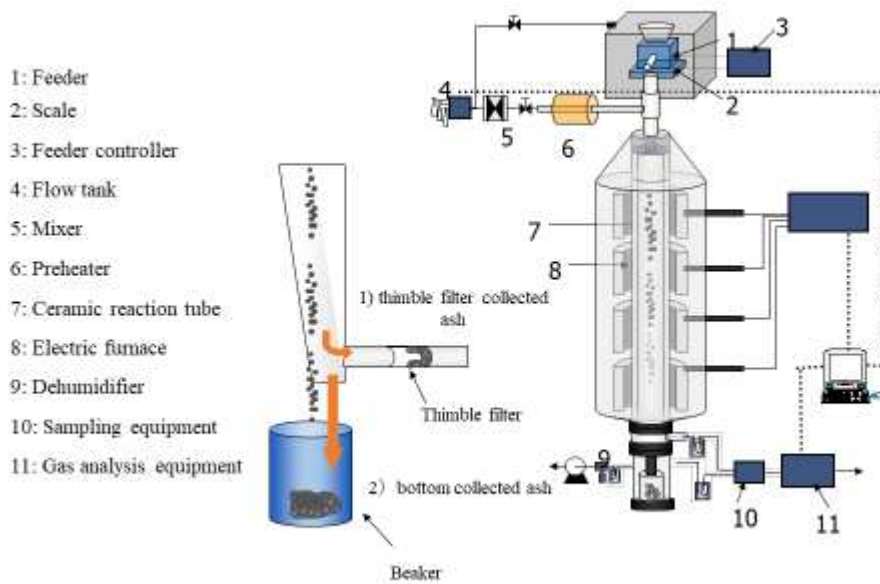


Figure 4-2. Schematic of a drop tube furnace for coal ash preparation to modify pulverized coal combustion conditions.

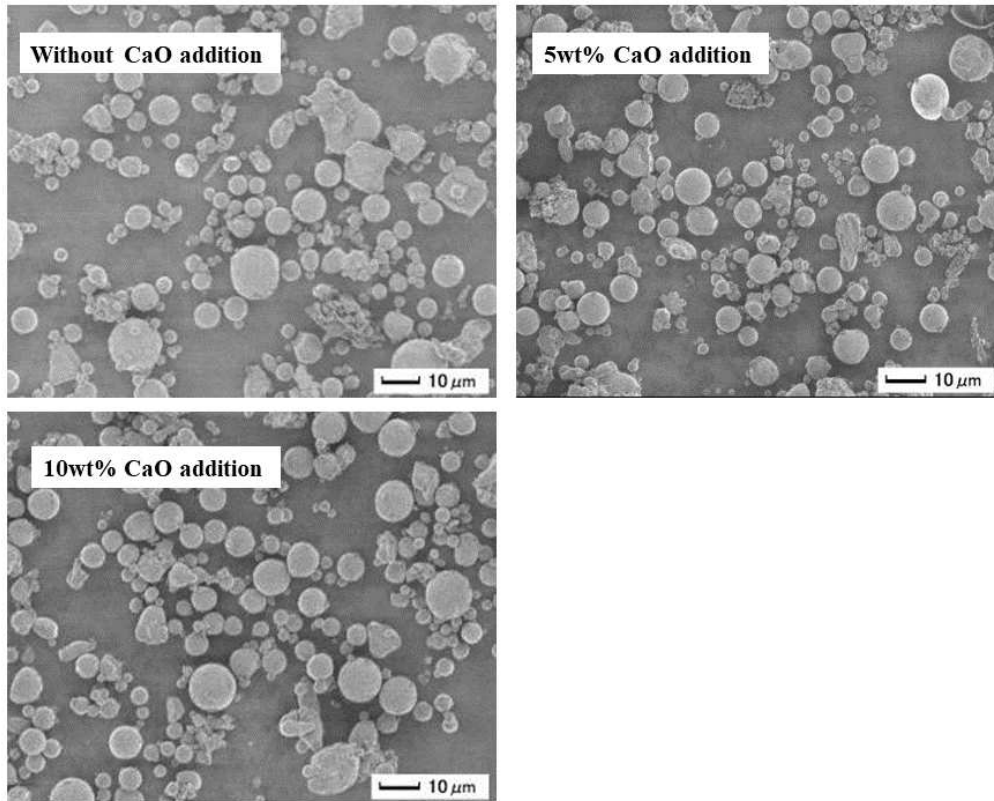


Figure 4-3. SEM observation of prepared ash particles with different Ca content by drop tube furnace.

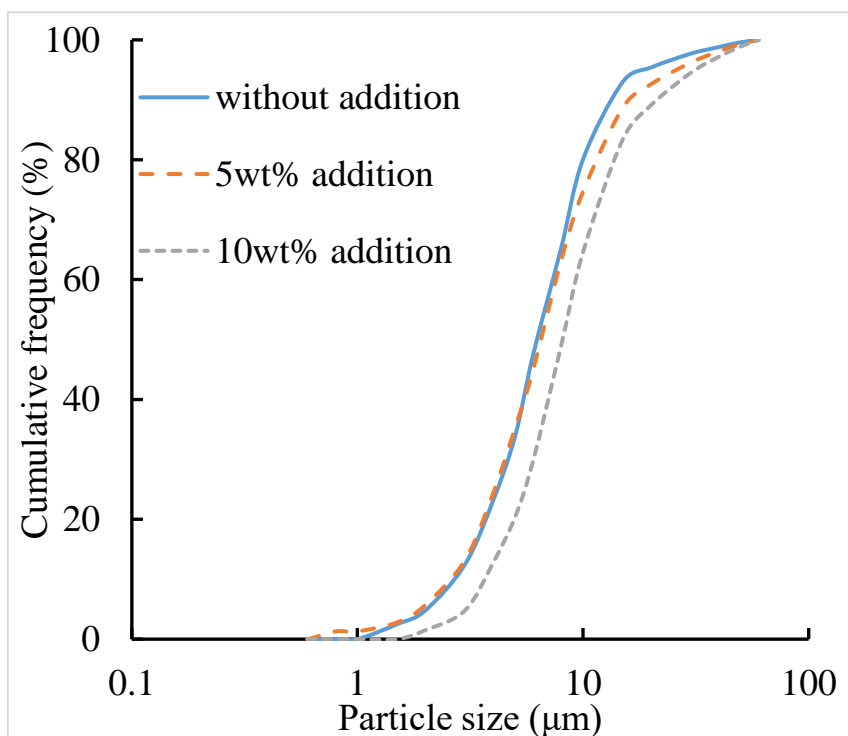


Figure 4-4. Size distributions of all coal ash samples.

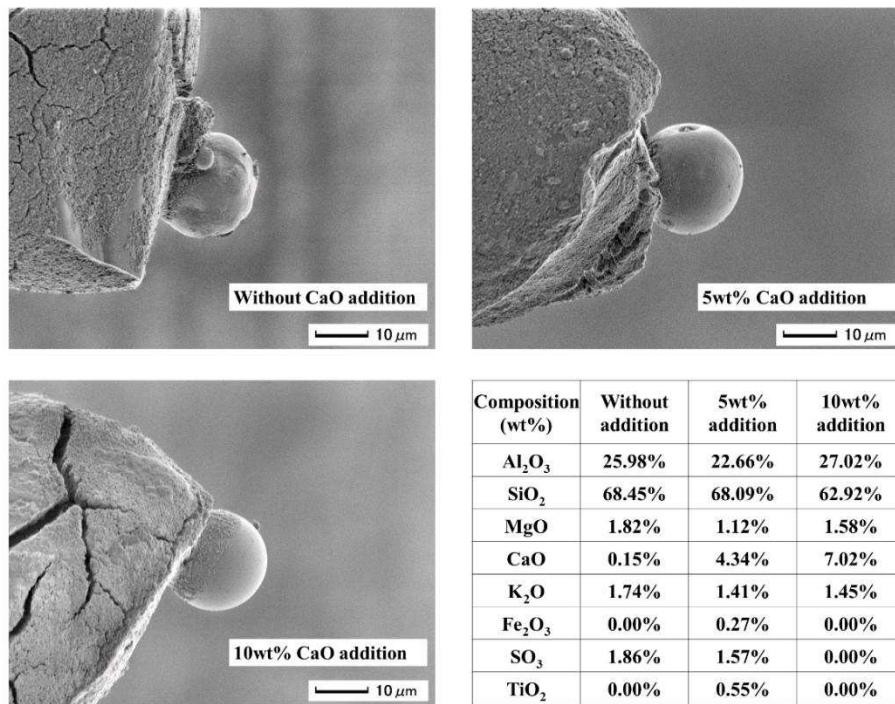
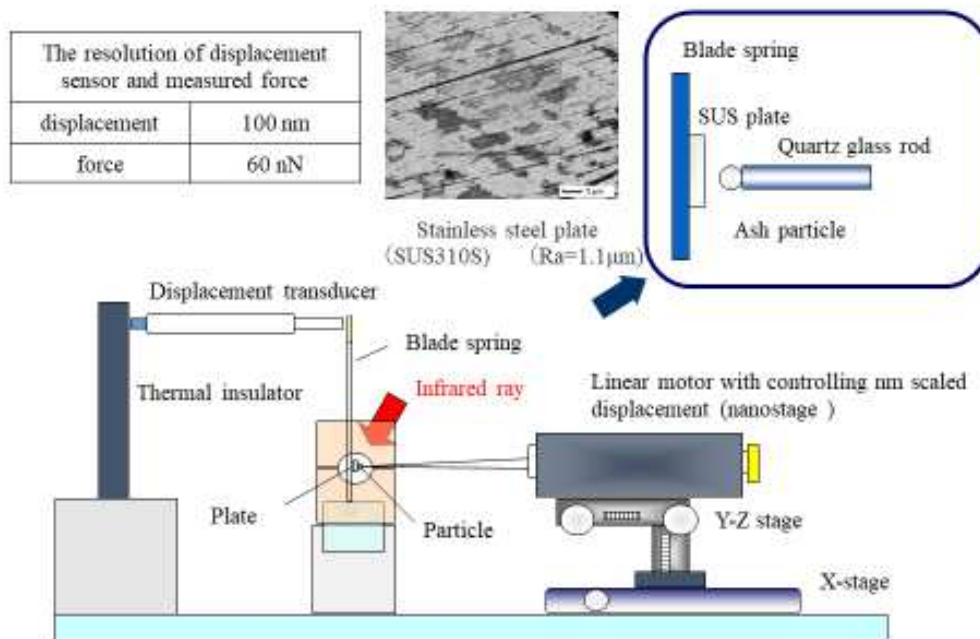
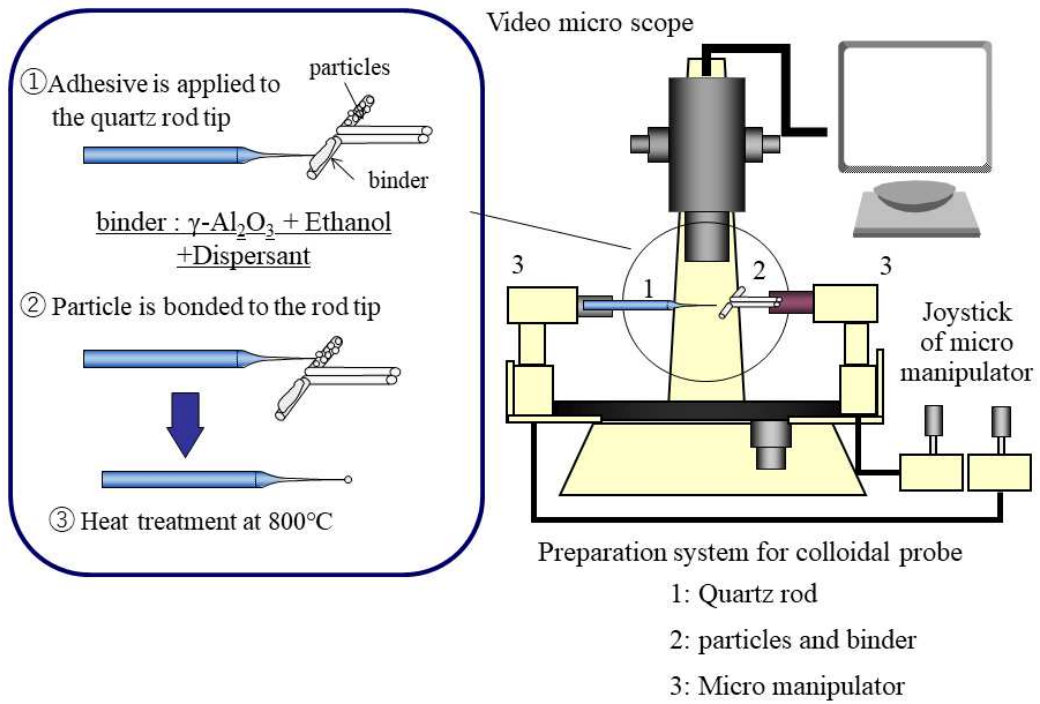


Figure 4-5. EDS results of sample real ash particles.



(a) Measurement system for adhesion force between single ash particle and metal substrate.



(b) Preparation system for single ash particle mounted on the top of quartz glass rod.

Figure 4-6. Schematic of single particle adhesion force measurement system and probe preparation system

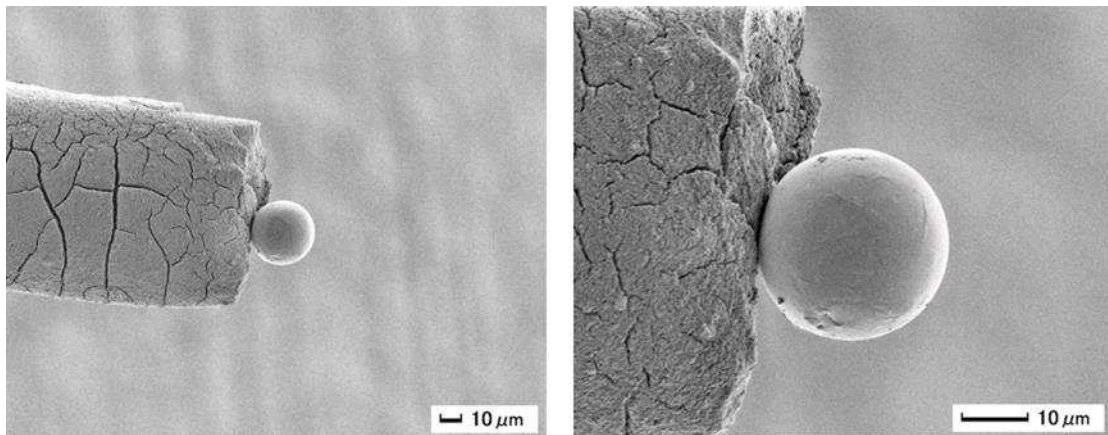


Figure 4-7. Morphology of one particle mounted onto the point of quartz rod.

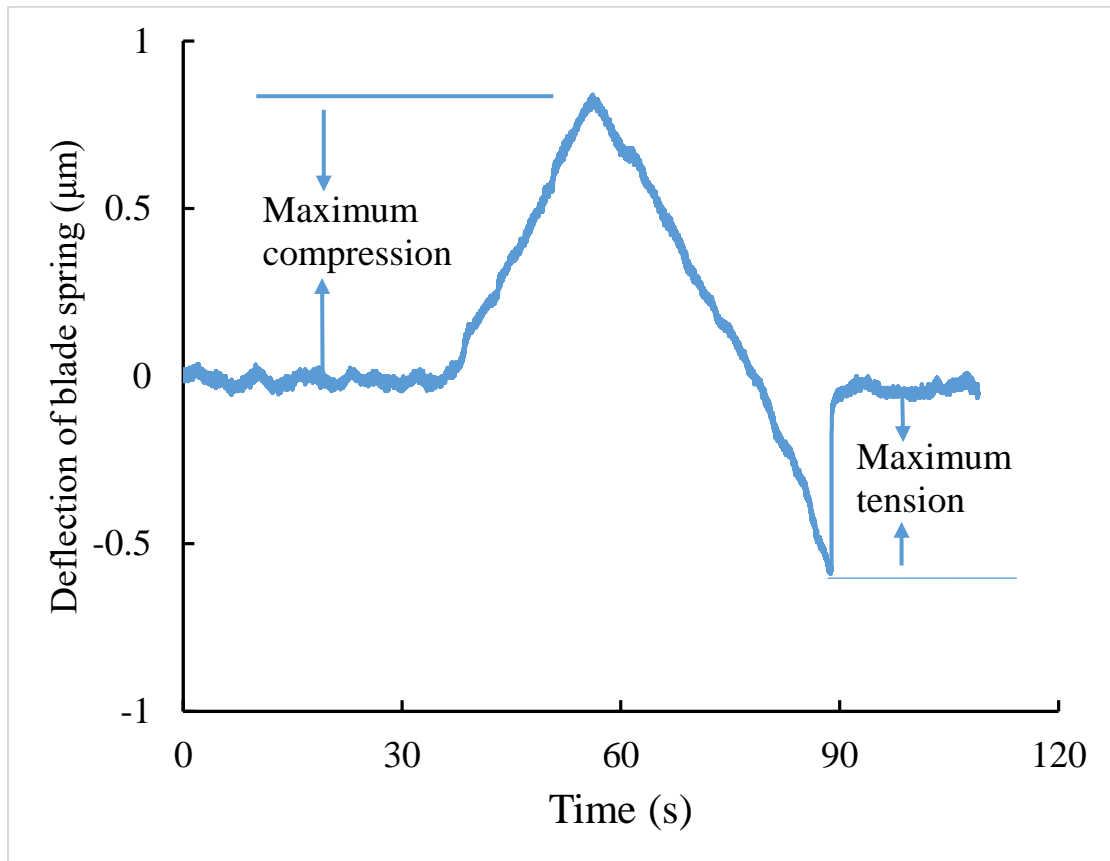


Figure 4-8. An example of spring deflection with time in one measurement.

Table 4-1. Chemical compositions of ash in pulverized coal samples at room temperature and after 950 °C heat treatment

Substance (wt%)	SiO ₂	Al ₂ O ₃	Fe ₂ O ₃	CaO	MgO	Na ₂ O	K ₂ O	SO ₃	P ₂ O ₅	TiO ₂	V ₂ O ₅	MnO
20°C	66	26	3.1	0.87	0.50	0.15	1.1	0.26	0.54	1.3	0.06	0.02
950°C	64.57	25.72	3.23	1.09	0.79	0.98	1.05	0.18	0.64	1.79	0	0

Table 4-2. Combustion conditions of coal samples in DTF

Pressure	1 atm
Temperature	1400 °C
Feed rate	0.42 g/min
Gas flow rate	0.64 NL/s
Stoichiometric air ratio	1.24
Residence time	1.36 s
Length of reaction tube	800 mm

4.3 Results and discussions

4.3.1 Shrinkage behaviors of different ash samples at elevated temperatures

TMA is used to analyze the mechanical properties of ash samples at elevated temperatures. The shrinking trend of TMA curves suggest the melting, softening or sintering behaviors of ash bulks and the starting shrinking temperature is usually used to represent the formation temperature of molten phase or slag phase. Therefore, the deformation behaviors of ash particles can be deduced based on the shrinkage curves. Figure 4-9 presents the TMA results for 5 samples including pure silica powders, model ash prepared from pure silica and alkali metals, and modified pulverized coal combusted with different CaO additional contents. The pure silica powders did not show distinct shrinkage till 1000 °C. Once alkali metals were introduced into silica powders, shown as model ash, the sample exhibited shrinkage from approximately 600 °C, as a consequence of the generation of eutectic phases (K_2O-SiO_2 , Na_2O-SiO_2). As the alkali metal content was low, the shrinkage of the model ash became stable from 850 to 1000 °C. With the temperature increasing to higher than 1000°C, the silica without alkali metals in model ashes started to shrink just like the shrinking behavior of pure silica powders, which was supported by the TMA curves of pure silica in Figure 4-9. At this temperature, the shrinking behavior of pure silica can be attributed to sintering or softening phenomena. The shrinkage curve of the model ash samples clearly shows the effect of alkali metals on decreasing ash melting or softening temperatures. For the pulverized coal ash samples, those with 0 and 5 wt% CaO

addition displayed higher shrinkage temperatures compared to the sample with 10 wt% CaO addition. Meanwhile, with increasing CaO content, the shrinkage became more significant with increasing temperature. At 1000 °C, samples without addition displayed the least shrinkage whilst the 10 wt% CaO sample showed the most serious shrinkage behavior. The differences among the three coal ash samples suggested that the addition of CaO ranging from 0 to 10 wt% in this coal may result in stronger adhesion forces among particles and greater deposition.

4.3.2 Adhesion force of model ash samples prepared from pure silica particles under different conditions

Firstly, the author tested whether the movement speed of the Nano-stage has an effect on the adhesion force, as shown in Figure 4-10. Particles under different movement speeds (5-40 nm/s) were arranged to measure the relationship between the compressive force and adhesion force at the same temperature (900 °C). Figure 4-10 indicates that although the stage speeds are different, the measured adhesion forces are similar and the slopes of the fitted lines are also similar, which suggests that a compression speed ranging from 5 to 40 nm/s has no effect on the adhesion force of an individual particle in this study. Based on these results, the compression and adhesion behaviors measurement were measured under 10 nm/s in the following experiments, because the measured forces were relatively stronger than at the other speeds.

The effect of temperature on the adhesiveness of the model ash particle to a metal substrate surface was measured and is shown in Figure 4-11. This figure shows the

adhesion forces of individual particles under increasing compression forces at 850 °C, 900 °C, and 950 °C. The movement speed of the Nano-stage was set at 10 nm/s and the compressive forces applied to the single ash particle ranged from several μN to approximately 30 μN . From this figure, the slopes of the relationships between the adhesion forces and compressive forces were dependent on measurement temperature. At 900 °C, the slope showed a maximum and a reduction was seen at 950 °C.

Considering the TMA result for this model ash, real coal ash, and pure silica particles (Figure 4-9), the model particle beds showed shrinkage at 850 °C, 900 °C, and 950 °C, which suggests that the contact point between particles partially softened. It can be assumed that, as a slight plastic deformation of particles during compression under these temperatures occurred, the adhesion force between the particles and substrate was increased. Had the particle undergone plastic deformation, the shape would not recover after the compression force was released. Therefore, if plastic deformation occurred at the contact point, higher compression forces would lead to a larger contact area between the particle and plate after compression in the measurement, causing the adhesion forces to also increase. Overall, it can be deduced that when particles were partially melted or underwent plastic deformation, the adhesion force positively correlated with the increase in compressive force. Based on the above mechanism, the fitted curves for some tests were calculated and the method for obtaining the approximate curves in Figure 4-11 will be described later.

Note that although there was no evident further shrinkage from 850 to 950 °C, the adhesion forces under the same compressive force first showed an increase and then a decrease. One possible model of these phenomena in this case is the enhanced sintering behavior between a single particle and a substrate plate from 850 to 900 °C, resulting in the adhesion force increased without further melting. With the temperature increased to 950 °C, alkali phases located on the contact point started to evaporate and were released due to high temperatures, and the contact area showed a slight reduction, causing the adhesion force to decrease. The result of our thermodynamics calculation is shown in Figure 4-12. Using the commercial software FactSage 7.3, the slag phase content in the ternary system at elevated temperatures under Gibbs energy minimization can be calculated. The slag phase formation temperature was approximately 600 °C, which fitted with the start temperature of remarkable shrinkage in the TMA curve.

4.3.3 Adhesion force of coal ash particles prepared by a drop tube furnace

Using simply structured model ash particles, we discussed the effect of some basic parameters on the adhesion forces between a single particle and an SUS plate. Results suggested that the adhesion force on one particle is affected by the compression force and temperature. However, the model ash samples prepared were of a simple structure which only contained Na, K, Si, and O, while real combustion ashes contain more complex chemical compositions and structures. Therefore, author prepared modified coal ashes by combustion of pulverized coals with different CaO contents using a drop

tube furnace. Size distributions of these three kinds of samples are presented in Figure 4-4. The mean diameters of the pure coal ash particles, ash with 5 wt% CaO addition, and ash with 10 wt% CaO addition were 7.11 μm , 7.07 μm and 7.37 μm respectively. No distinct differences in the size distribution were observed among the three kinds of coal ashes, which represented the success of modification with CaO additions. As the experiments were performed under micro-meter scale and the operations were sophisticated, many factors including sphericity, mounting angle, and especially particle size might have effects on the results. Meanwhile as author deduced that the contact area related to deformation was important to the tensile strength tests, to minimize the effect of these factors on the tensile force measurement results, the tests were performed on one particle for each ash sample. In the experiments, one particle was mounted to the top of a rod, the compressive forces on the single particle were applied from small to large rather than randomly which ensured the contact area between the particle and the plate increase gradually with the maximum compressive force increased. After a series of tests under 750 $^{\circ}\text{C}$, the temperature condition rose to 850 $^{\circ}\text{C}$ and 950 $^{\circ}\text{C}$, then new rounds of tests were performed successively. The diameters of measured particles for 0, 5 and 10 wt% CaO addition ashes were 21.3, 21.8 and 20.4 μm , respectively, which were estimated through the micro scope observation in Figure 4-5, therefore the sizes of three tested particles were similar.

Figure 4-13 shows the individual particle adhesion forces measured for the three kinds of ashes at different temperatures. In the 0 and 5 wt% CaO addition ashes, the adhesion forces did not depend on compression force at 750 and 850 $^{\circ}\text{C}$, and increased

with increasing temperature. When the temperature was increased to 950 °C, the adhesion forces increased significantly and were dependent on the compression force. In the 10 wt% CaO addition ash, the adhesion forces were dependent on the compression forces at all temperatures.

To discuss the effect of CaO addition and temperature on the adhesion force, the TMA curves in Figure 4-9 should be considered. Based on the TMA results, 0 and 5 wt% CaO-added ash did not shrink at temperatures lower than 850 °C, and almost no deformation was caused by liquid or molten phase generation at 750 and 850 °C. Therefore, the adhesion force did not depend on the compression force of ash particles in this temperature range. However, at 950 °C, due to the generation of a molten liquid phase, higher compressive forces led to a larger contact area between the molten particle and the plate, due to which the maximum adhesion force increased. In 10 wt% CaO ash, the maximum adhesion forces increase with increasing maximum compression forces at all measured temperatures as the ash started to shrink at lower temperatures; therefore, the maximum adhesion forces are sensitive to the compressive force change. Note that the maximum adhesion forces increased from 750 to 950 °C in 10 wt% CaO-added ashes more significantly than in the other ashes, which is in agreement with the largest shrinkage in the TMA results.

For the model ash prepared from pure silica and alkali metals, due to the limited elements and alkali metal contents, the shrinkage did not increase from 900 to 950 °C; consequently, adhesion forces influenced by deformations did not increase at 950 °C.

In contrast, as real ash includes more elements, such as CaO, the shrinkage of the ash layer continued at temperatures above 900 °C, thereby increasing the adhesion force.

Figure 4-14 represents the tensile strength of coal ash samples from 700 to 900°C measured by a split cell tensile strength test system. It can be clearly seen that the strength stayed at low level from low temperature to 800°C. Once the temperature increased to 900°C, the tensile strength got significant increased to about 3.12 kPa. Combined with the single particle adhesion measurement results, it can be deduced that at temperatures lower than 850°C, as no molten phase generated and the ash particle kept elastic deformation, the interaction forces among ash particles in ash bulk were not dominated by capillary force, the tensile strengths of ash bulks were not strong consequently. With the temperature increased to higher than 900°C, parts of the ash particles got soften, small liquid bridges among particles formed, therefore the tensile strengths of ash bulks got strongly promoted. Meanwhile, in single particle adhesion measurement process, the compression on ash particle would lead to plastic deformation and larger contact area between one particle to a plate, therefore the maximum tensile force got strengthen with the increase of maximum compressive force. The results of tensile force in macro scale agreed with the results on single ash particle in micro scale.

As our research was focused on a spherical particle to a flat, Hertz deformation theory was used to calculate the mathematical fittings for the relationships between maximum compressive force and maximum tensile force in coal ash samples at high

temperatures. Based on Hertz theory, when a sphere contacts with a flat, the radius of contact area can be expressed as:²⁶

$$a^3 = \frac{3}{4}R \left(\frac{1-\mu_1^2}{E_1} + \frac{1-\mu_2^2}{E_2} \right) F \quad (4-1)$$

where a is the radius of contact area, R is the radius of a sphere, μ_1 and μ_2 are the elastic modulus of the sphere and the flat, E_1 and E_2 are the poisson ratios of the sphere and the flat, F is the compression force acting on the sphere. If the maximum contact area was kept during unloading process of compression force by plastic deformation, the increase of contact area would cause the increase of tensile force.

From Equation 1, the relationship between sphere-flat contact area and the force can be derived as:

$$S \propto F^{\frac{2}{3}} \quad (4-2)$$

In our measurements, when the maximum compressive force is 0 μN , the tensile force between a particle and a flat should be the van der Waals force without plastic deformation. The author assumed that the maximum tensile force f is proportional to the residual contact area S after compressive force released, accordingly the relationship between tensile force and compressive force can be expressed as:

$$f = \varphi F^{\frac{2}{3}} + \omega \quad (4-3)$$

where φ is the coefficient determined by R , μ , E and other constants, ω is the van der Waals force between sphere and flat.

As the increase of tensile forces with increase of compression force measured at relatively lower temperature (below 850 °C) were not obvious, the author fitted the data measured at high temperatures (between 850 and 950 °C). The detailed fitting results of each coal combustion ash with different CaO additions are shown in Table 4-3. At 950 °C, the φ of 10wt% CaO addition ash is greater than 5wt% addition ash, 0wt% addition ash and Model ash samples sequentially and the trend is similar to the comparison of shrinkage among these samples in TMA results. It seems that φ can be summarized that have a positive correlation to the temperature and CaO content in this coal ash sample. Meanwhile, larger φ also suggests more molten slag phase or liquid phase were generated under the same conditions.

As Equation 4-1 describes elastic deformation, when the particles were in plastic deformation during compression process, the residual contact area caused by plastic deformation should be larger than the estimated elastic deformation after force released. On the contrary, if partially elastic and plastic deformation occurred during force release process, the residual contact area should be smaller than represented contact area by Equation 4-1.

In general, the author verified that the one-particle adhesion measurement system can be used not only for simple ternary model ash samples but also real coal combustion ash samples. The phenomena “tensile force increases with the increases of compressive force” were always accompanied by the shrinking behavior in TMA results for both model ash and coal ashes. The adhesion force between a particle and a plate is mainly

dominated by the particle deformation properties and contact area. TMA curves can be used to discuss the differences in the relationships between the compression force and adhesion force at different temperatures in all ash samples. For model ash prepared from pure silica and alkali metals, the generation of K_2O-SiO_2 and Na_2O-SiO_2 eutectic phases, which have low melting points, reduced the initial shrinkage temperature compared to pure silica bulks, thus the alkali metals should be one of the key factors relating to the deformation in the model ash system. Limited by the element types and low contents of alkali metals, the shrinkage behavior of model ash was not continuous at elevated temperatures, due to which the adhesion force could not increase at 950 °C. This was different from the results for the pulverized coal ash samples. As compounds with more kinds of elements, coal ash samples contained alkali metals and silica as well, but the start shrinking temperatures were higher than the model ash. This phenomenon could be attributed to the existence of alumina in coal ashes, which can suppress the formation of eutectic phases with low melting points.²⁷ For the coal ash samples, results showed that the CaO additive increased the adhesion force at elevated temperatures by decreasing the initial shrinkage temperature and increasing the molten phase contents. As the melting points of the ashes showed a tendency toward decreasing first and then increasing with increasing CaO content, 5 wt% and 10 wt% CaO provided decreased ash melting points; therefore, the adhesion forces increased with increasing CaO content.

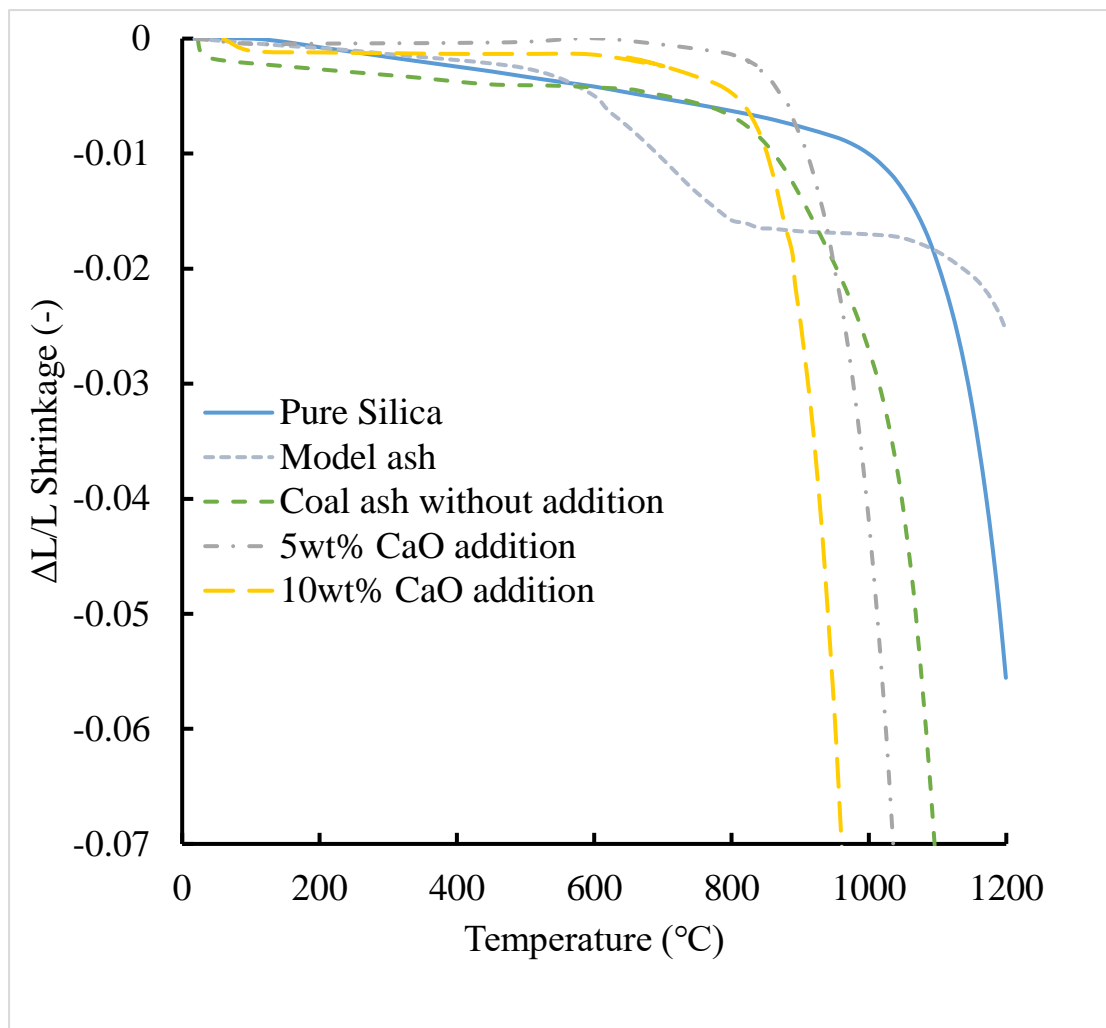


Figure 4-9. TMA curves of pure silica powders, model ash sample and coal ash samples at elevated temperature.

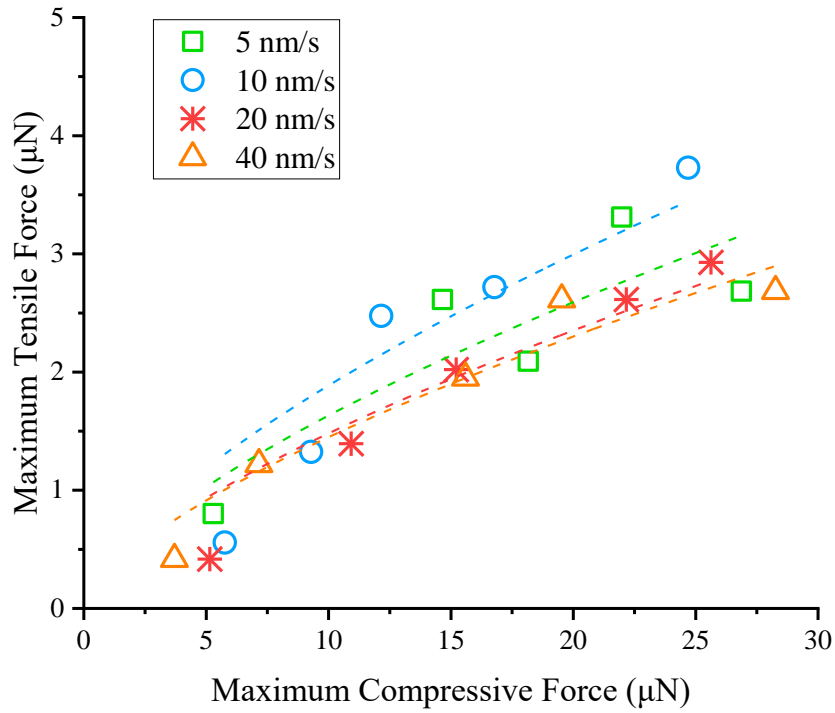


Figure 4-10. Effect of compressive speed and force on adhesion force of model ash sample.

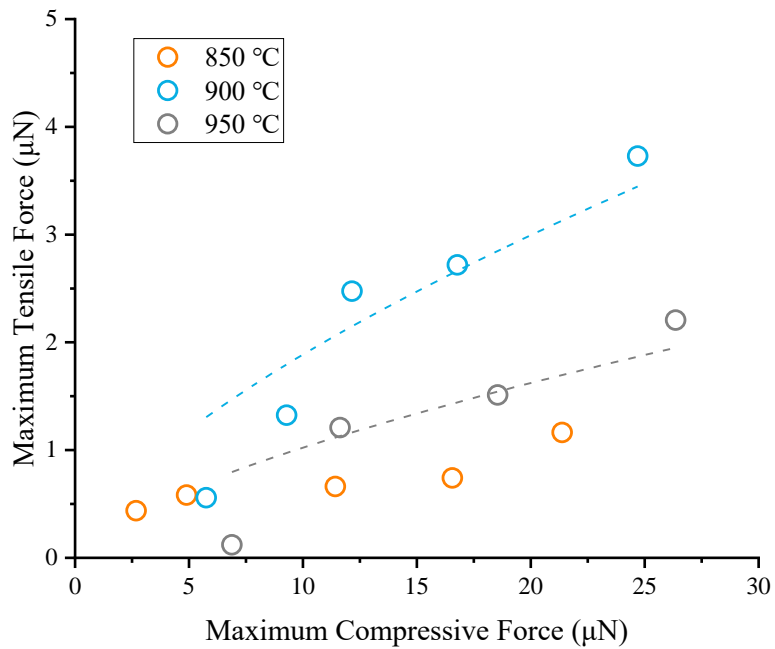


Figure 4-11. Effect of temperature and compressive force on adhesion force in model ash sample.

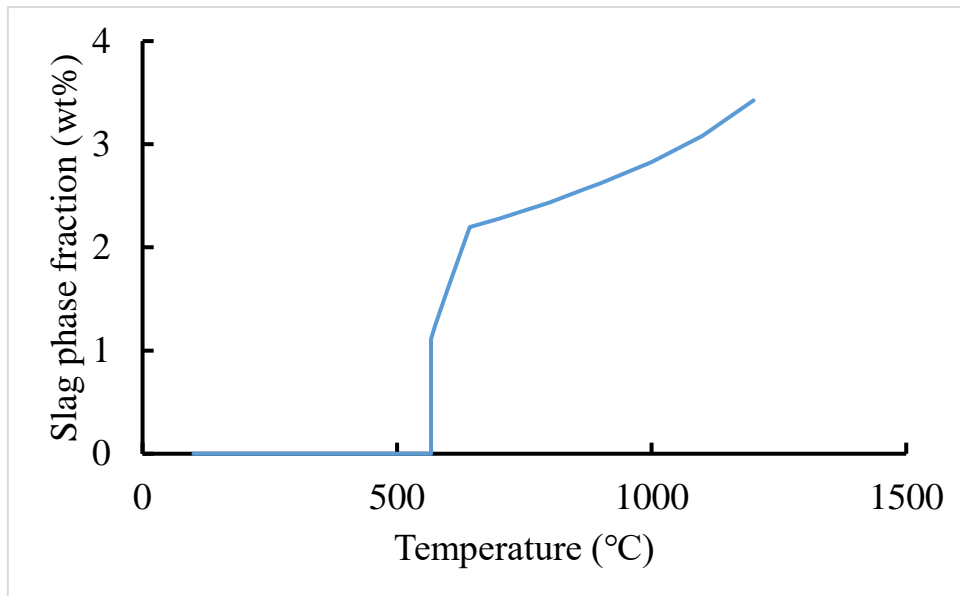
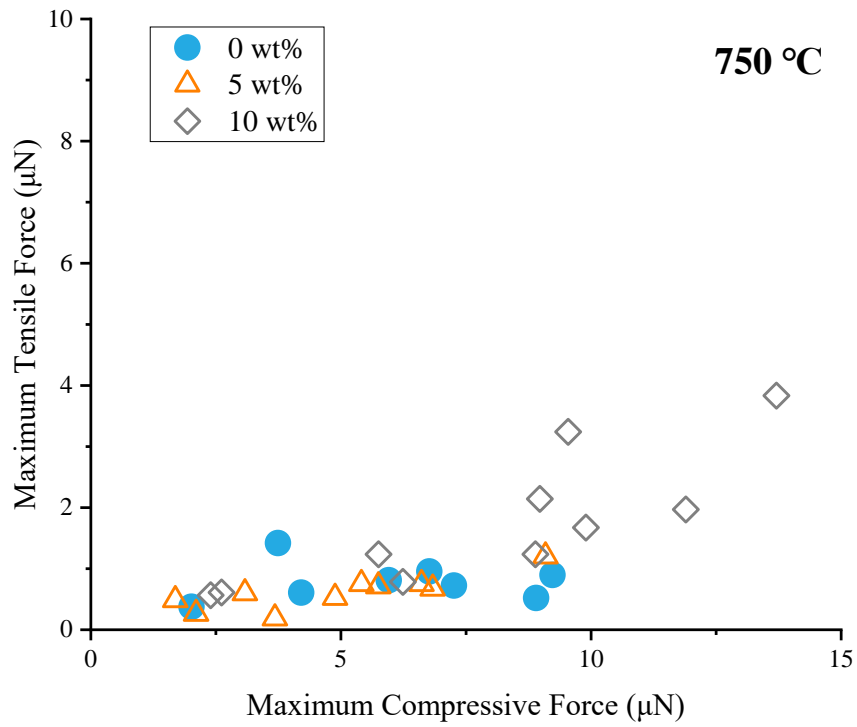
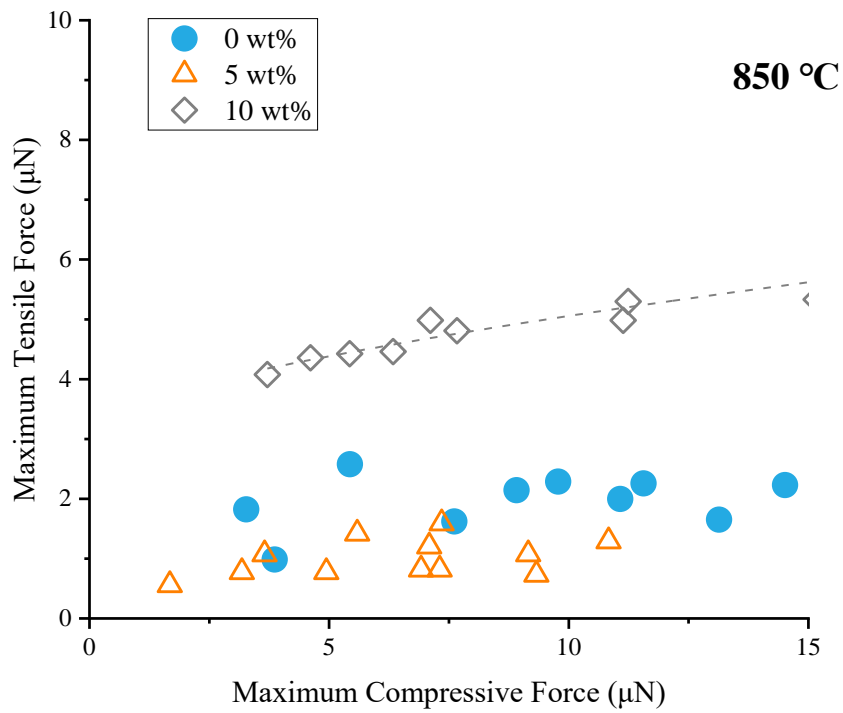


Figure 4-12. Mass fraction of slag phase in model ash at elevated temperature using thermodynamic equilibrium calculation.*

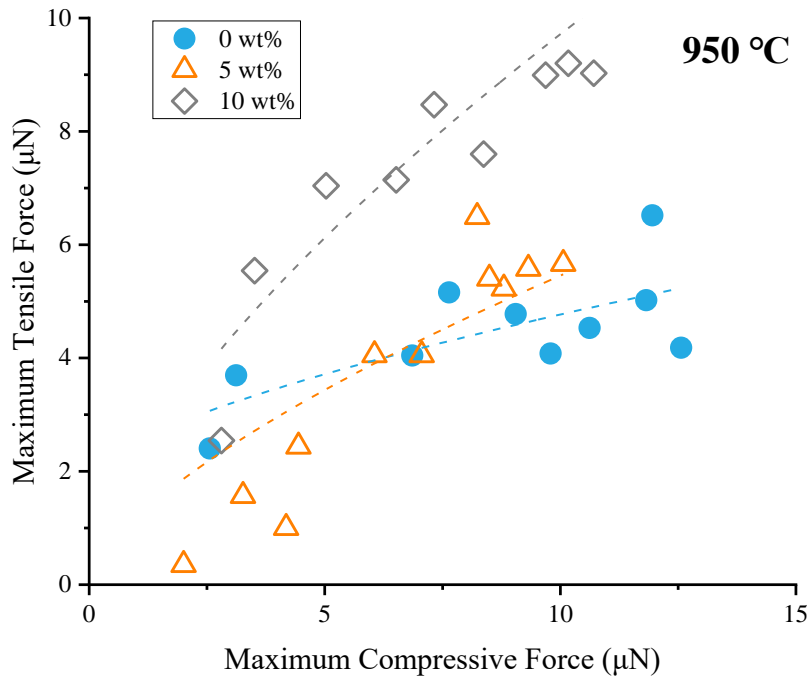
* Thermodynamic equilibrium calculations was carried out using commercial software, *Factsage 7.3*, *Equilib* module. Calculation databases were '*FToxid*' and '*FactPS*'. The calculation conditions were set at a temperature ranging from 20 °C to 1200 °C, and the temperature check point interval is 100 °C under a pressure of 1 atm.



(a)



(b)



(c)

Figure 4-13. Effect of temperature and compressive force on adhesion force of coal ash samples. (a) 750 °C, (b) 850 °C and (c) 950 °C.

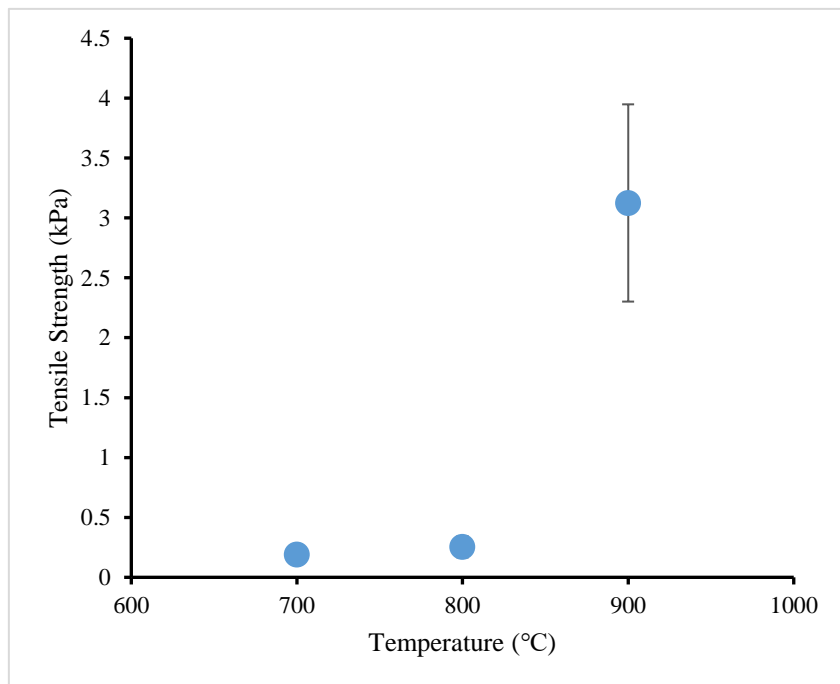


Figure 4-14. Tensile strength measurement results of pure coal ash samples at different temperatures.

Table 4-3. Parameters of fitted curves for different ash samples.

Samples	Fitted equations
Model ash (900°C)	$f = 0.406F_3^{\frac{2}{3}}$ ($R^2 = 0.842$)
Model ash (950°C)	$f = 0.220F_3^{\frac{2}{3}}$ ($R^2 = 0.766$)
10 wt% addition Coal ash (850°C)	$f = 0.392F_3^{\frac{2}{3}} + 3.2377$ ($R^2 = 0.884$)
0 wt% addition Coal ash (950°C)	$f = 0.613F_3^{\frac{2}{3}} + 1.9207$ ($R^2 = 0.513$)
5 wt% addition Coal ash (950°C)	$f = 1.18F_3^{\frac{2}{3}}$ ($R^2 = 0.744$)
10 wt% addition Coal ash (950°C)	$f = 2.09F_3^{\frac{2}{3}}$ ($R^2 = 0.798$)

4.4 Conclusions

1. A developed system were used to measure the adhesion force of both ternary model ash and pulverized coal ash samples with different CaO contents. This system offers a new method to quantify the adhesion force of a single particle by direct measurement.

2. By changing the measurement conditions, author confirmed and discussed the factors influencing the adhesion force between a particle and an SUS plate under high-temperature conditions combined with TMA. Physical state and deformation type of ash particles are important factors which can influence the adhesion behaviors.

3. By changing the movement speed of the Nano-stage, it was found that compressive speeds did not have a remarkable correlation with adhesion forces. In addition, by changing the CaO content in pulverized coal ashes, it was confirmed that in some range the addition of CaO could increase adhesion forces by changing ash deformation behaviors at high temperatures.

4.5 References

1. Kamiya, H.; Kimura, A.; Yokoyama, T.; Naito, M.; Jimbo, G., Development of a Split-type tensile-strength tester of inorganic fine powder bed for high-temperature conditions. *Powder Technology* **2002**, 127, 239-245.
2. Kamiya, H.; Kimura, A.; Tsukada, M.; Naito, M., Analysis of the high-temperature cohesion behavior of ash particles using pure silica powders coated with alkali metals. *Energy&Fuels* **2002**, 16 (2), 457-461.
3. Naganuma, H.; Ikeda, N.; Ito, T.; Matsuura, M.; Nunome, Y.; Ueki, Y.; Yoshiie, R.; Naruse, I., Reduction mechanisms of ash deposition in coal and/or biomass combustion boilers. *Fuel* **2013**, 106, 303-309.
4. Kamiya, H.; Kimura, A.; Horio, M.; Seville, J.; Kauppienen, E., Diametal compression characteristics of cohesive ash powder pellets at high temperature. *Journal of Chemical Engineering of Japan* **2000**, 33 (4), 654-656.
5. Pang, C. H.; Hewakandamby, B.; Wu, T.; Lester, E., An automated ash fusion test for characterisation of the behaviour of ashes from biomass and coal at elevated temperatures. *Fuel* **2013**, 103, 454-466.
6. Hemmer, G.; Kasper, G. Predicting the Operating Behavior of Ceramic Filters from Thermo-Mechanical Ash Properties; Verfahrenstechnik und Mechanik, Universitaet Karlsruhe (TH), D-76128 ...: **2002**.
7. Kamiya, H.; Deguchi, K.; Gotou, J.; Horio, M., Increasing phenomena of pressure drop during dust removal using a rigid ceramic filter at high temperatures. *Powder Technology* **2001**, 118 (1-2), 160-165.
8. Jiang, J.; Gong, J.; Liu, W.; Chen, T.; Zhong, C., Analysis on filtration characteristic of wall-flow filter for ash deposition in cake. *Journal of Aerosol Science* **2016**, 95, 73-83.
9. Heidenreich, S., Hot gas filtration—A review. *Fuel* **2013**, 104, 83-94.
10. Laursen, K.; Frandsen, F.; Larsen, O. H., Ash deposition trials at three power stations in Denmark. *Energy&Fuels* **1998**, 12 (2), 429-442.
11. Huang, L.; Norman, J.; Pourkashanian, M.; Williams, A., Prediction of ash deposition on superheater tubes from pulverized coal combustion. *Fuel* **1996**, 75 (3), 271-279.
12. Lin, J.-S.; Tsai, C.-J.; Tung, K.-L.; Chiang, H.-C., Thermophoretic particle deposition efficiency in turbulent tube flow. *Journal of the Chinese Institute of Chemical Engineers* **2008**, 39 (3), 281-285.
13. Baxter, L. L. Ash Deposit Formation and Deposit Properties. A Comprehensive Summary of Research Conducted at Sandia's Combustion Research Facility; Sandia National Labs., Albuquerque, NM (US); Sandia National Labs ...: **2000**.
14. Walsh, P. M.; Sayre, A. N.; Loehden, D. O.; Monroe, L. S.; Beér, J. M.; Sarofim, A. F., Deposition of bituminous coal ash on an isolated heat exchanger tube: effects of coal properties on deposit growth. *Progress in Energy and Combustion Science* **1990**, 16 (4), 327-345.
15. Kamiya, H.; Yamaguchi, N.; Koga, A.; Horio, M. In Development of a Direct Measurement System for a Single Particle Force at High Temperature, Preprints of Fall Meeting of Soc. Powder Technology. Japan, **1999**; pp 207-10.
16. Ferreira, O. D. S.; Gelinck, E.; de Graaf, D.; Fischer, H., Adhesion experiments using an AFM—Parameters of influence. *Applied Surface Science* **2010**, 257 (1), 48-55.
17. Kappl, M.; Butt, H. J., The colloidal probe technique and its application to adhesion force measurements. *Particle & Particle Systems Characterization: Measurement and Description of Particle*

- Properties and Behavior in Powders and Other Disperse Systems* **2002**, 19 (3), 129-143.
18. Broekmaat, J.; Brinkman, A.; Blank, D. H.; Rijnders, G., High temperature surface imaging using atomic force microscopy. *Applied Physics Letters* **2008**, 92 (4), 043102.
 19. KAMIYA, H., Direct measurement of the adhesion force for single ash particle at high temperature. *Ceramic Transaction* **2004**.
 20. Miles, T. R.; Miles Jr, T. R.; Baxter, L. L.; Bryers, R. W.; Jenkins, B. M.; Oden, L. L., Boiler deposits from firing biomass fuels. *Biomass and Bioenergy* **1996**, 10 (2-3), 125-138.
 21. Guan, R.; Li, W.; Li, B., Effects of Ca-based additives on desulfurization during coal pyrolysis. *Fuel* **2003**, 82 (15-17), 1961-1966.
 22. Wu, X.; Zhang, X.; Yan, K.; Chen, N.; Zhang, J.; Xu, X.; Dai, B.; Zhang, J.; Zhang, L., Ash deposition and slagging behavior of Chinese Xinjiang high-alkali coal in 3 MWth pilot-scale combustion test. *Fuel* **2016**, 181, 1191-1202.
 23. Wang, X.; Xu, Z.; Wei, B.; Zhang, L.; Tan, H.; Yang, T.; Mikulčić, H.; Duić, N., The ash deposition mechanism in boilers burning Zhundong coal with high contents of sodium and calcium: a study from ash evaporating to condensing. *Applied Thermal Engineering* **2015**, 80, 150-159.
 24. Song, W. J.; Tang, L. H.; Zhu, X. D.; Wu, Y. Q.; Zhu, Z. B.; Koyama, S., Effect of coal ash composition on ash fusion temperatures. *Energy&Fuels* **2009**, 24 (1), 182-189.
 25. Liu, B.; He, Q.; Jiang, Z.; Xu, R.; Hu, B., Relationship between coal ash composition and ash fusion temperatures. *Fuel* **2013**, 105, 293-300.
 26. Chaudhri, M.; Yoffe, E., The area of contact between a small sphere and a flat surface. *Philosophical Magazine A* **1981**, 44 (3), 667-675.
 27. Gao, J.; Matsushita, M.; Horiguchi, G.; Fujii, R.; Tsukada, M.; Okada, Y.; Kamiya, H., Toward Stable Operation of Sewage Sludge Incineration Plants: The Use of Alumina Nanoparticles to Suppress Adhesion of Fly Ash. *Energy&Fuels* **2019**, 33 (9), 9363-9366.

CHAPTER 5

General Conclusions

CHAPTER5

General conclusions

The major objective of this study is to have a better understand about ash deposition phenomena of fly ashes generated from combustions. Knowing the mechanisms of deposition have contributes to the normal operation and manufacture in real power plants or incinerators. In this work, different research methods in many aspects were applied to research on the ash deposition phenomena, the general conclusions are summarized as below.

In Chapter 2, real ashes from industries were chosen as the research targets. Four types of sewage sludge combustion ash with different adhesive properties were examined to determine the mechanism of ash adhesion at temperatures up to 1000°C. By measuring tensile strength of ash powder beds at 400-800°C and determining chemical composition, ashes with higher adhesiveness contained greater amounts of phosphorus, while ashes that did not adhere contained greater amounts of silicon and aluminum. Results from thermomechanical property analyses showed that the ashes with greater adhesiveness generated liquid or slag phases at lower temperatures compared with the stable operation ashes. This phenomenon was also confirmed by thermodynamic equilibrium calculations, which indicated that the slag formation temperature (initiation temperature of slag phase formation) was lower in ashes with high adhesiveness. Based on analysis of the adhesion mechanism of high-adhesiveness ashes, adding alumina particles may reduce adhesion force. Experimental results showed that the alumina additive effectively decreased the tensile strength of high-

adhesiveness ashes at high temperatures. In this chapter the mechanism of ash deposition phenomena were discussed that the generation of slag/liquid phase among ash particles is a main cause of strong adhesion forces among particles at high temperatures and some specific elements were researched to discuss their roles in the deposition issues.

Based on the results in Chapter 2, it is known that slag/liquid phases are the key point, so in Chapter 3, the author tried to have a deeper understanding of the effect of some other specific elements on deposition issues using synthetic model ash systems. In this chapter, a method of synthesizing sewage sludge combustion ashes was proposed and the corresponding model ashes based on the chemical composition of two real high-phosphorus ashes with different deposition issues were synthesized. The synthesized model ashes can modify the stickiness of real ashes to some extent. Since the rationality and effectiveness of this synthetic method, it become possible to research on the effect of specific elements on the deposition phenomena of ashes at high temperature by controlling the concentration of specific elements in model ashes. A group of ashes using Al to replace the Mg and Ca were prepared to make a comparison between the effects of Al and Mg/Ca, results showed that Mg and Ca have a better performance in resistance of slag phase generation compared to Al in the high phosphorus concentration sewage sludge ashes, the deposition phenomena would be controlled consequently.

Except for sewage sludge ashes, the deposition issues of coal combustion ashes are also an important research topic. Different from sewage sludge ashes, the treatment

temperature of coal samples are usually higher and the typical chemical compositions are different. Comprehensive considering different aspects including morphology and chemical compositions, direct measurement of adhesion force on single particle is an useful method on characterizing coal ash samples. In Chapter 4, the author measured the adhesion force of both ternary model ash and pulverized coal ash samples with different CaO contents using the developed single-particle adhesion measurement system. This system offers a new method to quantify the adhesion force of a single particle by direct measurement. By changing the measurement conditions, the author confirmed and discussed the factors influencing the adhesion force between a particle and an SUS plate under high-temperature conditions combined with TMA. The slightly molten deformation behavior of particles determined by mechanical properties appeared to have influenced adhesion forces. When the particles maintained solid states or elastic deformation during compression and release, the adhesion force would not increase with increasing compression force. When the deformation behaviors of the particles were plastic, the adhesion force had a positive correlation with the compressive force. Meanwhile, by changing the movement speed of the Nano-stage, the author found that compressive speeds did not have a remarkable correlation with adhesion forces. In addition, by changing the CaO content in pulverized coal ashes, it was confirmed that the addition of CaO could increase adhesion forces by changing ash deformation behaviors at high temperatures. Higher CaO addition leads to a higher adhesion force between a single particle and the substrate due to the more serious ash melting behavior.

In general, this thesis provides a systematic experimental research on the deposition phenomena of ashes. Partially generation of slag or liquid phases among particles is the main mechanism relating to the high adhesiveness of ashes. Consequently, the main method to suppress the adhesiveness is to reduce the generation of slag phase by increasing melting temperature using physical or chemical routes. In this thesis, the samples involved sewage ashes and coal ashes, the experimental subjects included real ashes and synthetic model ashes, the researched elements covers the main elements in ashes, the research scales ranged from ash bulks to single particle. Element-level researches are benefit for understanding the mechanism of ash deposition phenomena and also can contribute to the proposal of depressors or control methods. In all ash samples, alkali metal is a key factor relating to deposition issues. Phosphorus usually promotes deposition issues while aluminum can suppress the deposition by generating materials with higher melting points. The roles of magnesium and calcium are complex, they can influence the adhesiveness of different ashes in different way. In this work, calcium and magnesium are benefit for the control of ash adhesiveness. About research method, preparation of model ash is a convenient, useful and visualized method. With it, researchers can easily design and control the chemical composition of researched ash samples in a border way, the restrains of real ash samples can be removed consequently. About experimental facilities, it's impossible to evaluate every aspects of one property using only one equipment. In this work, the deposition property and adhesion property were evaluated using a split-cell tensile strength test system and a single particle adhesion force measurement system, both of these two system can be used to research

on the ash behaviors, but in different scales. Researches with multiple perspectives are beneficial to a comprehensive understanding about the mechanism of ash deposition phenomena. The general conclusions of this study is summarized above. I hope my researches could make some contributions to some researchers and engineers who is working on the fuel or combustion fields to solve some problems in some way in the future.

Acknowledgement

ACKNOWLEDGEMENT

Firstly, I would like to express my gratitude to all those who were with me during the period in my lab. Especially for my supervisor, Prof. Hidehiro Kamiya, he taught me knowledge in academics, supported me in life and guide me in mind. Without his guidance and encouragement, this thesis could not research its present form. I would also appreciate my team members including Okada sensei, Tsukada-san, Matsushita-san, Kawada-san, Horiguchi-san, Hariu-san, Fujii-san, Beppu-san and everyone in Kamiya lab, they helped me a lot in both experiments and lab life, also, we enjoyed many drinking parties in the past years.

Secondly, I would like to give my hearty thanks to my friends, we supported each other to today.

Last but not least, my thanks would go to my beloved family for their loving considerations and great confidence in me all through these years. Their supports are my greatest motivation to move forward in the future.